The Pennsylvania State University
The Graduate School

THERMODYNAMIC MODELING OF THE REACTIVE SINTERING OF ND:YAG

A Thesis in
Materials Science and Engineering
by
James E. Saal

Submitted in Partial Fulfillment
of the Requirements
for the Degree of

Master of Science

May 2008

The thesis of James E. Saal was reviewed and approved* by the following:

Zi-Kui Liu
Professor of Materials Science and Engineering
Thesis Advisor

Gary L. Messing
Distinguished Professor of Ceramic Science and Engineering
Head, Department of Materials Science and Engineering

Elizabeth C. Dickey
Associate Professor of Materials Science and Engineering

*Signatures are on file in the Graduate School.

Abstract

This thesis describes the use of thermodynamic modeling to study the reactive sintering of Nd:YAG by evaluating the Al_2O_3-Nd_2O_3-SiO_2-Y_2O_3 system. Such modeling predicts the phase equilibria during the high temperature sintering, data that is difficult to directly determine experimentally. To describe the this system, a previous modeling of the Al_2O_3-SiO_2-Y_2O_3 system is taken as the foundation upon which Nd_2O_3 is added. This is accomplished by evaluating the three pseudo-binary oxide systems that contain Nd_2O_3 (Al_2O_3-Nd_2O_3, Nd_2O_3-SiO_2, and Nd_2O_3-Y_2O_3) using experimental phase equilibria and thermochemical data from the literature and performing first-principles calculations on the compounds in the systems. To complete the modeling of the pseudo-quaternary system, the description of the Gibbs free energy of Nd:YAG is determined by calculating, from first-principles, the enthalpy of mixing of Nd in the Y sublattice of YAG for several compositions.

The phase equilibria during reactive sintering is then predicted. For a typical composition of Nd:YAG, a liquid phase is present in appreciable quantities (about 10% by mole fraction), supporting the hypothesized role of SiO_2 as a sintering aid due to the formation of liquid. Interestingly, SiO_2 is also predicted to stabilize a small amount of $NdAl_{11}O_{18}$ (about 1% by mole fraction), the quantity and stable temperature region of which change with the amount of Nd_2O_3 and SiO_2.

From these results, a model is proposed describing the abnormal grain growth observed in YAG. It is theorized that $NdAl_{11}O_{18}$ particles precipitate in the YAG grain boundaries during sintering. Near temperatures where the particles begin to melt, abnormal grain growth arises because the distribution of the particles fluctuates, allowing a few grains to grow faster than others. Under this model, the CALPHAD evaluation of the phase equilibria predicts the temperature at which abnormal grain growth occurs is around 2000K. Predictions are made as to the size of the particles and how the temperature at which abnormal grain growth occurs changes with the composition of the system.

Table of Contents

List of Figures

List of Tables

Acknowledgments

I would like to thank the following people for making this possible:

- My advisor, Zi-Kui Liu, for the opportunity to work and learn from him and for always pressing me to work harder and aim higher.
- My committee members, Gary Messing and Elizabeth Dickey, for their time and support. Special thanks to Gary Messing for the chance to work on this project.
- Everyone at the Phases Research Lab for their help and support, especially Ray, Sara, Arkapol, and Venki. I wish to especially thank Dongwon Shin for his infinite patience in teaching me the finer points of materials modeling and for proofreading my thesis.
- Adam Stevenson for the many times I bugged him about Nd:YAG.
- My family and friends for their love and support.

Dedication

To my mother, father, and brother, without whom this would not be possible.

Chapter 1

Introduction

1.1 Nd:YAG Properties and Processing

An essential component of the solid state laser is the laser emitting material, which consists of a host crystal or glass doped with ions that, once excited to higher energy states, will emit the high power light when they relax. The first solid state laser was demonstrated by Maiman[1] who used a chromium-doped ruby crystal as the emitting material. Advances have since been made in both the understanding of the physics responsible for solid state lasers and in the materials which are capable of the phenomenon.

Discovered in 1964 by Geusic[2], neodymium-doped yttrium aluminum garnet ($(Y_{1-x}Nd_x)_3Al_5O_{12}$) or Nd:YAG is currently the most widely used solid-state laser emitting material. YAG is an ideal host for the ions as it is strong mechanically, is easy to produce, and has a high thermal conductivity which allows for high output power without degrading the quality of the laser. Trivalent neodymium ions replace trivalent yttrium in the oxide by up to about x=0.01 for single crystal growth[3]. Single crystal Nd:YAG would be the ideal form for a device. However the growth of the crystal introduces defects and stresses due to an inhomogeneous distribution of Nd across the crystal, leaving only 25% of the material in a usable form. Furthermore, single crystal growth of YAG is a time-consuming and expensive process. Polycrystalline Nd:YAG does not suffer from these complications, and a method to produce the material via reactive sintering was developed by Ikesue in 1995[4] in which the resulting ceramic has nearly the same laser properties

as the single crystal. This process involves sintering the component oxides (Al_2O_3, Nd_2O_3, and Y_2O_3) in the ratio of Nd:YAG. Silica is added as a sintering aid as it is found to promote densification and improve the incorporation of Nd into YAG.

Investigation into the sintering of Nd:YAG by this method has shown that the density of the ceramic is strongly influenced by the sintering temperature[5]. At higher temperatures, porosity is kept at a minimum. However, it is observed that at approximately 2100K the regularity of the grain size is disrupted by the presence of some excessively large grains. A time dependence also exists whereby, at lower temperatures, these large grains will arise if sintered at longer times. Such a phenomenon, commonly referred to as exaggerated or abnormal grain growth (AGG), has been observed in numerous ceramic oxides, notably Al_2O_3[6].

1.2 Objectives

Direct observation of the phase equilibria during reactive sintering is difficult as it takes place during high temperatures. Such information, however, is necessary to fully understand the growth mechanisms and properties of the material during processing. A method that can be used to provide some insight is to model the Gibbs energies of all the pertinent phases in the system and then determine the phase equilibria by the CALPHAD approach, detailed in the next chapter. Therefore, the goal of this thesis is to investigate the phase equilibria during the reactive sintering of Nd:YAG by thermodynamically modeling the Al_2O_3-Nd_2O_3-SiO_2-Y_2O_3 system. This is accomplished by adding Nd_2O_3 to the previously modeled Al_2O_3-SiO_2-Y_2O_3 system[7].

As an example of how thermodynamic modeling can bring insight into the behavior of a materials system, the phenomenon of AGG is investigated in the thesis. As the presence of particles of a solid phase at the grain boundaries is theorized to be an essential component to AGG[8], an important step in understanding this effect is to examine the phase equilibria at the sintering conditions to determine if such particles exist. Experimental investigation can be difficult as the size and amount of these particles may be too small to be detectable with common imaging and characterization techniques and yet be large enough to bring about changes in the growth of the Nd:YAG grains. Therefore, the modeling of the Al_2O_3-Nd_2O_3-

SiO_2-Y_2O_3 system can provide insight into AGG by predicting the whether these particles exist.

1.3 Outline

This thesis is divided into eight chapters. Chapter 2 provides a brief review of the methods employed, including CALPHAD thermodynamic modeling and first-principles calculations. Chapters 3, 4, and 5 detail the modeling of the Al_2O_3-Nd_2O_3, Nd_2O_3-SiO_2, and Nd_2O_3-Y_2O_3 systems, respectively, including a review of the available experimental data in the literature and results of the first-principles calculations of the compounds for those systems. Chapter 6 discusses the construction of the Al_2O_3-Nd_2O_3-SiO_2-Y_2O_3 system from the previously modeled Al_2O_3-SiO_2-Y_2O_3 system and the new pseudo-binary systems, including a review of the available experimental data concerning the pseudo-quaternary system and results for first-principles calculations on Nd:YAG. Chapter 7 provides details on the phase equilibria present in the sintering conditions of Nd:YAG when AGG is observed and proposes a model for the abnormal growth. The thesis concludes with Chapter 8, which summarizes the findings of the current work and proposes possible avenues for future study.

Chapter 2

Computational Methodology

2.1 Introduction

The goal of this thesis is to predict the phase stability during the reactive sintering of Nd:YAG through the CALPHAD (Computer Coupling of Phase Diagrams and Thermochemistry) approach to thermodynamic modeling. This method entails describing the Gibbs energy of phases as a function of temperature, pressure, and composition. This enables the calculation of properties derived from the Gibbs energy, such as the chemical potential, and of phase equilibria. The specific parameters that dictate the behavior of the Gibbs energy equation are determined by fitting the equation onto experimental thermochemical and phase equilibria data. For instances where such data may be unavailable or unreliable, first-principles density functional theory simulations have been shown to ably predict the thermochemical properties of phases. Afterwards, useful predictions can be made by extrapolating the equations into regions where data is not available (i.e. the properties of a metastable phase or the equilibria of a high-order system from lower-order ones). The phases present during the reactive sintering of Nd:YAG can be determined by modeling the individual pseudo-binary oxide systems and extrapolating into the higher-order Al_2O_3-Nd_2O_3-SiO_2-Y_2O_3 system. In this section, the underlying concepts of thermodynamic modeling and density functional theory will be reviewed, followed by details of the calculations performed in the current work.

2.2 CALPHAD Thermodynamic Modeling

Thermodynamic modeling involves representing the thermochemical behavior of phases with numerical descriptions of the Gibbs energy as a function of temperature, pressure, and composition. The CALPHAD approach determines these functions by fitting them to data that they ought to reproduce. This can be thermochemical data for an individual phase, such as experimentally determined activities or the enthalpy of formation from first-principles calculations. Phase equilibria can also be used as they are determined by the relative quantity of a phase's Gibbs energy with respect to another's. The thermodynamic modeling of a materials system is the process of determining the parameters of the Gibbs energy functions, and the usefulness of such a thermochemical description is the ability to extrapolate and interpolate the functions into areas where there is no data and make predictions about how the system will behave.

The Gibbs energy can be separated into enthalpy and entropy terms:

$$G = H - TS \tag{2.1}$$

Above room temperature, the temperature dependent form of the Gibbs energy typically used for pure element phases and stoichiometric compounds is

$$G_m - H_m^{SER} = a + bT + cT\ln T + dT^2 + eT^3 + fT^{-1} \tag{2.2}$$

where H_m^{SER} is the molar enthalpy of the phase at 298K and 1 atm and a,b,c,d,e, and f are model parameters. This form works well in cases where there are plentiful datasets for the phase. In fact, this modeling has been performed in detail for most of the elements[9] and their phase descriptions are widely used. For cases where data may not be plentiful, such as a stoichiometric compound made up of more than one element, the Neumann-Kopp rule can be applied, where the heat capacity of the stoichiometric compound is approximated to be the sum of the heat capacities of its elements. Thus, equation 2.2 can be simplified as

$$G^{A_iB_j} = x_A{}^oG_A^{SER} + x_B{}^oG_B^{SER} + a + bT \tag{2.3}$$

where $G^{A_iB_j}$ is the molar Gibbs energy of the phase, ${}^oG_A^{SER}$ and ${}^oG_B^{SER}$ are the molar Gibbs energies of components A and B, respectively, in their stable state, and a and b are model parameters corresponding to the enthalpy and entropy of formation of the compound, respectively.

For the case of oxides, the same concepts can be applied. For example, the Gibbs energy of an ABO_3 perovskite could be expressed as

$$G^{ABO_3} = \frac{1}{2}{}^oG_{A_2O_3}^{SER} + \frac{1}{2}{}^oG_{B_2O_3}^{SER} + a + bT \tag{2.4}$$

where G^{ABO_3} is the molar Gibbs energy of the perovskite, ${}^oG_{A_2O_3}^{SER}$ and ${}^oG_{A_2O_3}^{SER}$ are the molar Gibbs energies of the component oxides in their stable state, and a and b are model parameters corresponding, in this case, to the enthalpy and entropy of formation of the perovskite from the monoxides. This formulation of the Gibbs energy for an oxide is more convenient when applying first-principles calculations to an oxide system, as will be discussed in the next section.

For solution phases, the compound energy formalism is often employed[10]. For a phase described by the mixture of A-, B-, C-, and D-type atoms in a two-sublattice model $(A,B)_i(C,D)_j$, there are four ideal "endmembers" (A_iC_j, A_iD_j, B_iC_j and B_iD_j) and the energy of the solution phase is a mixture of the energies of the endmembers. The molar Gibbs energy of the phase, G_m, is split into three portions

$$G_m = {}^oG_m + {}^{ideal}\Delta G_{mix} + {}^{xs}\Delta G_{mix} \tag{2.5}$$

where ${}^oG_m$ is the Gibbs energy due to the mechanical mixing of the endmembers in the disordered phase, ${}^{ideal}\Delta G_{mix}$ is the Gibbs energy due to the ideal mixing of A/B and C/D atoms within each sublattice and ${}^{xs}\Delta G_{mix}$ is the Gibbs energy due to interactions between the A/B and C/D atoms within each sublattice not accounted for in the other two terms. The first of the three terms is given as:

$${}^oG_m = y_A^I y_A^{II} {}^oG_{A:C} + y_A^I y_B^{II} {}^oG_{A:D} + y_B^I y_A^{II} {}^oG_{B:C} + y_B^I y_B^{II} {}^oG_{B:D} \tag{2.6}$$

where ${}^oG_{A:C}$, ${}^oG_{A:D}$, ${}^oG_{B:C}$, and ${}^oG_{B:D}$ are the Gibbs energy of each endmember,

defined by equation 2.3. The ideal mixing is defined by

$$^{ideal}\Delta G_{mix} = iRT(y_A^I \ln y_A^I + y_B^I \ln y_B^I) + jRT(y_C^{II} \ln y_C^{II} + y_D^{II} \ln y_D^{II}) \tag{2.7}$$

Lastly, the excess mixing is given as a Redlich-Kister polynomial[11]:

$$\begin{aligned} ^{xs}\Delta G_{mix} = y_A^I y_B^I \left(y_C^{II} \sum_{k=0}^{} {}^{k}L_{A,B:C}(y_A^I - y_B^I)^k + y_D^{II} \sum_{k=0}^{} {}^{k}L_{A,B:D}(y_A^I - y_B^I)^k \right) \\ + y_C^{II} y_D^{II} \left(y_A^I \sum_{k=0}^{} {}^{k}L_{A:C,D}(y_C^{II} - y_D^{II})^k + y_B^I \sum_{k=0}^{} {}^{k}L_{B:C,D}(y_C^{II} - y_D^{II})^k \right) \end{aligned} \tag{2.8}$$

where ${}^{k}L_{A,B:C}$ is the k^{th} order mixing parameter between A and B in the first sublattice when C is in the second sublattice. Such terms are used as model parameters.

For solutions where charged species occupy the sublattices and the charge of the sublattice can change, considerations need to be made to ensure that the phase remains charge neutral. For solids, this involves constraining the site occupancies of each species so as to balance the charges. For liquids, a specialized model[12] can be used where the ratio of the different sublattices (i and j in $(\text{A,B})_i(\text{C,D})_j$) changes. The principles of determining the Gibbs energy of such phases remains the same.

2.3 Density Functional Theory

Typically in the literature, phase equilibria data is more plentiful than thermochemical data for individual phases, but relying solely on phase equilibria for the modeling of a system is not sufficient to ensure an accurate model. Different functions for the Gibbs energies of the phases in a system can reproduce the same phase equilibria data as such data is determined by the relative values of the Gibbs energies of the pertinent phases, giving only a superficial understanding of the Gibbs energy of a phase. On the other hand, thermochemical data for a single phase, such as the enthalpy of formation, constrains the Gibbs energy in an absolute way, producing a more unique function. Unfortunately, the thermochemical data necessary for an accurate assessment of a system by the CALPHAD approach can

be difficult or even impossible to obtain experimentally, especially for complex, multi-component compounds.

Density functional theory can help to constrain the Gibbs energy functions by predicting thermochemical data for particular phases. From the atomic coordinates and atomic numbers of the atoms in a periodic solid, density functional theory applies the concepts of quantum mechanical electronic theory to determine the total energy of the crystalline structure. Such calculations are usually referred to as first-principles since they are performed "from the beginning" or without any experimental or empirical observations. From these total energy calculations, the relative stability of different phases can be determined, even for hypothetical phases.

The time-independent Schrödinger Equation describes the quantum mechanical behavior of particles in space at a snapshot in time by defining the wavefunction of such a system, from which the total energy can be determined. It is given as

$$\hat{H}\Psi = E\Psi \tag{2.9}$$

where $\hat{H}$ is the Hamiltonian operator, Ψ is the wavefunction, and E is the energy of the system. However, this equation is only solvable for a single particle, and the systems of interest are electrons in a crystalline solid, the quantity of which is in the order of 10^{23}. The system can be simplified by using periodic boundary conditions and calculating the simplest repeating unit (a primitive cell), but such systems still contain more than one electron.

To avoid solving an infinitely complex problem, a method was developed by which the density of electrons, $\rho(\vec{r})$, is described as opposed to the actual wavefunction [13, 14]. The assumption is that this density uniquely defines the wavefunction and, thus, determines all the properties of the system, including total energy. The total energy is a functional of this charge density (hence density functional theory)

$$E_T = E[\rho(\vec{r})] \tag{2.10}$$

and the electronic groundstate of the system is determined by minimizing E_T. The

energy of the system is considered the sum of several components:

$$E[\rho] = T_0[\rho] + V_{\text{ext}}[\rho] + V_{\text{Hartree}}[\rho] + E_{\text{xc}}[\rho] \tag{2.11}$$

where $\mathrm{T_0}$ is the kinetic energy of the electrons without interactions, $\mathrm{V_{ext}}$ is the potential energy of the ions interacting with the electrons, and $\mathrm{V_{Hartree}}$ is the Coulombic interaction between a single electron with the rest of the system. The last term, $\mathrm{E_{xc}}$, is the exchange and correlation energy which accounts for the complex interactions not included in the other three terms, such as the interactions of all the electrons in the system with each other. The exact form of this term is not known and approximations are employed, notably the local density approximation and the generalized gradient approximation.

The value of the total energy of a system is not directly applicable towards CALPHAD modeling, primarily because there is no meaningful reference state. Therefore, other systems must be calculated to provide such a reference. For instance, the enthalpy of formation of a compound (the a parameter in equation 2.3) is described in reference to the energy of its components at room temperature and pressure. Therefore, to calculate the enthalpy of formation from first-principles, the total energy of three structures are necessary. The following general relationship is followed:

$$\Delta H_f(A_iB_j) = E(A_iB_j) - x_A E(A) - x_B E(B) \tag{2.12}$$

where $\Delta H_f(A_iB_j)$ is the enthalpy of formation of the compound, $E(A_aB_b)$ is the total energy of the compound, and $E(A)$ and $E(B)$ are the total energies of the components that make up the compound. Typically, the components are the individual elements that make up the phase. However, reliably calculating the total energy of oxygen gas from first-principles is difficult as there are many contributions to the total energy of gases that are not taken into account, such as the rotational, translational, and vibrational motions of the oxygen molecule. To avoid this issue, the reference state for the Gibbs energies of the binary oxides considered in the present work are the monoxides, as detailed in the previous section. In this way, A and B in 2.12 can be considered monoxide components of a binary oxide phase $\mathrm{A}_i\mathrm{B}_j$.

A similar process is used to determine the enthalpy of mixing of Nd:YAG with $Y_3Al_5O_{12}$ and the hypothetical $Nd_3Al_5O_{12}$ taken as the reference states:

$$\Delta H^{mix}_{(Y_{1-i}Nd_i)_3Al_5O_{12}} = E((Y_{1-i}Nd_i)_3Al_5O_{12}) - iE(Nd_3Al_5O_{12}) - (1-i)E(Y_3Al_5O_{12}) \tag{2.13}$$

where $\Delta H^{mix}_{(Y_{1-i}Nd_i)_3Al_5O_{12}}$ is the enthalpy of mixing of Nd:YAG, $E((Y_{1-i}Nd_i)_3Al_5O_{12})$ is the total energy at a given composition, i, of Nd:YAG, and $E(Nd_3Al_5O_{12})$ and $E(Y_3Al_5O_{12})$ are the total energies of $Nd_3Al_5O_{12}$ and $Y_3Al_5O_{12}$, respectively. This data is used to determine the interaction parameter, L, found in the function of the excess Gibbs energy of mixing in equation 2.8.

First-principles calculations do not implicitly consider temperature-induced effects such as atomic vibrations, so such calculations are assumed to represent the system at 0K. However, the energies are still applicable to a CALPHAD modeling as it is found that enthalpies of formation do not change appreciably from 0K to room temperature. Therefore, an assumption is made that the enthalpy of formation for compounds are independent of temperature and any contributions to the Gibbs free energy that may occur due to such changes can be incorporated into the temperature-dependent entropy term. Such assumptions become necessary when simultaneously using experimental and first-principles data in a thermodynamic modeling.

2.4 Calculation Details

The CALPHAD evaluation of model parameters was performed with the PARROT module of the Thermo-Calc software. The description of the Al_2O_3-Nd_2O_3-SiO_2-Y_2O_3 system was constructed by adding Nd_2O_3 to the Al_2O_3-SiO_2-Y_2O_3 system[7]. To do so, the Al_2O_3-Nd_2O_3, Nd_2O_3-SiO_2, and Nd_2O_3-Y_2O_3 system must be modeled first and then combined with the Al_2O_3-SiO_2-Y_2O_3 system. For the sake of simplicity, the only phase considered to be capable of non-stoichiometry is Nd:YAG, the behavior of which was determined by first-principles calculations. In this way, the phase equilibria in the Al_2O_3-Nd_2O_3-SiO_2-Y_2O_3 system can be extrapolated as there are no reported ternary or quaternary oxide compounds.

All first-principles calculations were performed within density functional theory

as implemented within the Vienna *Ab-initio* Simulation Package(VASP)[15]. The projector augmented wave pseudopotentials were used. The exchange and correlation energy was approximated using the generalized gradient method. The k-point matrices were constructed to obtain a density of k-points of approximately 5,000 per atom in reciprocal space. Convergence of the the total energy and volume was tested for and achieved with this value. The cutoff energy for the planewave basis set was set at 520 eV, as determined by the oxygen pseudopotential. Likewise, it was found that the total energy and volume of the structures were sufficiently converged with this value. All degrees of freedom of the crystal structures were fully relaxed to determine the minimum energy. The atomic coordinates and lattice vectors of all the structures discussed in the thesis can be found in Appendix B.

2.5 Conclusion

When coupled with DFT-based first-principles calculations, CALPHAD thermodynamic modeling is a method by which to study the behavior of a materials system that may be difficult or even impossible to do experimentally. By describing the Gibbs energy of individual phases numerically and determining model parameters by fitting experimental and first-principles data, a description of a system is constructed with which properties can be predicted as a function of temperature, pressure, and composition. In the thesis, this approach is used to construct a model of the Al_2O_3-Nd_2O_3-SiO_2-Y_2O_3 system.

Chapter 3

Thermodynamic Modeling of the Al_2O_3-Nd_2O_3 System

3.1 Introduction

The Al_2O_3-Nd_2O_3 system contains three compounds: $NdAl_{11}O_{18}$ (β-Al_2O_3), the perovskite $NdAlO_3$ which is found to melt congruently, and $Nd_4Al_2O_9$, the stability of which is a matter of debate. Experimental and first-principles derived data are used to determine the parameters of the Gibbs energy equations for the phases in the system. The first section of this chapter offers a review of the available experimental data and of previous modelings of the system. Next, the results of the first-principles calculations are given, followed by the details of the present modeling and the parameters of the phase descriptions.

3.2 Literature Review

A summary of the phase equilibria of the Al_2O_3-Nd_2O_3 system from both experiment and calculations is found in Table 3.1. The three experimental investigations of the phase diagram differ in the number of phases present in the system and the temperatures of the invariant reactions. The equilibria reported by Coutures[16] containing three binary oxide compounds ($NdAl_{11}O_{18}$, $NdAlO_3$ and $Nd_4Al_2O_9$) are accepted in the present work. The phase diagram by Toropov and Kiseleva[17]

Table 3.1. Invariant equilibria in the Al_2O_3-Nd_2O_3 system.

Reaction	Type	T(K)	Liquid at.%Nd_2O_3	Reference
Al_2O_3+Liquid ↔ $NdAl_{11}O_{18}$	Peritectic	2165	10.25	This Work
		2068	∼18.00	Exp.[18]
		2173	10.00	Exp.[16]
		2070	19.00	CALPHAD[21]
		∼2162	∼14.00	CALPHAD[22]
		2078	19.08	CALPHAD[23]
Liquid ↔ $NdAl_{11}O_{18}$+$NdAlO_3$	Eutectic	2027	23.65	This Work
		1993	23.00	Exp.[18]
		2023	20.00	Exp.[16]
		1986	25.00	CALPHAD[21]
		∼2019	∼23.00	CALPHAD[22]
		2070	20.00	CALPHAD[23]
Liquid ↔ $NdAlO_3$	Congruent	2368	50.00	This Work
		2343	50.00	Exp.[17]
		2438	50.00	Exp.[18]
		2363	50.00	Exp.[16]
		2373	50.00	CALPHAD[21]
		∼2367	50.00	CALPHAD[22]
		2348	50.00	CALPHAD[23]
$Nd_4Al_2O_9$ ↔ $NdAlO_3$+Liquid	Peritectic	2175	68.00	This Work
		2178	69.00	Exp.[16]
		2178	∼70.00	CALPHAD[21]
		∼2146	∼76.00	CALPHAD[22]
Liquid ↔ $Nd_4Al_2O_9$+Nd_2O_3	Eutectic	2076	79.73	This Work
		2073	77.50	Exp.[16]
		2126	78.00	CALPHAD[21]
		∼2066	∼82.00	CALPHAD[22]

contains only $NdAlO_3$. Mizuno et al.[18] reports two compounds, $NdAl_{11}O_{18}$ and $NdAlO_3$, and the invariant equilibria differ greatly from the other two authors. However, the reported liquidus qualitatively agrees with Coutures[16].

Experimental thermochemical data of this system is limited to calorimetry of the $NdAlO_3$ perovskite by Kanke and Navrotsky[19] and Zhang and Navrotsky[20]. They report an enthalpy of formation from the oxides of -41.36 and -52.9 kJ/mol-form, respectively. The difference between the two experimental values may be due to how Zhang and Navrotsky[20] determined the enthalpy of formation from differences in enthalpies of vitrification, the uncertainties of which may have accumulated into a large error for the enthalpy of formation. Kanke and Navrotsky[19], on the other hand, performed a direct measurement of the enthalpy of formation.

There have been several modelings of the Al_2O_3-Nd_2O_3 system, some of them before the $NdAlO_3$ thermochemical data had been reported, forcing those modelings to be based entirely from phase equilibria data. The error from such an approach can be seen in the first two modelings of the system, by Wu and Pelton[21] and Li et al.[22], where the predicted enthalpies of formation differ greatly from experiment and the first-principles calculations detailed in the next section, as shown in Table 3.3. A more recent modeling by Fabrichnaya and Seifert[23] incorporates the experimental enthalpy of formation into their evaluation of the system. However, the enthalpy of formation reported by Zhang and Navrotsky[20] was accepted, which disagrees with the first-principles prediction. In addition, the authors did not consider the $Nd_4Al_2O_9$ phase stable, again in disagreement with first-principles calculations. Therefore, a remodeling of the Al_2O_3-Nd_2O_3 system is necessary to resolve discrepancies between the results from the first-principles calculations and the previous modelings concerning the enthalpies of formation and the stability of $Nd_4Al_2O_9$. In addition, the Al_2O_3-Nd_2O_3 system must be made consistent with the previously modeled Al_2O_3-SiO_2-Y_2O_3 system by using the same description of the Al_2O_3 phases and an ionic model for the liquid.

3.3 First-Principles Calculations

As thermochemical data only exists for one compound in the system, first-principles calculations will be necessary to accurately constrain the descriptions of the three phases. However, the enthalpies of formation for only two of them, $NdAlO_3$ and $Nd_4Al_2O_9$, were examined with first-principles calculations. The crystal structure of the third one, $NdAl_{11}O_{18}$, contains partial occupancy of neodymium and aluminum sites to produce the stoichiometry of 1:11[24], which made a first-principles study of the energetics of the phase prohibitively complex.

Thus, four structures are examined with first-principles: $NdAlO_3$, $Nd_4Al_2O_9$ and their oxide reference states (Corundum and Nd_2O_3-A). The predicted crystal structures are compared to experiments in Table 3.2. Such a comparison provides a check to ensure the validity of the calculations. The errors are fairly small, on the order of 1%, which is typical for DFT-based calculations. As the crystal structures are fairly accurate, it is assumed the total energies are as well. From

these energies, as detailed in Chapter 2, the enthalpies of formation for $NdAlO_3$ and $Nd_4Al_2O_9$ are predicted and shown in Table 3.3. The prediction for $NdAlO_3$ agrees well with the experimental value from Kanke and Navrotsky[19], suggesting that the determination by Zhang and Navrotsky[20] may have been inaccurate.

With the enthalpies of formation for $Nd_4Al_2O_9$ and its neighboring phase, $NdAlO_3$, calculated from first-principles, the low-temperature stability of $Nd_4Al_2O_9$ can be predicted. This is significant as there is contradictory evidence for the stability of the $Nd_4Al_2O_9$ phase in the literature, where one study was unable to synthesize the compound[27] whereas others could[16, 28]. Consequently, previous modelings of the system have treated this phase differently. Wu and Pelton[21] has the phase as a stable compound at low temperatures, Li et al.[22] reproduces Couture's metastable behavior of the phase and the assessment by Fabrichnaya and Seifert[23] does not include the phase at all. From the current first-principles calculation, the predicted enthalpy of formation of $Nd_4Al_2O_9$ is about 1.5 kJ/mol-atom less than the enthalpy of formation of an ideal solution of $NdAlO_3$ and pure Nd_2O_3, illustrated in Figure 3.1. As the temperature of first-principles calculations are taken to be 0K, this result suggests that $Nd_4Al_2O_9$ is stable at low temperatures, which is how the phase is treated in the current modeling.

3.4 Thermodynamic Modeling

With the information from the first-principles calculations, the Al_2O_3-Nd_2O_3 system can be sufficiently constrained to determine the Gibbs energy functions of the phases in the system. All three oxide phases ($NdAl_{11}O_{18}$, $NdAlO_3$ and $Nd_4Al_2O_9$)

Table 3.2. Crystal structures of the compounds in the Al_2O_3-Nd_2O_3 system. Percent difference between calculated and experimental values are given.

Phase	Space	Lattice Parameters (Å)						$\beta(^\circ)$	Error	Source
	Group	a	Error	b	Error	c	Error			
Al_2O_3	$R\bar{3}c$	4.803	0.8%	4.803	0.8%	13.107	0.8%			DFT
(Corundum)		4.763		4.763		13.003				Exp[25]
Nd_2O_3-A	$P\bar{3}m1$	3.860	0.8%	3.860	0.8%	6.079	1.5%			DFT
		3.831		3.831		5.991				Exp[25]
$NdAlO_3$	$R\bar{3}c$	5.376	1.1%	5.376	1.1%	12.991	0.6%			DFT
		5.32		5.32		12.916				Exp[26]
$Nd_4Al_2O_9$	$P2_1/c$	7.787	1.7%	10.943	0.8%	11.463	1.4%	109.336	0.1%	DFT
		7.740		10.854		11.308		109.450		Exp[27]

are treated as stoichiometric compounds for the sake of simplicity. Like many other sesquioxides, Nd_2O_3 exhibits polymorphism, with three temperature-dependent polymorphs at ambient pressure, Nd_2O_3-A, Nd_2O_3-H, and Nd_2O_3-X. The description for these phases are accepted from a previous modeling of the Nd_2O_3-Y_2O_3 system by Huang et al.[29]. The Al_2O_3 phase, corundum, is accepted from the assessment of the Al_2O_3-SiO_2-Y_2O_3 system[7]. The following ionic model is used for the liquid phase:

$$(Nd^{+3})_p(O^{-2}, AlO_{3/2})_q$$

Nd^{+3} in the first sublattice describes the contribution of Nd_2O_3 to the liquid and $AlO_{3/2}$ in the second sublattice for Al_2O_3, which is retained from the previous modeling of the Al_2O_3-SiO_2-Y_2O_3 system[7] for consistency. The descriptions for the Al_2O_3 and Nd_2O_3 liquid phases are taken from the previous modelings[7, 29].

The parameters of the Gibbs energies of $NdAl_{11}O_{18}$, $NdAlO_3$, $Nd_4Al_2O_9$, and liquid were evaluated using the liquidus data and invariant reactions from Coutures

Table 3.3. Enthalpies of formation of the compounds in the Al_2O_3-Nd_2O_3 system.

Phase	ΔH_f (kJ/mol-form)	Method	Reference
$NdAl_{11}O_{18}$	-71.876	CALPHAD	This Work
	86.5335	CALPHAD	[21]
	-522.461	CALPHAD	[22]
	-59.000	CALPHAD	[23]
$NdAlO_3$	-41.100	First-Principles	This Work
	-41.197	CALPHAD	This Work
	-31.937	CALPHAD	[21]
	-150.520	CALPHAD	[22]
	-41.36±3.44	Experiment	[19]
	-52.9±1.7	Experiment	[20]
	-51.705	CALPHAD	[23]
$Nd_4Al_2O_9$	-104.522	First-Principles	This Work
	-104.334	CALPHAD	This Work
	-188.33	CALPHAD	[21]
	188.619	CALPHAD	[22]

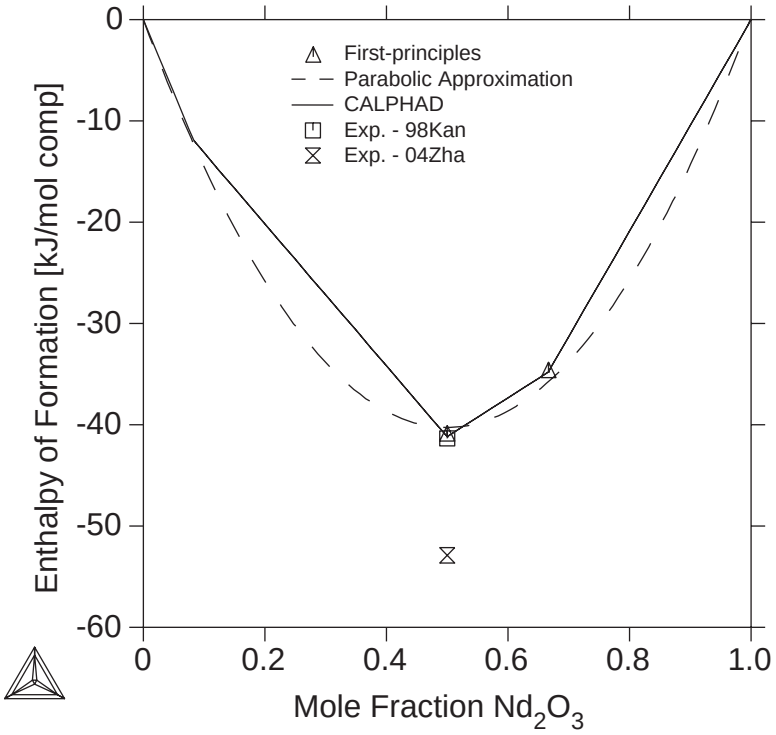

Figure 3.1. Enthalpies of formation for compounds in the Al_2O_3-Nd_2O_3 system at 298K. First-principles results are in triangles and the dashed line is the parabolic approximation. Experimental data from Kanke and Navrotsky[19] and Zhang and Navrotsky[20] also included.

[16] and the enthalpies of formation derived from first-principles calculations. The starting value for the enthalpy of formation of $NdAl_{11}O_{18}$ was estimated by fitting a parabola to the two calculated compounds, as illustrated in Figure 3.1, which has been shown to be an effective method of estimation for many binary oxides[30]. It is argued that such an approximation is applicable to systems that exhibit symmetry about the 50-50% composition (in terms of the distribution of stable compounds and magnitudes of their melting points) as the stability of the system is not skewed in either direction. For the case of $NdAl_{11}O_{18}$, the phases of the Al-Nd and Al_2O_3-Nd_2O_3 systems are evenly distributed at various compositions and the liquidus for the Al_2O_3-Nd_2O_3 system is fairly symmetric about $NdAlO_3$, which has the highest melting point. Therefore, a parabola is assumed to be an acceptable approximation for the behavior of the enthalpies of formation in the Al_2O_3-Nd_2O_3 system. Furthermore, the fit of the parabola onto the four data points (Al_2O_3,

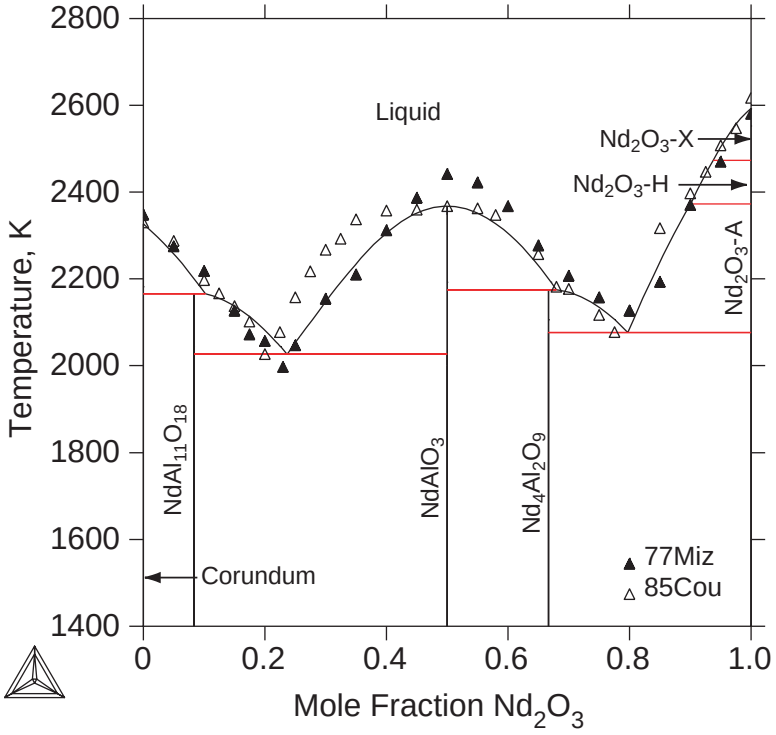

Figure 3.2. Calculated Al_2O_3-Nd_2O_3 phase diagram with experimental liquidus data from Mizuno et al.[18] and Coutures[16].

Nd_2O_3, $NdAlO_3$, and $Nd_4Al_2O_9$) has an R^2 value of 0.999, suggesting the known enthalpies of formation are behaving symmetrically.

The evaluated phase descriptions are listed in Table 3.4. The resulting phase diagram, Figure 3.2, shows partial agreement with the data from Coutures[16] as the liquidus near the perovskite exhibits a particularly flat shape that is not reproduced in the modeling. Thus, the phase diagram has been reproduced with Gibbs energy functions that are constrained by results from the first-principles calculations.

3.5 Conclusion

As the Al_2O_3-Nd_2O_3 system is an essential component to the Al_2O_3-Nd_2O_3-SiO_2-Y_2O_3 system, it has been modeled via the CALPHAD method, including the

Table 3.4. Phase descriptions for the Al_2O_3-Nd_2O_3 system. The values of $G^{Nd_2O_3}$, $G^{Al_2O_3}$ and the function GAL2O3L can be found in the Appendix.

Phase	Sublattice Model	Phase Description
$NdAl_{11}O_{18}$	$(Nd^{+3})(Al^{+3})_{11}(O^{-2})_{18}$	${}^0G^{NdAl_{11}O_{18}}_{Nd^{+3}:Al^{+3}:O^{-2}}$=0.5$G^{Nd_2O_3}$+5.5$G^{Al_2O_3}$-71876-58.807T
$NdAlO_3$	$(Nd^{+3})(Al^{+3})(O^{-2})_3$	${}^0G^{NdAlO_3}_{Nd^{+3}:Al^{+3}:O^{-2}}$=0.5$G^{Nd_2O_3}$+0.5$G^{Al_2O_3}$-41197-45.843T
$Nd_4Al_2O_9$	$(Nd^{+3})_4(Al^{+3})_2(O^{-2})_9$	${}^0G^{Nd_4Al_2O_9}_{Nd^{+3}:Al^{+3}:O^{-2}}$=2$G^{Nd_2O_3}$+$G^{Al_2O_3}$-104334-100.571*T
Ionic Liquid	$(Nd^{+3})_p(O^{-2},AlO_{3/2})_q$	${}^0G^{\text{Ionic Liquid}}_{Nd^{+3}:O^{-2}}$=143621-56.785T+$G^{Nd_2O_3}$
		${}^0G^{\text{Ionic Liquid}}_{AlO_{3/2}}$=0.5GAL2O3L
		${}^0L^{\text{Ionic Liquid}}_{Nd^{+3}:O^{-2},AlO_{3/2}}$=291926-364.060T
		${}^1L^{\text{Ionic Liquid}}_{Nd^{+3}:O^{-2},AlO_{3/2}}$=-154645

$NdAl_{11}O_{18}$, $NdAlO_3$, and $Nd_4Al_2O_9$ compounds. By calculating the enthalpies of formation for the compounds by first-principles, $Nd_4Al_2O_9$ was found to be stable below room temperature. An ionic model was used for the liquid phase. The parameters of the Gibbs energy functions were determined by utilizing the published experimental data for the phase equilibria and first-principles calculations of the enthalpies of formation of the compounds. A parabolic approximation was applied to determine the enthalpy of formation of $NdAl_{11}O_{18}$. The evaluated parameters accurately describe the thermochemical data and phase equilibria of the system.

Chapter 4

Thermodynamic Modeling of the Nd_2O_3-SiO_2 System

4.1 Introduction

Although a minute amount of SiO_2 is added when sintering Nd:YAG, the phase equilibria in the Nd_2O_3-SiO_2 system will influence this process. Therefore, the modeling of the Nd_2O_3-SiO_2 system is necessary. There are three phases found in the system: Nd_2SiO_5, $Nd_{14}Si_9O_{39}$, and $Nd_2Si_2O_7$, the latter of which is metastable at low temperatures. As there are no experimental thermochemical data for these phases, first-principles calculations will be necessary in guiding the modeling of the system. The chapter begins with a review of the pertinent literature, including experimental phase equilibria and a previous modeling. Next, the results of the first-principles calculations are presented. Lastly, the thermodynamic modeling is discussed and the assessed parameters are given.

Table 4.1. Invariant equilibria in the Nd_2O_3-SiO_2 system.

Reaction	Type	T(K)	Liquid at.%SiO_2	Method
Liquid ↔ Nd_2O_3+Nd_2SiO_5	Eutectic	1956	36.24	This Work
		1953	∼33.00	Exp.[31]
		1948	∼35.00	Exp.[32]
		∼1953	∼33.00	CALPHAD[22]
		∼1930	∼35.00	Exp.[33]
Liquid+$Nd_{14}Si_9O_{39}$ ↔ Nd_2SiO_5	Peritectic	1990	38.40	This Work
		∼1980	∼36.00	Exp.[33]
Liquid ↔ $Nd_{14}Si_9O_{39}$	Congruent	2223	56.25	This Work
		2233	60.00	Exp.[31]
		2223	60.00	Exp.[32]
		∼2222	∼60.00	CALPHAD[22]
		2193	56.25	Exp.[33]
$Nd_{14}Si_9O_{39}$+Liquid ↔ $Nd_2Si_2O_7$	Peritectic	1965	74.54	This Work
		2023	∼68.00	Exp.[31]
		1953	∼70.00	Exp.[32]
		∼2021	∼67.00	CALPHAD[22]
		∼1940	∼69.00	Exp.[33]
$Nd_2Si_2O_7$ ↔ $Nd_{14}Si_9O_{39}$+SiO_2	Eutectoid	1815		This Work
		1813		Exp.[32]
Liquid ↔ $Nd_2Si_2O_7$+SiO_2	Eutectic	1908	77.14	This Work
		1873	72.00	Exp.[31]
		1908	∼74.00	Exp.[32]
		∼1881	∼71.00	CALPHAD[22]
		∼1896	∼72.00	Exp.[33]
Liquid ↔ Liquid2[a]+SiO_2	Eutectic	1978	78.24, 99.82	This Work
		1933	∼74.00,∼98.00	Exp.[31]
		∼1973	∼79.00,∼98.00	Exp.[32]
		∼1950	∼75.00,∼98.00	CALPHAD[22]

[a] The second liquid composition in the miscibility gap.

4.2 Literature Review

The invariant phase equilibria for the Nd_2O_3-SiO_2 system reported in the literature are summarized in Table 4.1. All three experimental investigations[31–33] report three binary oxide compounds. Nd_2SiO_5 was reported by Toropov[31] and Miller and Rase[32] to melt congruently. This led to a peculiar phase diagram as another phase, $Nd_4Si_3O_{12}$, was also found to melt congruently, producing a eutectic in the center of the system. A reexamination of the phase equilibria by Masubuchi et al.[33] found that Nd_2SiO_5 melts incongruently, and a new phase

diagram was reported. Masubuchi et al.[33] also found that the composition of the second phase reported by Toropov[31] and Miller and Rase[32], $Nd_4Si_3O_{12}$, is actually much closer to $Nd_{9.33}(SiO_4)_6O_2$ (herein referred to stoichiometrically as $Nd_{14}Si_9O_{39}$). Although the third phase, $Nd_2Si_2O_7$, was reported by all three authors, only Miller and Rase[32] claim this phase is metastable at low temperatures since this was the the only investigation to examine the low temperature equilibria. The invariant equilibria reported by Miller and Rase[32] and Toropov[31] are accepted as Masubuchi et al.[33] do not report specific temperatures.

However, the shape of the liquidus from Masubuchi et al.[33] is what was reproduced by the modeling. Data concerning the liquidus is lacking as the compositions of the liquid phase reported by Miller and Rase[32] and Toropov[31] were not determined with great accuracy. However, it was confirmed by both investigations that a miscibility gap forms in the liquid phase in the SiO_2-rich side of the phase diagram, although no specific data was provided.

As there is no experimental thermochemical data in the literature, only one modeling has been performed on the Nd_2O_3-SiO_2 system, by Li et al.[22], where phase equilibria is the only data used to determine the Gibbs energy functions. As discussed in the previous chapter, such an approach can produce functions that have correct values relative to one another but with absolute values that are inaccurate. In the case of the modeling by Li et al.[22], positive enthalpies of formation are reported for the three compounds, stabilized by entropies of formation. This is unlikely as it suggests that all the phases are not stable at low temperatures, which is in disagreement with the first-principles calculations detailed in the next section. For this reason, the parameters of the Gibbs energies are reevaluated.

4.3 First-Principles Calculations

As there is no experimental thermochemical data for Nd_2O_3-SiO_2 system, first-principles calculations are necessary to adequately constrain the system and determine the Gibbs energy functions. However, of the three compounds, only Nd_2SiO_5 was calculated. The $Nd_{14}Si_9O_{39}$ phase contains vacancies in two neodymium crystallographic sites[34] which makes it prohibitively complex for first-principles calculations. Calculations of the $Nd_2Si_2O_7$ phase were not included in the assessment

as there is ambiguity as to its true crystal structure in the stable temperature range[35]. Table 4.2 summarizes the crystallographic results of the first-principles calculations for the two reference state structures, Nd_2O_3 and SiO_2, and Nd_2SiO_5, showing good agreement between the calculated and experimentally determined lattice parameters. The enthalpy of formation predicted for Nd_2SiO_5 by first-principles calculations is -139.665 kJ/mol-form.

Table 4.2. Crystal structures of the phases in the Nd_2O_3-SiO_2 system. Percent difference between calculated and experimental values are given.

Phase	Space	Lattice Parameters (Å)						$\beta(^\circ)$	Error	Source
	Group	a	Error	b	Error	c	Error			
Nd_2O_3-A	$P\bar{3}m1$	3.860	0.8%	3.860	0.8%	6.079	1.5%			This Work
		3.831		3.831		5.991				Exp[25]
SiO_2	$P3_21$	4.992	1.6%	4.992	1.6%	5.484	1.5%			This Work
		4.913		4.913		5.405				Exp[25]
Nd_2SiO_5	$P2_1/c$	9.350	1.1%	7.279	0.3%	6.962	0.5%	107.812	0.5%	This Work
		9.250		7.258		6.886		108.3		Exp[36]

Although this value is specific only to the Nd_2SiO_5 phase, it can be used to determine the upper and lower limits of the enthalpy of formation of $Nd_{14}Si_9O_{39}$. The the enthalpy of formation for the compounds are plotted in Figure 4.1. For $Nd_{14}Si_9O_{39}$ to be stable at room temperature, its enthalpy of formation must be more negative than the mixture of pure SiO_2 and Nd_2SiO_5 (a straight line connecting these values). Similarly, $Nd_{14}Si_9O_{39}$ must be less negative than the mixture of pure Nd_2O_3 and Nd_2SiO_5 to ensure that Nd_2SiO_5 is stable at room temperature. With these limits, we can constrain the enthalpy of formation of $Nd_{14}Si_9O_{39}$ within a small range. Furthermore,the enthalpy of formation for $Nd_2Si_2O_7$ must be more positive than the mixture of $Nd_{14}Si_9O_{39}$ and SiO_2 to be meta-stable at low temperatures. Thus, a single known value of enthalpy of formation in a system containing multiple compounds, such as Nd_2O_3-SiO_2, can be used to constrain the values of all the phases in the system.

4.4 Thermodynamic Modeling

The thermodynamic modeling of the Nd_2O_3-SiO_2 system was performed by treating all compounds as stoichiometric phases for simplicity. For consistency, the

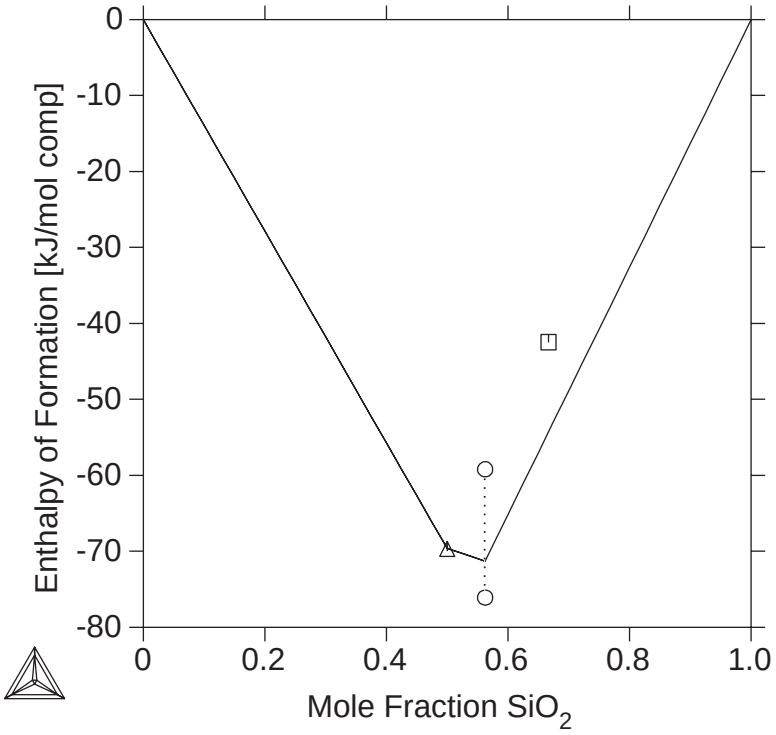

Figure 4.1. Enthalpies of formation for the Nd_2O_3-SiO_2 system at 298K. The triangle corresponds to the first-principles result for Nd_2SiO_5, the square is the CALPHAD predicted value for $Nd_2Si_2O_7$, the circles and dotted line is the range the value for $Nd_{14}Si_9O_{39}$ can take so that both $Nd_{14}Si_9O_{39}$ and Nd_2SiO_5 are stable, and the solid line is the result of the modeling.

descriptions of the SiO_2 phases (tridymite, cristobalite, and quartz) are accepted from the modeling of the Al_2O_3-SiO_2-Y_2O_3 system[7] and the Nd_2O_3 phases from the Nd_2O_3-Y_2O_3[29] system. The following ionic liquid model was used:

$$(Nd^{+3})_p(O^{-2}, SiO_4^{-4}, SiO_2)_q$$

SiO_4^{-4} and SiO_2 are used to describe liquid SiO_2 to remain consistent with the Al_2O_3-SiO_2-Y_2O_3 system[7]. The liquid phase descriptions for Nd_2O_3 and SiO_2 were accepted from the previous modelings. A miscibility gap was modeled, although none of the investigations into the system reported the shape of the gap. To reproduce the miscibility gap, it was assumed that the Nd^{+3}:SiO_4^{-4},SiO_2 species interaction in the ionic liquid is similar to that of Y^{+3}:SiO_4^{-4},SiO_2 in the SiO_2-Y_2O_3

system, as reported in the modeling of the Al_2O_3-SiO_2-Y_2O_3 system[7]. This assumption was made as Nd and Y form solid solutions in the binary system[37] and pseudo-binary oxide system[29], suggesting that Nd and Y are similar thermochemically.

The eutectic temperatures reported by Miller and Rase[32], the liquidus shape reported by Masubuchi et al.[33], and the calculated enthalpy of formation of Nd_2SiO_5 were used to evaluate the parameters of the Gibbs energy. The parabolic estimation made in the Al_2O_3-Nd_2O_3 system has not been applied here to the $Nd_{14}Si_9O_{39}$ phase as the system is asymmetric in regards to the melting points of the phases and there is not enough data to ensure that the enthalpies of formation would fit a parabola. Instead, the enthalpies of formation of the other two compounds were restrained in the approach described in the previous section, the results of which are shown in Table 4.3. The phase descriptions of the system are summarized in Table 4.4.

Table 4.3. Enthalpies of formation for the Nd_2O_3-SiO_2 system.

Phase	ΔH_f (kJ/mol form)	Method	Source
Nd_2SiO_5	-139.665	DFT	This Work
	-139.229	CALPHAD	This Work
	106.569	CALPHAD	[22]
$Nd_{14}Si_9O_{39}$	-1140.666	CALPHAD	This Work
	1066.774	CALPHAD	[22]
$Nd_2Si_2O_7$	-127.444	CALPHAD	This Work
	188.620	CALPHAD	[22]

Good agreement is found in the calculated phase diagram in comparison with experimental data, as shown in Figure 4.2. However, more detailed data of the phase equilibria, particularly for the liquidus and miscibility gap, is necessary to improve the quality of the modeling as the uncertainty in the existing experimental data is large. For instance, deviations in the compositions of the two eutectics is acceptable as Miller and Rase[32] do not claim specific compositions.

Table 4.4. Phase descriptions for the Nd_2O_3-SiO_2 system. The values of $G^{Nd_2O_3}$, G^{SiO_2} and the function GSIO2LIQ can be found in the Appendix.

Phase	Model	Phase Description
Nd_2SiO_5	$(Nd^{+3})_2(Si^{+4})(O^{-2})_5$	${}^0G^{Nd_2SiO_5}_{Nd^{+3}:Si^{+4}:O^{-2}}$=$G^{Nd_2O_3}$+$G^{SiO_2}$-139229+6.855T
$Nd_{14}Si_9O_{39}$	$(Nd^{+3})_{14}(Si^{+4})_9(O^{-2})_{39}$	${}^0G^{Nd_{14}Si_9O_{39}}_{Nd^{+3}:Si^{+4}:O^{-2}}$=7$G^{Nd_2O_3}$+9$G^{SiO_2}$-1140666+10.882T
$Nd_2Si_2O_7$	$(Nd^{+3})_2(Si^{+4})_2(O^{-2})_7$	${}^0G^{Nd_2Si_2O_7}_{Nd^{+3}:Si^{+4}:O^{-2}}$=$G^{Nd_2O_3}$+2$G^{SiO_2}$-127444-18.429T
Ionic Liquid	$(Nd^{+3})_p(O^{-2},SiO_4{}^{-4},SiO_2)_q$	${}^0G^{\text{Ionic Liquid}}_{Nd^{+3}:O^{-2}}$=143621-56.785T+$G^{Nd_2O_3}$
		${}^0G^{\text{Ionic Liquid}}_{Nd^{+3}:SiO_4^{-4}}$=2${}^0G^{\text{Ionic Liquid}}_{Nd^{+3}:O^{-2}}$+3GSIO2LIQ-171104+103.632T
		${}^0G^{\text{Ionic Liquid}}_{SiO_2}$=GSIO2LIQ
		${}^0L^{\text{Ionic Liquid}}_{Nd^{+3}:O^{-2},SiO_2}$=-356871+52.132T
		${}^1L^{\text{Ionic Liquid}}_{Nd^{+3}:O^{-2},SiO_2}$=-768443+225.508T
		${}^0L^{\text{Ionic Liquid}}_{Nd^{+3}:SiO_4^{-4},SiO_2}$=2${}^0L^{\text{Ionic Liquid}}_{Nd^{+3}:O^{-2},SiO_2}$
		${}^1L^{\text{Ionic Liquid}}_{Nd^{+3}:SiO_4^{-4},SiO_2}$=2${}^1L^{\text{Ionic Liquid}}_{Nd^{+3}:O^{-2},SiO_2}$
		${}^0L^{\text{Ionic Liquid}}_{Nd^{+3}:O^{-2},SiO_4^{-4}}$=731822-573.973T

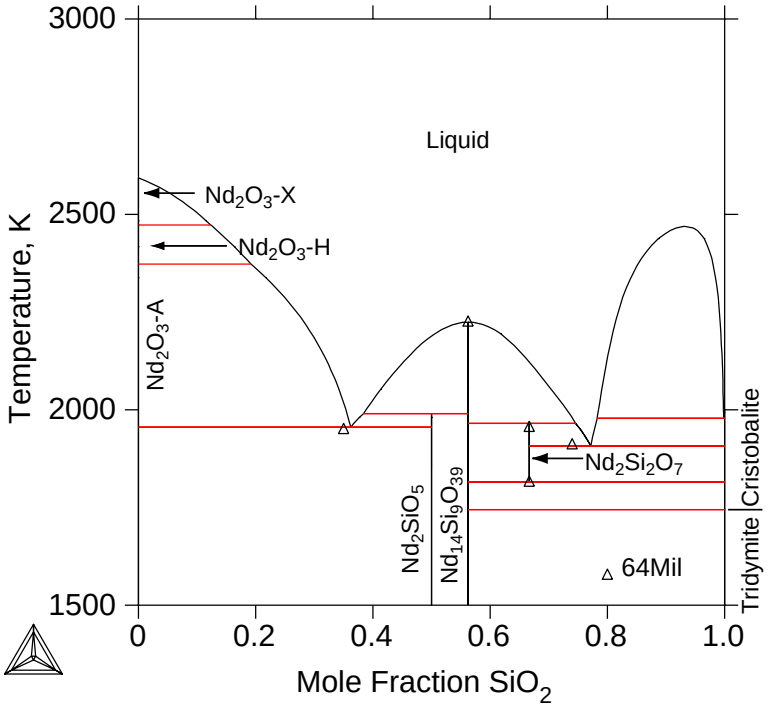

Figure 4.2. Nd_2O_3-SiO_2 phase diagram with experimental invariant equilibria data from Miller and Rase[32].

4.5 Conclusion

By way of the CALPHAD approach, the Nd_2O_3-SiO_2 system has been modeled. Experimental investigations disagree as to the shape of the liquidus but agree on the presence of three binary compounds: Nd_2SiO_5, $Nd_{14}Si_9O_{39}$, and $Nd_2Si_2O_7$. With no experimental thermochemical data, the first-principles enthalpy of formation for Nd_2SiO_5 was necessary to constrain the system and estimate the ranges of the enthalpies of formation for $Nd_{14}Si_9O_{39}$ and $Nd_2Si_2O_7$. The experimental data is accurately reproduced by the current phase descriptions, but more information is needed to improve the quality of model, such as an experimental determination of the stability limits of the liquid miscibility gap.

Chapter 5

Thermodynamic Modeling of the Nd_2O_3-Y_2O_3 System

5.1 Introduction

Unlike the two pseudo-binary systems studied in the previous chapters, the Nd_2O_3-Y_2O_3 system is composed entirely of solid solutions which are polymorphs of the sesquioxide structure shared by Nd_2O_3 and Y_2O_3. The phase equilibria has been studied by several authors, cumulating in a modeling by Huang et al.[29]. This modeling is accepted in the present work and modified for compatibility with the other systems to assemble the Al_2O_3-Nd_2O_3-SiO_2-Y_2O_3 system. The chapter begins with a review of the available experimental data in the literature. This is followed by details of the re-modeling of the system and the parameters of the Gibbs energy functions.

5.2 Literature Review

Experimental data for the Nd_2O_3-Y_2O_3 system in the literature is exclusively phase equilibria. The system has been studied by three groups. Coutures et al.[38], Tikhonov et al.[39], and Adylov et al.[40] found it comprised of five sesquioxide solid solutions: X, H, A, B, and C polymorphs. They generally agree on the high-temperature phase equilibria, except Tikhonov et al.[39] reports a significantly

lower liquidus. Furthermore, they disagree on the specific shape of the B+C two-phase region, which may be attributed to slow kinetics at low temperatures.

No accurate thermochemical data, such as the enthalpy of mixing, is reported in the literature. However, as the available experimental phase equilibria are plentiful and the solid solutions share the accurately modeled Nd_2O_3 and Y_2O_3 phases, a modeling using exclusively phase equilibria can adequately predict the Gibbs energies. Huang et al.[29] performed a thermodynamic modeling of the system, utilizing their own experimental data and that from the literature, accurately reproducing the experiments. A second modeling by Zinkevich[41] is featured in a reevaluation of the thermodynamic functions of the rare-earth sesquioxides. In that work, the liquid was treated as an ideal solution and the solid phases as regular solutions. However, the goal of that work was to test the reliability of the parameters of the sesquioxides and not to reliably model the system. Therefore, the assessed parameters by Huang et al.[29] are preferred.

5.3 Thermodynamic Modeling

Although the modeling of the Nd_2O_3-Y_2O_3 system by Huang et al.[29] is accepted in the present work, it must be modified to be consistent with the other phases in the proposed pseudo-quaternary system. Specifically, the associative models for the solid and liquid phases must be replaced by ionic models and the Y_2O_3 phase descriptions need to be replaced with those from Al_2O_3-SiO_2-Y_2O_3 system of Fabrichnaya et al.[7]. The system is essentially remodeled, using the parameters determined by Huang et al.[29] as starting values in the evaluation. The experimental phase equilibria reported by Coutures et al.[38], Adylov et al.[40], and Huang et al.[29] are used in the evaluation of the parameters. The resulting phase descriptions are given in Table 5.1.

Good agreement is found with most of the phase equilibria in the calculated phase diagram, shown in Figure 5.1, except for the boundaries of the Nd_2O_3-B/Y_2O_3-R two phase field as the behavior of this region varies amongst the experimental investigations. An accurate determination of the phase equilibria in this area is necessary to further improve the accuracy of the modeling. Furthermore, the lack of experimental thermochemical data, while not as critical as for the other

Table 5.1. Phase descriptions for the Nd_2O_3-Y_2O_3 system. The values of $G^{Nd_2O_3}$, $G^{Y_2O_3}$ and the functions GY2O3H and GY2O3LIQ can be found in the Appendix.

Phase	Model	Phase Description
Nd_2O_3-X	$(Nd^{+3},Y^{+3})_2(O^{-2})_3$	${}^0G^{Nd_2O_3-X}_{Nd^{+3}:O^{-2}}=G^{Nd_2O_3}$+44489-18.555T
		${}^0G^{Nd_2O_3-X}_{Y^{+3}:O^{-2}}=G^{Y_2O_3}$+55220-20T
		${}^0L^{Nd_2O_3-X}_{Nd^{+3},Y^{+3}:O^{-2}}$=120129-53.29T
Nd_2O_3-A	$(Nd^{+3},Y^{+3})_2(O^{-2})_3$	${}^0G^{Nd_2O_3-A}_{Nd^{+3}:O^{-2}}=G^{Nd_2O_3}$
		${}^0G^{Nd_2O_3-A}_{Y^{+3}:O^{-2}}=G^{Y_2O_3}$+74728
		${}^0L^{Nd_2O_3-A}_{Nd^{+3},Y^{+3}:O^{-2}}$=-185399+26.790T
		${}^1L^{Nd_2O_3-A}_{Nd^{+3},Y^{+3}:O^{-2}}$=67934
Nd_2O_3-B	$(Nd^{+3},Y^{+3})_2(O^{-2})_3$	${}^0G^{Nd_2O_3-B}_{Nd^{+3}:O^{-2}}=G^{Nd_2O_3}$-399+1.684T
		${}^0G^{Nd_2O_3-B}_{Y^{+3}:O^{-2}}=G^{Y_2O_3}$+70632
		${}^0L^{Nd_2O_3-B}_{Nd^{+3},Y^{+3}:O^{-2}}$=-522337+170.606T
		${}^1L^{Nd_2O_3-B}_{Nd^{+3},Y^{+3}:O^{-2}}$=-107806+109.644T
Y_2O_3-H	$(Nd^{+3},Y^{+3})_2(O^{-2})_3$	${}^0G^{Y_2O_3-H}_{Nd^{+3}:O^{-2}}=G^{Y_2O_3}$+33189-13.986T
		${}^0G^{Y_2O_3-H}_{Y^{+3}:O^{-2}}$=GY2O3H
Y_2O_3-R	$(Nd^{+3},Y^{+3})_2(O^{-2})_3$	${}^0G^{Y_2O_3-R}_{Nd^{+3}:O^{-2}}=G^{Nd_2O_3}$-1311+6.55T
		${}^0G^{Y_2O_3-R}_{Y^{+3}:O^{-2}}=G^{Y_2O_3}$
		${}^0L^{Y_2O_3-R}_{Nd^{+3},Y^{+3}:O^{-2}}$=-337902+146.609T
		${}^1L^{Y_2O_3-R}_{Nd^{+3},Y^{+3}:O^{-2}}$=26200
Ionic Liquid	$(Nd^{+3},Y^{+3})_p(O^{-2})_q$	${}^0G^{Ionic\ Liquid}_{Nd^{+3}:O^{-2}}=G^{Nd_2O_3}$+143621-56.785T
		${}^0G^{Ionic\ Liquid}_{Y^{+3}:O^{-2}}$=GY2O3LIQ
		${}^0L^{Ionic\ Liquid}_{Nd^{+3},Y^{+3}:O^{-2}}$=730719-290T
		${}^1L^{Ionic\ Liquid}_{Nd^{+3},Y^{+3}:O^{-2}}$=831407-326T

pseudo-binaries, is a consideration in determining the accuracy of the modeling and incorporating experimental or first-principles values of the enthalpy of mixing for the solid solution phases would improve the quality of the thermochemical predictions.

5.4 Conclusion

With five solid solution phases, the Nd_2O_3-Y_2O_3 system has been modeled by reevaluating the parameters of a previous modeling to be consistent with the other

phases in the Al_2O_3-Nd_2O_3-SiO_2-Y_2O_3 system. The new parameters are shown to accurately reproduce the phase diagram, but the lack of experimental thermochemical data may limit the accuracy of the modeling.

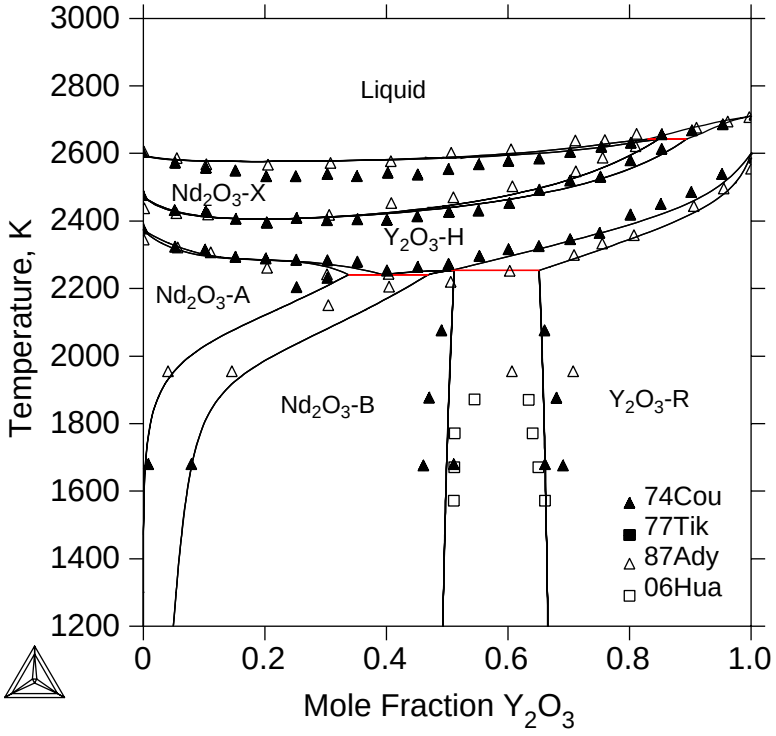

Figure 5.1. Nd_2O_3-Y_2O_3 phase diagram with experimental phase equilibria data from Coutures et al.[38], Tikhonov et al.[39], Adylov et al.[40], and Huang et al.[29].

Chapter 6

Thermodynamic Modeling of the Al_2O_3-Nd_2O_3-SiO_2-Y_2O_3 System

6.1 Introduction

The phase equilibria during Nd:YAG sintering is described within the Al_2O_3-Nd_2O_3-SiO_2-Y_2O_3 system by combining the descriptions of the pseudo-binary systems and incorporating any experimental data of the pseudo-ternary systems. Therefore, the experimental data and previous modelings concerning the four pseudo-ternary systems within Al_2O_3-Nd_2O_3-SiO_2-Y_2O_3 are discussed. As a result, only one new ternary oxide, Nd:YAG, is added to the system. Therefore the reported data concerning the solubility of neodymium in YAG is also reviewed. This phase is modeled by incorporating first-principles calculations of the enthalpy of mixing of Nd in YAG, the results of which are detailed.

6.2 Literature Review

With all of the pseudo-binary systems in the Al_2O_3-Nd_2O_3-SiO_2-Y_2O_3 system modeled, the modeling at the pseudo-ternary and pseudo-quaternary levels must now be considered. Although the pseudo-ternary phase equilibria can be accurately extrapolated from the pseudo-binaries, these must be checked against the available experimental data and any new phases must be included as well. Therefore, what

follows is a review of the literature concerning these pseudo-ternary systems.

The Al_2O_3-SiO_2-Y_2O_3 system has been modeled by Fabrichnaya et al.[7] using an ionic model for the liquid and treating the YAG phase as a stoichiometric compound. The authors performed an extensive literature review and their own experimental investigation for the system. This modeling is accepted in the current work.

The Al_2O_3-Nd_2O_3-SiO_2 system has been investigated and reviewed by Kaiser et al.[42]. No ternary oxide compounds are observed, but Al was claimed to be soluble in the $Nd_{14}Si_9O_{39}$ phase. This solubility is ignored in the present work for the sake of simplicity. The phase equilibria reported by Kaiser et al.[42] in this system at 1623K includes the $Nd_2Si_2O_7$ phase, whereas Miller and Rase's[32] investigation into the Nd_2O_3-SiO_2 system show this phase as being unstable below 1800K. Toropov and Kiseleva[17] studied the effects of Al_2O_3 on the miscibility gap of the Nd_2O_3-SiO_2 system and found that it is present despite addition of Al_2O_3. Li et al.[22] has modeled the Al_2O_3-Nd_2O_3-SiO_2 system. However, the shortcomings of the authors' modelings of Al_2O_3-Nd_2O_3 and Nd_2O_3-SiO_2 systems discussed in Chapters 3 and 4, respectively, cast doubt on the reliability of the predictions.

Bakradze et al.[43] and Soboleva and Chirkin[44] studied the phase equilibria around the Al_2O_3-rich corner of the Al_2O_3-Nd_2O_3-Y_2O_3 system and reported no pseudo-ternary compounds. Klimm et al.[45] modeled the phase equilibria along the $Y_3Al_5O_{12}$-$Nd_3Al_5O_{12}$ isopleth using the thermodynamic functions developed by Wu and Pelton[21], which, as discussed in Chapter 3, did not incorporate any experimental thermochemical data. These functions predict that an $Nd_3Al_5O_{12}$ or NAG phase is stable up to 1200K and the authors use this calculation to explain the behavior of results from differential thermal analysis of heavily doped Nd:YAG. However, as will be shown in the next section, first-principles calculations predict that NAG is not stable at low temperatures.

The only new ternary oxide phase in the current modeling is Nd-doped YAG. The solubility limit of Nd in YAG has been studied by several authors and it is found that the reported limit varies depending on the method by which the material is produced. These limits range from about 1% replacement of yttrium in single crystals[46] to 27.5% by the sol-gel method[47]. The differences in the reported

value can be attributed to effects driving the system away from equilibrium. For instance, single crystals of YAG typically exhibit an uneven distribution of Nd in the lattice, which may introduce strains and defects in the crystal. Klimm et al.'s[45] modeling predicts a limit of about 80%. The solubility of Nd in YAG by ceramic processing, taken to be the limit under which high-quality transparent material can be produced, has been found to be about 9%[3]. As the crystals in the ceramic are smaller than those grown in single crystals of YAG, the solubility limit reported by the ceramic method may be considered the more accurate value. Therefore, 9% is accepted as the solubility limit of Nd in the Y sublattice in YAG.

6.3 First-Principles Calculations

Nd:YAG is treated as a solid solution between Nd and Y in YAG, where the enthalpy of mixing defines the stability of the phase. With no experimental thermochemical data reported in the literature, the enthalpy of mixing will be predicted by first-principles calculations with the method detailed in Chapter 2. As a unit cell of YAG has twelve Y sites, compositions of 1/12 and 11/12 were readily calculated, changing one out of the twelve sites. However, a value in the middle of the composition space at 50% is needed to determine the behavior of the enthalpy of mixing across the entire composition range.

It is assumed that as Nd dopes on Y sites, the distribution of Nd and Y is random. First-principles calculations for such disordered structures must be handled with care as density functional theory uses periodic boundary conditions to simplify calculations, imposing short-range order on the unit cell. Large supercells of YAG where the Nd and Y atoms are randomly distributed would normally be needed to represent a disordered solid solution, but such structures would be costly to calculate. One approach to resolve this issue is to construct a special quasirandom structure (SQS)[48], where correlation functions are used to ensure that short-range order around each atom is removed. Thus, a relatively small structure can approximate the behavior of the random solid solution by assuming that long-range order has little effect on the properties of interest. In this case, an SQS was constructed to calculate the 50% composition of Nd:YAG with a supercell of 160 atoms or two primitive cells. The result of the calculation, 13.886 kJ/mol-form,

suggests a positive curve for the enthalpy of mixing, the magnitude of which could not have been estimated from the 1/12 and 11/12 values alone. The predicted a lattice parameter for the different compositions of Nd:YAG are shown in Table 6.1 and generally show an increasing parameter with increasing Nd content. However, the SQS results in an a lower than expected parameter. The results of the three enthalpy of mixing calculations are given in Table 6.2 and plotted in Figure 6.1.

Table 6.1. Crystallographic parameter of Nd-doped YAG predicted by first-principles calculations.

% Nd in Y sublattice	Lattice Parameter a (Å)
0	12.122
8.333	12.143
50	12.128
91.667	12.336
100	12.355

Table 6.2. First-principles calculation results for the enthalpy of mixing of Nd in YAG.

% Nd in Y sublattice	Enthalpy of Mixing (kJ/mol-form)
8.333	1.394
50	13.886
91.667	1.175

Another component of the modeling of Nd:YAG as a solution phase is that the energies of the two endmembers must be described. For $Y_3Al_5O_{12}$, the Gibbs energy from the modeling of the Al_2O_3-SiO_2-Y_2O_3 system[7] is used. For the hypothetical $Nd_3Al_5O_{12}$ or NAG phase, the enthalpy of formation from first-principles calculations is used to describe the Gibbs energy. The enthalpy of formation of NAG is calculated to be -116.389 kJ/mol-form. Wu and Pelton[21] estimated this value by extrapolating the thermodynamic functions from the stable rare-earth garnets and found it to be -125.105784 kJ/mol-form. When the first-principles calculated value is compared to the enthalpies of formation for the other phases in the Al_2O_3-Nd_2O_3 system (Figure 3.1), NAG is metastable at low temperatures.

This is in agreement with the three experimental investigations into the system[16–18] which did not report the presence of this phase.

6.4 Thermodynamic Modeling

The thermodynamic functions determined in the previous three chapters for the Al_2O_3-Nd_2O_3, Nd_2O_3-SiO_2, and Nd_2O_3-Y_2O_3 systems are combined with the functions from the previously modeled Al_2O_3-SiO_2-Y_2O_3 system[7]. Ternary interactions for the liquid phase were considered as ideal as there is not sufficient thermochemical or phase equilibria data to determine them.

As stated earlier, the only new ternary oxide phase included in the modeling is Nd:YAG, which is described by amending the YAG model with Nd^{+3} ions in the Y^{+3} sublattice:

$$(Nd^{+3}, Y^{+3})_3(Al^{+3})_5(O^{-2})_{12}$$

The evaluated parameters are detailed in Table 6.3. The enthalpy of formation for NAG was taken from the first-principles calculations. The entropy of formation was estimated from the other phases in the Al_2O_3-Nd_2O_3 system by using a similar ratio of $\Delta_f H$ to $\Delta_f S$. For NAG, this ratio was assumed to be 1100. The NAG phase remains metastable in the Al_2O_3-Nd_2O_3 system after the addition of the entropy term. As the 1/12 and 11/12 enthalpy of mixing calculations have a large uncertainty, only the zeroth order interaction parameter was considered, producing a positive, parabolic shape to the enthalpy of mixing as shown in Figure 6.1. The two terms of this parameter were determined from the SQS calculation of the enthalpy of mixing at 50% replacement of Y with Nd in YAG and from the experimental solubility limit for Nd in YAG, taken to be 9% replacement of Y at 2000K.

Table 6.3. Phase description for YAG. The values for $G^{Nd_2O_3}$ and $G^{Al_2O_3}$ and the function GYAG are given in the Appendix.

Phase	Model	Phase Description
YAG	$(Nd^{+3},Y^{+3})_3(Al^{+3})_5(O^{-2})_{12}$	${}^0G^{YAG}_{Nd^{+3}:Al^{+3}:O^{-2}}$=1.5$G^{Nd_2O_3}$+2.5$G^{Al_2O_3}$-116389-109T ${}^0G^{YAG}_{Y^{+3}:Al^{+3}:O^{-2}}$=GYAG ${}^0L^{YAG}_{Nd^{+3},Y^{+3}:Al^{+3}:O^{-2}}$=56000-5T

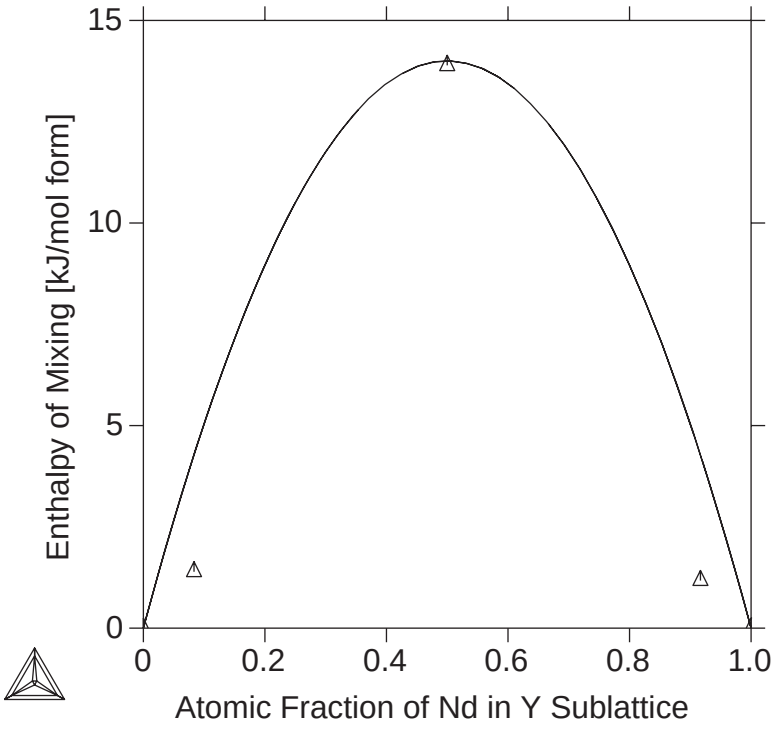

Figure 6.1. Enthalpy of mixing of Nd in YAG from first-principles calculations (triangles) and CALPHAD modeling.

With Nd:YAG modeled, the phase equilibria of the pseudo-ternary systems can be examined. Isothermal sections of the four pseudo-ternary phase diagrams at 2000K, a typical sintering temperature for Nd:YAG, are given in the Appendix as Figures A.1, A.2, A.3, and A.4. The ternary miscibility gap behavior reported by Toropov and Kiseleva[17] for the Al_2O_3-Nd_2O_3-SiO_2 system is reproduced, namely that the gap persists well towards the Al_2O_3 direction.

6.5 Conclusion

The Al_2O_3-Nd_2O_3-SiO_2-Y_2O_3 system has been modeled and the parameters of the Gibbs energy functions of the Nd:YAG phase have been presented. The parameters were evaluated by the CALPHAD approach, utilizing first-principles calculations of the enthalpy of mixing for Nd in YAG and experimental solubility data. The enthalpy of mixing for Nd in YAG was determined to be positive and symmetric.

First-principles calculations were also used to determine the enthalpy of formation of the hypothetical $Nd_3Al_5O_{12}$ phase, predicted to be metastable in the Al_2O_3-Nd_2O_3 system.

Chapter 7

Phase Equilibria During Nd:YAG Sintering

7.1 Introduction

From the modeling detailed in the previous chapters, the phase equilibria during reactive sintering of Nd:YAG will be predicted. The following discussion of the results will aim to shed light on several open questions concerning Nd:YAG processing, such as whether a liquid phase is present, what other phases are present, and what is the cause of the abnormal grain growth (AGG). Particular attention will be paid to the last question, where a model for AGG will be presented.

7.2 Phase Equilibria During Sintering

With the modeling complete, the phase equilibria during reactive sintering can now be predicted. The composition of the system is chosen to be similar to that where experimental observations are made[5], specifically, a stoichiometric amount of Al_2O_3 and Y_2O_3 for YAG with 1% of the Y_2O_3 replaced with Nd_2O_3 and 0.014 mole fraction SiO_2. The quantities of phases present at this composition as a function of temperature are shown in Figure 7.1 for the temperature range where ceramic YAG is typically sintered, 1950K to 2150K.

A vertical slice of this diagram would represent the predicted equilibria at a

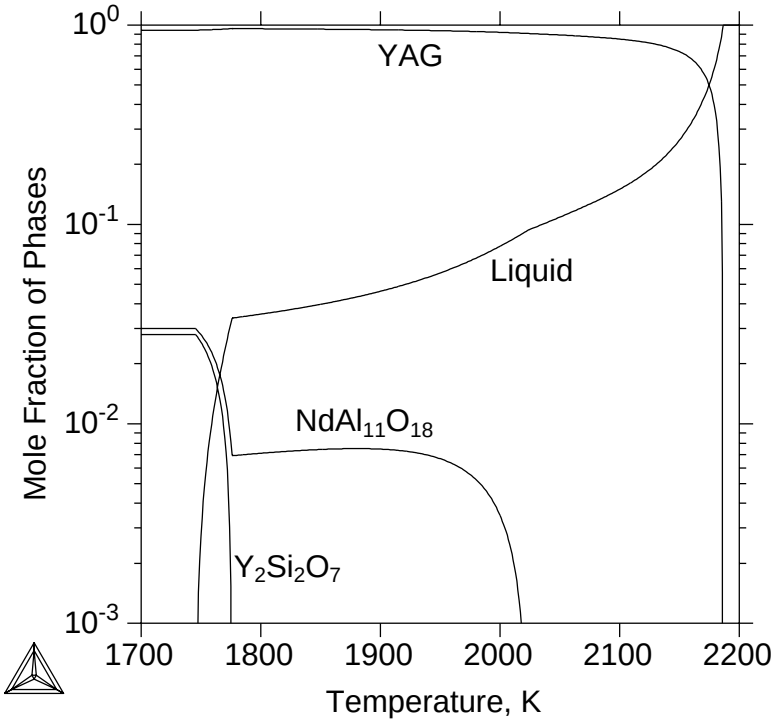

Figure 7.1. The amount of phases present vs. temperature for a typical composition to produce Nd:YAG by reactive sintering (1% Nd in YAG and 0.014 mole fraction SiO_2).

given sintering temperature. At all temperatures, YAG is the dominant phase, with approximately 1% Nd doped within it. Liquid is also present at temperatures above ∼1775K. This liquid phase is stable only when SiO_2 is present in the system, supporting the hypothesis that silica acts as a sintering aid due to the formation of a liquid phase. The composition of this liquid as a function of temperature is given in Figure 7.2. Note that even though SiO_2 is responsible for its presence, the liquid is rich in Al_2O_3 and Y_2O_3 as the dissolution of YAG into the liquid occurs.

Another interesting result of Figure 7.1 is the presence of a small amount of $NdAl_{11}O_{18}$, ∼0.01 mole fraction, below 2000K. For such quantities, $NdAl_{11}O_{18}$ can form particles and may have a large effect on the sintering of Nd:YAG, as will be examined in detail in the next section. The stability of this phase is dependent on the amount of Nd_2O_3 and SiO_2 added to the system, as illustrated in Figures 7.3 and 7.4. Increasing the quantity of Nd_2O_3 that replaces Y_2O_3 increases the quantity and decomposition temperature of $NdAl_{11}O_{18}$. With no Nd_2O_3 added to the system, another solid, corundum, forms instead. For increasing SiO_2, the

quantity of $NdAl_{11}O_{18}$ increases as more liquid phase is forming. However, the decomposition temperature is almost independent of SiO_2 concentration, at least less dependent than on Nd_2O_3 concentration. It should be noted that the formation of $NdAl_{11}O_{18}$ alters the composition of the liquid, as the decomposition temperature corresponds to a kink in the compositions predicted in Figure 7.2.

7.3 Abnormal Grain Growth in Nd:YAG

The phase equilibria detailed in the previous section can be applied to examine specific processing issues, such as abnormal grain growth (AGG). The phenomenon of AGG has been observed in many systems, where the grain size distribution is not normal due to the presence of few, extremely large grains. In a fundamental sense, the cause of AGG is the same in all cases: the properties of the grain boundaries of a polycrystalline material are inhomogeneous in a way that allows particular grains to grow at a faster rate than others. However, the source of

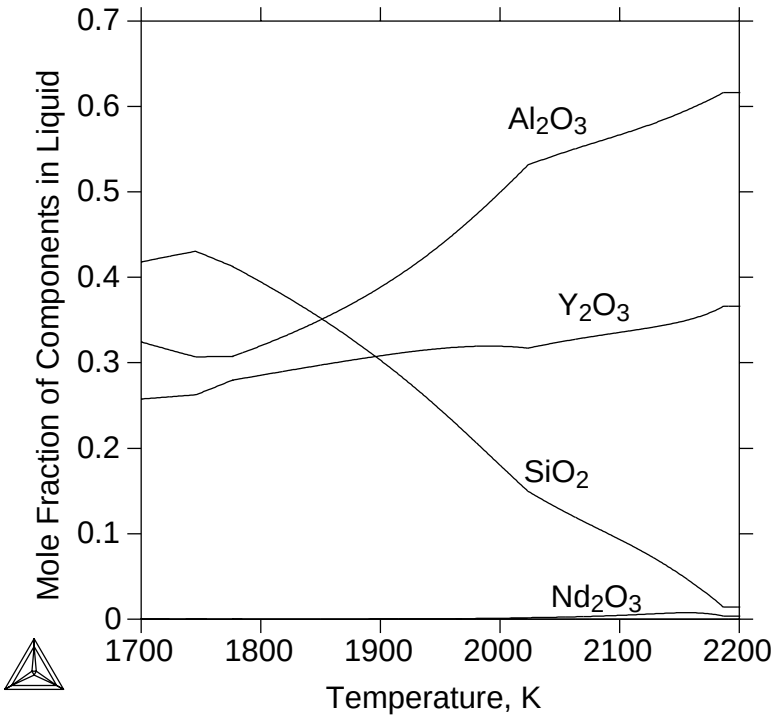

Figure 7.2. Calculated fractions of the component oxides in liquid as a function of temperature.

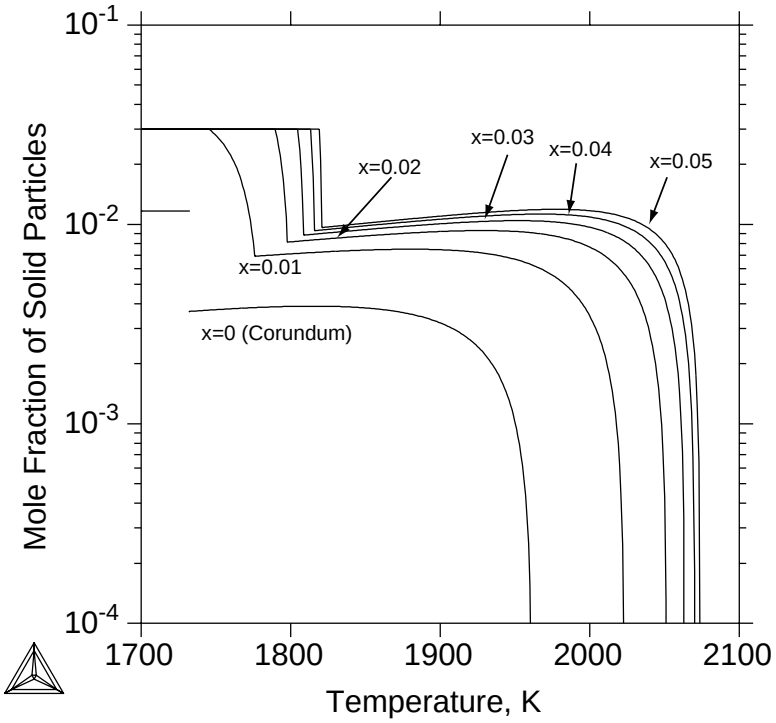

Figure 7.3. Mole fractions of the secondary solid phases for various concentrations, x in $(Y_{1-x}Nd_x)_3Al_5O_{12}$ and 0.014 mole fraction SiO_2.

the inhomogeneity is highly debated. For instance, alumina doped with yttria and silica exhibits AGG, and HRTEM images of the grain boundaries show the presence of a second, amorphous phase[49], which is theorized to promote growth. On the other hand, investigations into AGG of neodymium barium cuprates[50] show clean grain boundaries with no secondary phases. These two cases suggest that the cause of AGG may vary from system to system or that the underlying cause is simply not well understood.

Hillert[8] offered a model for AGG in which particles of a solid phase alter the growth of most grains, allowing some grains to grow much larger than the others. In his model, the quantity of these particles must fall within two constraints:

- The particles must be plentiful enough to alter the growth rate of a grain.
- The particles must be minute enough so as not to affect all the grains equally.

When such conditions are in place, some grains will have different growth rates from others and AGG can occur.

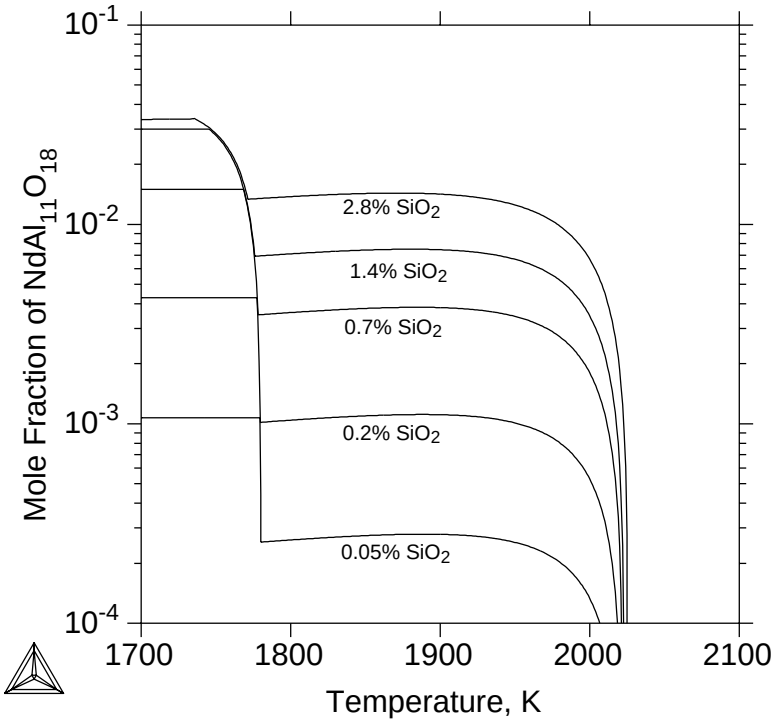

Figure 7.4. Mole fractions of the secondary solid phases for various concentrations of SiO_2 and 1% Nd in YAG.

The results of Figure 7.1 predict that Hillert's model may be applicable when sintering Nd:YAG with SiO_2 as a secondary solid phase, $NdAl_{11}O_{18}$, is predicted to be stable. At typical sintering temperatures from around 1800-1950K, the quantity of $NdAl_{11}O_{18}$ remains consistent at about 0.01 mole fraction, which could be enough to allow particles to be homogenously distributed across the grain boundaries (as will be examined later in this section), affecting the growth rate of all the grains. Thus, AGG is not observed at these temperatures. However, at approximately 2000K, the particles would be in the process of decomposing, causing fluctuations in the quantity of the particles. In such a situation, it is possible that an inhomogeneity of the particle distribution in the grain boundaries causes some grains to grow faster than others, as some grains would have fewer particles around them, resulting in AGG. Furthermore a time dependence would also be predicted due to the kinetics of the decomposition and the coarsening of the particles.

Under this scenario, Figures 7.3 and 7.4 can be used to make predictions on how grain growth is affected by changes in the composition of the system. For

instance, an increase the concentration of Nd_2O_3 should slow or even halt grain growth due to an increase in the quantity of particles. Furthermore, the temperature at which AGG occurs should increase as well as the particles are predicted to decompose at higher temperatures. Similarly, increasing the amount of SiO_2 increases the quantity of $NdAl_{11}O_{18}$, slowing grain growth. However, the decomposition temperature remains almost fixed, so the AGG temperature ought not to change much with SiO_2.

Another prediction made with this particle model is that under a similar composition as experiments, the predicted temperature for abnormal growth would be around 2000K, qualitatively agreeing with the experimentally observed AGG temperature at approximately 2100K. As the calculated peritectic temperature for $NdAl_{11}O_{18}$ is 2165K, it is reasonable to assume that the decomposition of $NdAl_{11}O_{18}$ occurs at a lower temperature at the composition of Nd:YAG sintering. Therefore, a predicted temperature of 2000K appears reasonable. The $\sim$100K difference between the experimental AGG temperature and the one predicted by the current model can be accounted for partly by uncertainty in the modeling but also by the kinetics of the reactions during sintering. The duration of the sintering process undoubtedly affects whether or not AGG occurs and, as the predicted temperature is lower than the observed temperature, kinetics may affect the formation, melting, or coarsening of $NdAl_{11}O_{18}$ particles.

Although the current modeling makes no statements concerning how these particles could alter the grain growth rate, classical grain growth mechanics can be used to predict the size of the particles as a first approximation. The ability for a spherical particle to stop the growth of a grain by a pinning mechanism can be described by the following equation from Porter and Easterling[51]:

$$\bar{D}_{max} = \frac{4r}{3f} \tag{7.1}$$

where $\bar{D}_{max}$ is the length of the largest grain, f is the volume fraction of the particles, and r is the mean radius of the particles so that pinning completely stops grain growth. $\bar{D}_{max}$ can be determined from experiment[5], where for 1% Nd:YAG at 2023K and 2073K, $\bar{D}_{max}$ is approximately 20μm and 50μm, respectively. Therefore, Equation 7.1 can be rewritten for r as a function of f, which

is plotted in Figure 7.5 for both temperatures. Assuming an equivalence between volume fraction and mole fraction, the volume fraction of particles predicted by the thermodynamic modeling is 0.01, resulting in a particle size to completely stop grain growth by pinning on the order of 100nm. As grain growth still occurs at low sintering temperatures such as 2023K, the particle size is predicted to be smaller than 100nm but large enough to affect grain growth, under the proposed AGG model. While pinning is not claimed as a mechanism for how particles could alter the growth rate of Nd:YAG grains, this analysis suggests that the quantity of particles is large enough to have some effect on the grain growth, making feasible the proposed model for AGG in Nd:YAG.

However, particles of a solid phase for these sizes and mole fractions would be readily visible under SEM, but no such reports have been made for samples

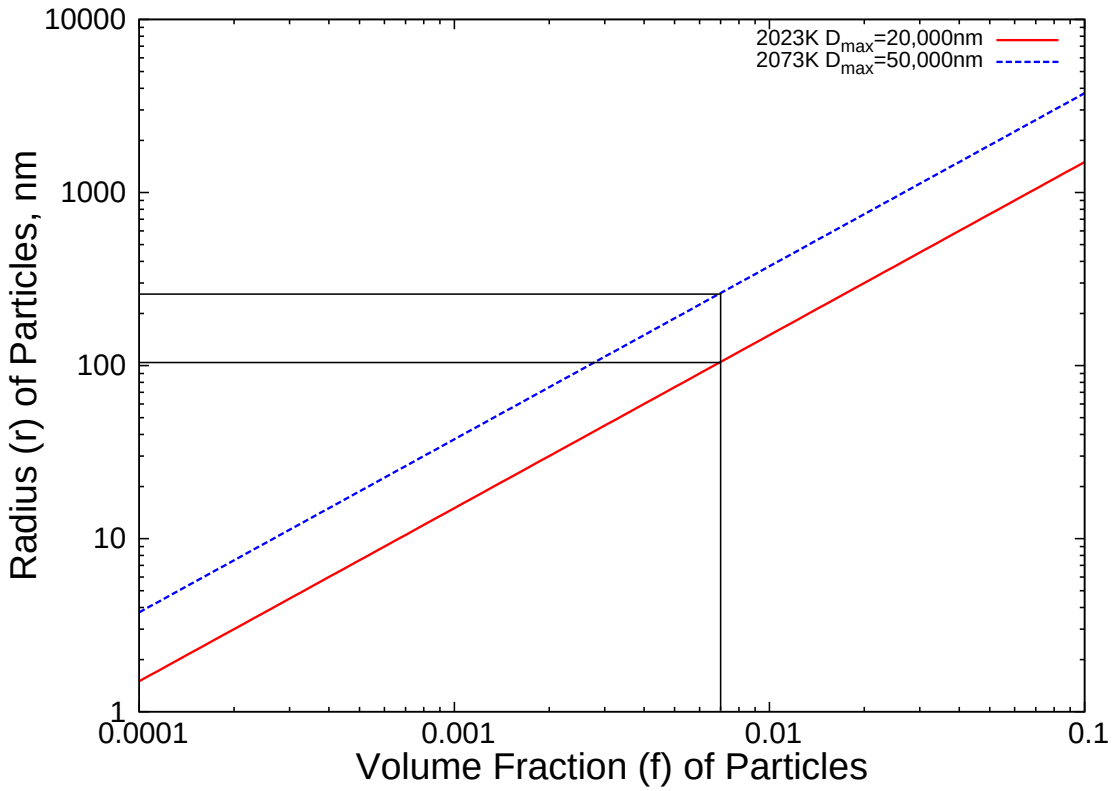

Figure 7.5. The particle size at a given volume fraction of particles necessary to completely stop grain growth by a pinning mechanism for two temperatures. Dark lines are guides for the eyes.

quenched from high temperatures. One possible reason is that there is some behavior in the system that is not accurately reproduced in the modeling that will affect the predicted phase equilibria, for instance the solubility of SiO_2 in Nd:YAG. This has been suggested as an explanation for why, given the amount SiO_2 added to the system, no secondary phases are observed at the grain boundaries. Such solubility has not been considered in the modeling as this has not been confirmed by experiments. Ignoring the changes to the thermochemical properties of Nd:YAG, SiO_2 solubility would only affect the system by reducing the amount of SiO_2 outside of Nd:YAG. Therefore, SiO_2 solubility can be approximated in the modeling by simply reducing the amount of SiO_2 in the system. The effects of such changes on the quantity of $NdAl_{11}O_{18}$ were described in Figure 7.4. Ultimately, such SiO_2 solubility shrinks the amount of the secondary solid phase, reducing the size and quantity of the particles that would form, possibly to a degree that the particles would be difficult to observe experimentally but still be capable of affecting grain growth and causing AGG.

7.4 Conclusion

The phase equilibria during sintering was examined and it is predicted that, along with YAG, liquid and minute amounts of $NdAl_{11}O_{18}$ are present as well. It is theorized that $NdAl_{11}O_{18}$ may form particles and, under a model developed by Hillert, may be responsible for the observed abnormal grain growth of Nd:YAG at approximately 2100K. The modeling accurately predicts this temperature and also suggests how this temperature and the grain growth rate change as a function of Nd_2O_3 and SiO_2 concentration. Although the precise mechanism by which the particles alter the grain growth rate is unknown, a pinning mechanism is assumed to obtain a rough estimate for the size of these particles of less than 100nm.

Chapter 8

Conclusions and Future Work

8.1 Conclusions

To study the reactive sintering of Nd:YAG, the Al_2O_3-Nd_2O_3-SiO_2-Y_2O_3 system has been thermodynamically modeled via the CALPHAD approach. Such a modeling predicts the phase equilibria during the high temperature sintering, information that is difficult to directly determine experimentally. To describe the Al_2O_3-Nd_2O_3-SiO_2-Y_2O_3 system, a previous modeling of the Al_2O_3-SiO_2-Y_2O_3 system was taken as the foundation upon which Nd_2O_3 was added. This was accomplished by evaluating the three pseudo-binary oxide systems that contain Nd_2O_3 and combining them with the previously modeled system.

The first of the three pseudo-binary systems, Al_2O_3-Nd_2O_3, includes three binary oxide phases ($NdAl_{11}O_{18}$, $NdAlO_3$ and $Nd_4Al_2O_9$). First-principles calculations were performed on $NdAlO_3$ and $Nd_4Al_2O_9$ to determine their enthalpies of formation. From these results, it was found that $Nd_4Al_2O_9$ is a stable compound at low temperatures, a fact debated in the literature. By utilizing the available experimental data and first-principles calculations, the Gibbs energies for the phases in the Al_2O_3-Nd_2O_3 system were determined. Likewise, the Nd_2O_3-SiO_2 system was evaluated. Three compounds are present in this system (Nd_2SiO_5, $Nd_{14}Si_9O_{39}$ and $Nd_2Si_2O_7$) as well as a miscibility gap in the liquid phase. First-principles calculations were again used to determine the enthalpy of formation for Nd_2SiO_5. The parameters of the Gibbs energies were ascertained by fitting to this data, as well as experimental phase equilibria. Lastly, a previous modeling of the Nd_2O_3-

Y_2O_3 system was used to describe that system. However, Y_2O_3 and liquid phases were inconsistent with the other systems. Therefore, the parameters of the Gibbs energies were reevaluated from the old values.

To complete the modeling of the Al_2O_3-Nd_2O_3-SiO_2-Y_2O_3 system, the description of the Gibbs energy of Nd:YAG was determined by using the experimental solubility limit of 9% replacement of Y with Nd and calculating the enthalpy of mixing of Nd in the Y sublattice of YAG for several compositions. A supercell was constructed for low and high concentrations of Nd and a special quasirandom structure for 50% replacement. It was found that the enthalpy of mixing is largely positive and that $Nd_3Al_5O_{12}$ is not a stable compound.

The phase equilibria during reactive sintering was then predicted. For a typical composition of Nd:YAG of about 1% Nd in the Y sublattice and a small amount of SiO_2, besides YAG a liquid phase is also stable, supporting the hypothesized role of SiO_2 as a sintering aid due to the formation of liquid. Interestingly, SiO_2 is also predicted to stabilize $NdAl_{11}O_{18}$, the quantity and stable temperature region of which change with the amount of Nd_2O_3 and SiO_2.

From these results, a model is proposed describing the abnormal grain growth observed in YAG. It is theorized that $NdAl_{11}O_{18}$ may form particles in the YAG grain boundaries during sintering. Near temperatures where the particles begin to melt, abnormal grain growth arises because the distribution of the particles fluctuates, allowing few grains to grow faster than others. Under this model, the CALPHAD evaluation of the phase equilibria predicts the temperature at which abnormal grain growth occurs to be around around 2000K, agreeing with experiment. Predictions are made as to the size of the particles and how the temperature at which abnormal grain growth occurs changes with the composition of the system.

8.2 Future Work

- Improve the quality of the modeling by incorporating new data, from either experiment or first-principles, into the evaluation of the parameters
  - Enthalpies of formation for compounds where experimental data were

not available or first-principles calculations were not performed, particularly the $NdAl_{11}O_{18}$ phase

  - Enthalpies of mixing for the solid solution phases in the Nd_2O_3-Y_2O_3 system
  - Thermodynamic properties of the liquid phase
  - Detailed phase equilibria in the pseudo-ternary systems
  - Enthalpies of mixing for Nd:YAG from experiment or for more compositions by first-principles calculations

- Use first-principles calculations to predict the defect mechanisms of SiO_2 incorporation into YAG and Nd:YAG.
- Experimental confirmation of a liquid phase during sintering and the location of SiO_2 after processing
- Experimental confirmation of the presence of $NdAl_{11}O_{18}$ at the grain boundaries of AGG Nd:YAG
- Further data on the conditions under which Nd:YAG will exhibit AGG such as the effect of temperature and composition on the probability AGG will occur

Appendix A

Isothermal Sections of the Pseudo-ternary Phase Diagrams

The modeling of the pseudo-binary systems in a consistent manner assures that the evaluated phase descriptions have values that, when compared with phases in the other systems, are physically meaningful. Therefore, higher order phase equilibria, such as those found in the pseudo-ternary systems, can be readily investigated. Isothermal sections of the four pseudo-ternary systems in the Al_2O_3-Nd_2O_3-SiO_2-Y_2O_3 system are provided to illustrate such equilibria.

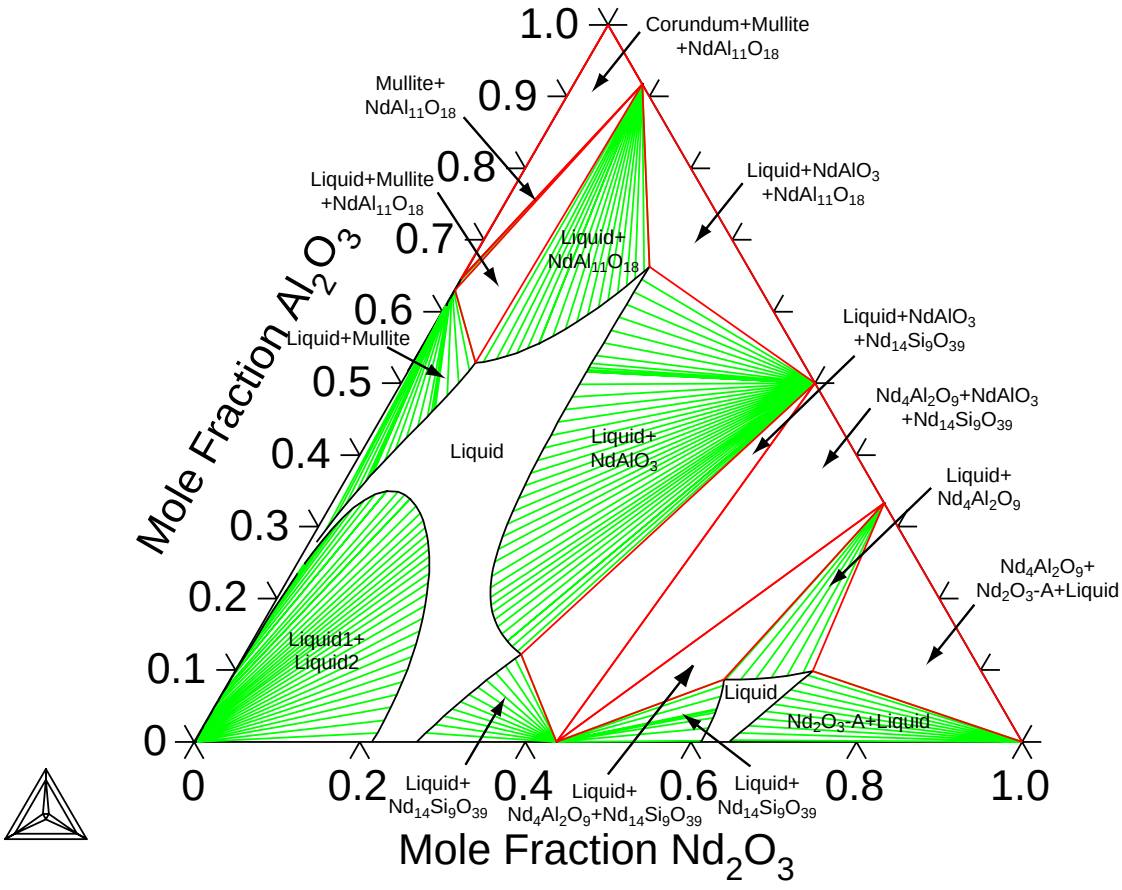

Figure A.1. Isothermal section of the Al_2O_3-Nd_2O_3-SiO_2 system at 2000K.

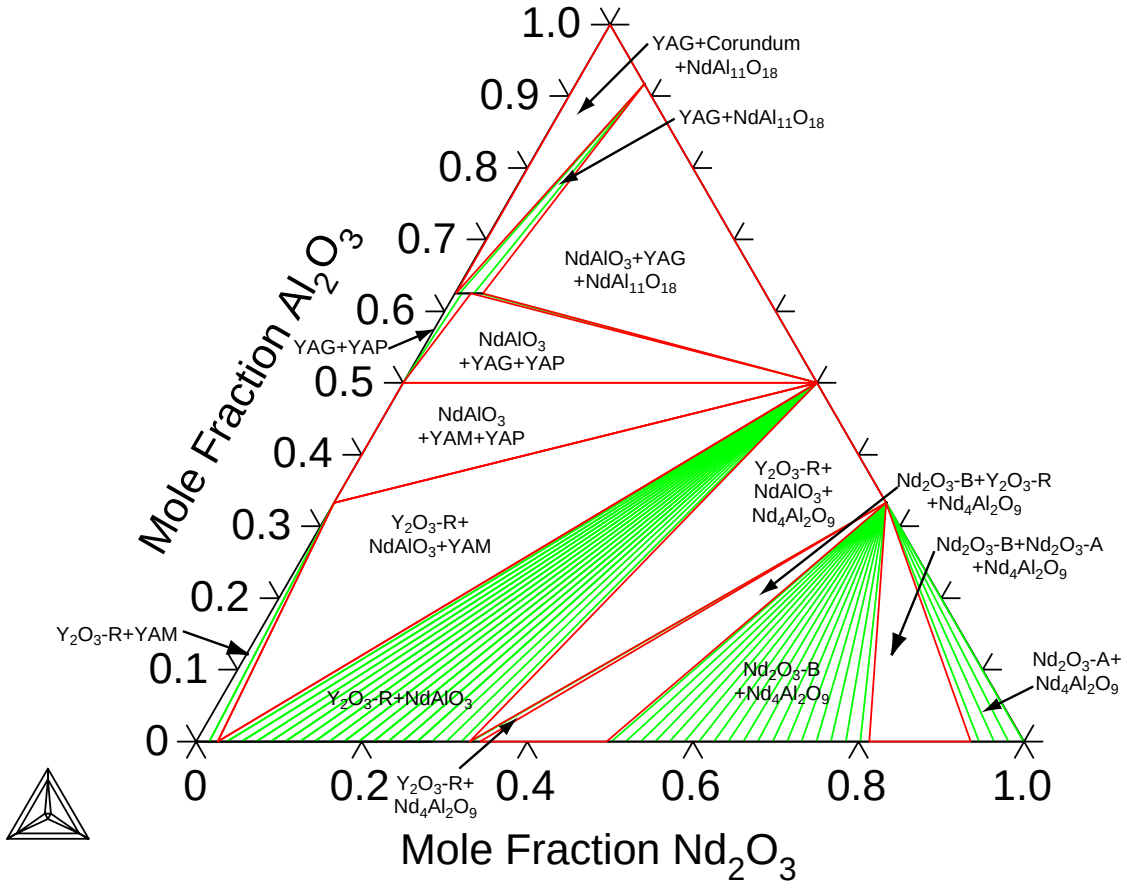

Figure A.2. Isothermal section of the Al_2O_3-Nd_2O_3-Y_2O_3 system at 2000K.

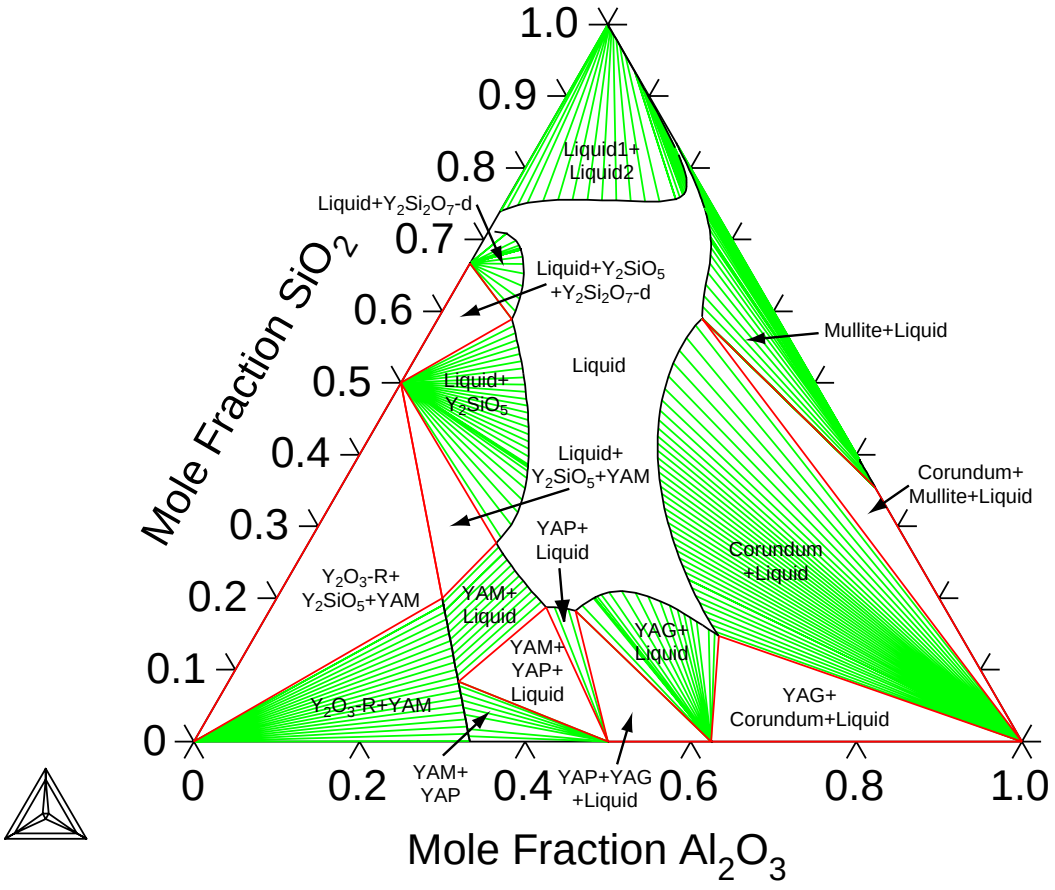

Figure A.3. Isothermal section of the Al_2O_3-SiO_2-Y_2O_3 system at 2000K.

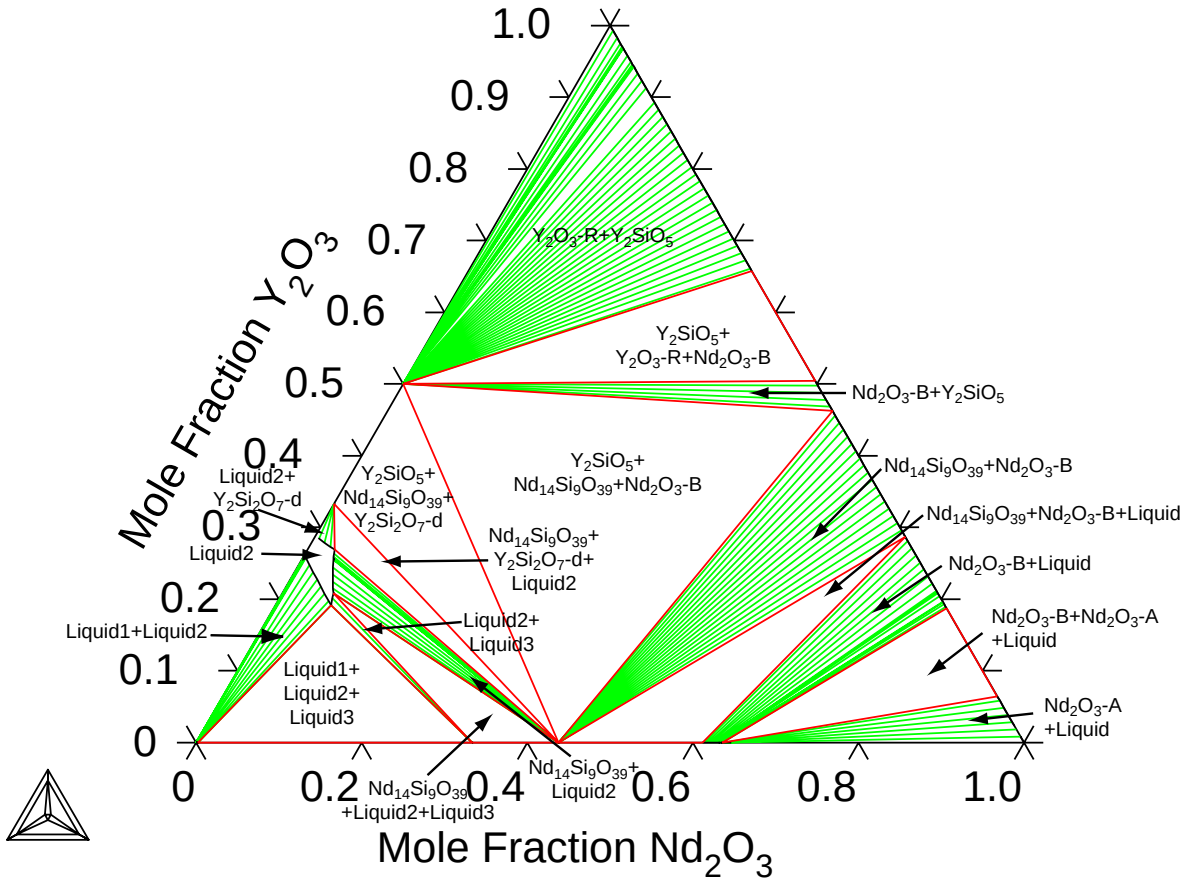

Figure A.4. Isothermal section of the Nd_2O_3-SiO_2-Y_2O_3 system at 2000K.

Appendix B

Crystal Structures

The following structures have been fully relaxed with respect to all degrees of freedom with the Vienna *Ab-initio* Simulation Package, as detailed in Chapter 2. The forms of the GGA-PAW pseudopotentials used for the ions were: Al, Nd_3, O, Si, and Y_sv.

These structures are given in the POSCAR file format. The first line is a label for the structure. The second is a scaling factor for volume. The next three are the lattice vectors. Afterwards, the quantity of each type of atom is given. For the following structures, this is in the same order as the label in the first line. The next line states the format in which the coordinates are given. Lastly, the atomic coordinates themselves are shown.

B.1 Al_2O_3 (Corundum)

```
Al2O3
    1.000000000000000
     0.0000000000000000   -2.7732042387409300    4.3689948743273930
     2.4016654951645750    1.3866021193704650    4.3689948743273930
    -2.4016654951645750    1.3866021193704650    4.3689948743273930
   4   6
Direct
  0.8521847851517563  0.8521847851517563  0.8521847851517563
  0.1478145221088667  0.1478145221088667  0.1478145221088667
  0.3521855163766503  0.3521855163766503  0.3521855163766503
  0.6478145605943908  0.6478145605943908  0.6478145605943908
  0.0562195326627517  0.7499994434138557  0.4437807352819902
  0.9437805443082894  0.2500006335571854  0.5562193416890509
  0.7500008743471440  0.4437807103738578  0.0562181266375958
  0.2499992026238971  0.5562193665971833  0.9437819503334524
  0.4437812454705892  0.0562185870099299  0.7499998788780644
  0.5562188315004519  0.9437814899611112  0.2500001980929767
```

B.2 Nd_2O_3-A

```
Nd2O3
    1.000000000000000
     3.8597510723562200    0.0000000000000000    0.0000000000000000
    -1.9298755361781100    3.3426420447476990    0.0000000000000000
     0.0000000000000000    0.0000000000000000    6.0791122979480060
   2   3
Direct
  0.3333326293456622  0.6666652586913315  0.2485628066656105
  0.6666670689453369  0.3333341378906667  0.7514371933343895
  0.0000000000000000  0.0000000000000000  0.0000000000000000
  0.3333326293456622  0.6666652586913315  0.6451665438193643
  0.6666670689453369  0.3333341378906667  0.3548334561806357
```

B.3 SiO_2 (α-Quartz)

```
SiO2
    1.000000000000000
     4.9922946685225250    0.0000000029282627    0.0000000000000000
    -2.4961473367972120    4.3234540034247320    0.0000000000000000
     0.0000000000000000    0.0000000000000000    5.4840801174453740
   3   6
Direct
  0.9999995993013044  0.4723457921098246  0.3333342639529207
  0.5276535822527490  0.5276533751310194  0.0000011901269161
  0.4723464658799842  0.0000001276272314  0.6666669805276868
```

```
  0.2631974298926306  0.4144554910670536  0.2109630490433671
  0.5855446684618272  0.8487416240942604  0.8776284821929066
  0.1512579646254000  0.7368038250145805  0.5442957656181333
  0.4144556318695095  0.2632004492386624  0.7890391041298672
  0.8487447208201086  0.5855454846359991  0.1223729308700543
  0.7368004699642984  0.1512557114331788  0.4557063875551011
```

B.4 $NdAlO_3$

```
NdAlO3
    1.000000000000000
    -2.6881957321706930   -1.5520304612274640   -4.3304367307095960
     0.0000000000000001    3.1040609224549280   -4.3304367307095960
     2.6881957321706930   -1.5520304612274640   -4.3304367307095960
   2   2   6
Direct
  0.7499999806351667  0.7499999806351667  0.7499999806351667
  0.2499999419054930  0.2499999419054930  0.2499999419054930
  0.0000000000000000  0.0000000000000000  0.0000000000000000
  0.4999999612703334  0.4999999612703334  0.4999999612703334
  0.8031785324135399  0.2499994925600575  0.6968211036088263
  0.1968213901271199  0.7500004299806022  0.3031788189318334
  0.6968208831121387  0.8031784600565075  0.2499997854137774
  0.3031790394285210  0.1968214624841522  0.7500001371268823
  0.2499996336411741  0.6968209589984440  0.8031785359428127
  0.7500002888994857  0.3031789635422157  0.1968213865978470
```

B.5 $Nd_4Al_2O_9$

```
Nd4Al2O9
    1.000000000000000
     7.7870740635786330    0.0000000000000000   -0.0103498249446414
     0.0000000000000000   10.9423725002215700    0.0000000000000000
    -3.7814137328651750    0.0000000000000000   10.8222603185470100
   16  8  36
Direct
  0.0258182994993229  0.4132441386929320  0.3100441907092423
  0.0258183173993226  0.0867558762070710  0.8100441641092434
  0.1640784156402078  0.6228018342228474  0.0866788846717859
  0.1640784333402110  0.8771981806771556  0.5866788581717891
  0.3342181027969147  0.1253447900124679  0.4307056090357136
  0.3342181205969197  0.3746552248875280  0.9307056123357086
  0.4755560879283539  0.8979824568193855  0.2120389738392171
  0.4755561058283536  0.6020175580806103  0.7120389771392190
  0.5244439297716492  0.3979824717193886  0.2879610294607850
  0.5244439476716489  0.1020175431806144  0.7879610029607811
  0.6657819149030814  0.6253448049124709  0.0692943942642884
```

0.6657819327030793	0.8746552099875322	0.5692943678642862
0.8359216021597902	0.1228018193228443	0.4133211186282089
0.8359216199597881	0.3771981955771516	0.9133211219282110
0.9741817183006750	0.9132441237929289	0.1899558125907598
0.9741817361006730	0.5867558911070740	0.6899558158907548
0.2234803954097115	0.1895165201221871	0.1285422108565576
0.2234804131097076	0.3104834947778088	0.6285422140565578
0.3477523657691483	0.6877437401436357	0.3806754406232847
0.3477523835691462	0.8122562747563673	0.8806754140232860
0.6522476520308496	0.1877437252436327	0.1193245626767103
0.6522476698308546	0.3122562896563632	0.6193245659767124
0.7765196224902883	0.6895165350221902	0.3714577925434392
0.7765196401902915	0.8104834798778128	0.8714577660434422
0.0768510235064023	0.9965619078252919	0.3936178277825316
0.0768510413064074	0.5034381070747039	0.8936178310825335
0.0804780795893054	0.2656683481057364	0.4810646205920894
0.0804780973893033	0.2343316667942666	0.9810645940920997
0.2172419386983159	0.7769956350848783	0.2530192611912568
0.2172419564983210	0.7230043798151176	0.7530192644912588
0.2167226269746816	0.0333379952574373	0.1626409481694822
0.2167226447746866	0.4666620196425658	0.6626409514694843
0.2317081501075415	0.2737735344076575	0.2633665022321687
0.2317081679075466	0.2262264804923384	0.7633664758321665
0.2986841841179986	0.5356953596043112	0.3266580633061780
0.2986842018179947	0.9643046552956847	0.8266580368061812
0.3583981816518565	0.7726344840243043	0.0318364343293186
0.3583981993518598	0.7273655308757058	0.5318364376293135
0.4347253396226209	0.2407562644964814	0.1173979957710061
0.4347253573226170	0.2592437504035216	0.6173979990710081
0.4331791294251989	0.5092597983750570	0.1039627112468718
0.4331791472252039	0.9907402165249460	0.6039626846468731
0.5668208882748043	0.0092597834750541	0.3960372920531232
0.5668209061748040	0.4907402314249489	0.8960372954531270
0.5652746782773789	0.7407562793964773	0.3826020076289907
0.5652746960773839	0.7592437355035186	0.8826019811289939
0.6416018361481414	0.2726344989242931	0.4681635689706835
0.6416018539481464	0.2273655159757027	0.9681635424706865
0.7013158336820063	0.0356953447043153	0.1733419400938187
0.7013158514820042	0.4643046701956877	0.6733419432938189
0.7682918676924563	0.7737735195076616	0.2366335010678333
0.7682918854924543	0.7262264953923414	0.7366335042678336
0.7832773908253163	0.5333380101574402	0.3373590551305127
0.7832774085253195	0.9666620047425699	0.8373590286305157
0.7827580791016820	0.2769956499848813	0.2469807422087399
0.7827580969016799	0.2230043649151217	0.7469807157087431
0.9195219382106925	0.7656683332057334	0.0189353827079056
0.9195219559106958	0.7343316816942625	0.5189353859078986
0.9231489942935957	0.4965619227252949	0.1063821756174652
0.9231490120935936	0.0034380921747081	0.6063821490174666

B.6 Nd_2SiO_5

```
Nd2SiO5
    1.000000000000000
     9.3485306807722050    0.0000000000000000   -0.1480402508248150
     0.0000000000000000    7.2787151092607900    0.0000000000000000
    -2.0244056087218040    0.0000000000000000    6.6611305317240790
   8  4  20
Direct
  0.1131805483909511  0.3532085230455360  0.9174070085195519
  0.1131805584909537  0.1467914918544669  0.4174069655195521
  0.4773554649027874  0.3733248485744118  0.7674519674264414
  0.4773554750027829  0.1266751663255912  0.2674519540264368
  0.5226445049972154  0.8733248634744076  0.7325481319735633
  0.5226445149972163  0.6266751514255883  0.2325480889735631
  0.8868194215090515  0.8532085081455330  0.5825930906804492
  0.8868194316090470  0.6467915067544628  0.0825930774804480
  0.2018582594130939  0.9170686833161001  0.9636598252956990
  0.2018582693130929  0.5829313315838958  0.4636597822956992
  0.7981417105869106  0.4170686684161043  0.5363402740043039
  0.7981417205869114  0.0829313464838987  0.0363402607043009
  0.0992008889148604  0.7369272974197147  0.9555922815473295
  0.0992008990148560  0.7630727174802883  0.4555922383473330
  0.1307624507548808  0.0428759878723866  0.7593622288880204
  0.1307624607548817  0.4571240270276164  0.2593621857880186
  0.2062203276287986  0.4299790683722033  0.6440184008690599
  0.2062203377288012  0.0700209465277928  0.1440183876690587
  0.3825579687700235  0.6299023967531749  0.5050330011952221
  0.3825579787700244  0.8700976181468210  0.0050329878952192
  0.3828933086281795  0.1221151679588041  0.5503701471993879
  0.3828933185281786  0.3778848469411989  0.0503701039993843
  0.6171066613718179  0.6221151530588011  0.9496299522006167
  0.6171066713718187  0.8778848618412020  0.4496299390006159
  0.6174420011299721  0.1299024116531778  0.9949670982047754
  0.6174420112299747  0.3700976032468252  0.4949670551047808
  0.7937796421712024  0.9299790832722062  0.8559816985309377
  0.7937796521712032  0.5700209316277967  0.3559816553309413
  0.8692375191451150  0.5428759729723836  0.7406378704119825
  0.8692375291451159  0.9571240419276123  0.2406378572119814
  0.9007990809851423  0.2369272825197118  0.5444078178526680
  0.9007990909851431  0.2630727323802841  0.0444078046526670
```

B.7 Nd:YAG - 0/12 Nd (YAG)

```
Al5O12Y3
    1.000000000000000
     6.0611392815115380   -6.0611392815115380    6.0611392815115380
     6.0611392815115380    6.0611392815115380   -6.0611392815115380
```

```
    -6.0611392815115380    6.0611392815115380    6.0611392815115380
  20  48  12
Direct
  0.0000000000000000  0.0000000000000000  0.0000000000000000
  0.5000000000000000  0.0000000000000000  0.5000000000000000
  0.3750000000000000  0.2500000000000000  0.6250000000000000
  0.0000000000000000  0.5000000000000000  0.5000000000000000
  0.8750000000000000  0.1250000149000030  0.7500000149000030
  0.3750000000000000  0.6250000000000000  0.7500000000000000
  0.1250000149000030  0.7500000149000030  0.8750000000000000
  0.7500000000000000  0.3750000000000000  0.6250000000000000
  0.0000000000000000  0.0000000000000000  0.5000000000000000
  0.5000000000000000  0.0000000000000000  0.0000000000000000
  0.0000000000000000  0.5000000000000000  0.0000000000000000
  0.5000000000000000  0.5000000000000000  0.5000000000000000
  0.2500000000000000  0.6250000000000000  0.3750000000000000
  0.2500000000000000  0.1250000000000000  0.8750000000000000
  0.6250000000000000  0.3750000000000000  0.2500000000000000
  0.1250000000000000  0.8750000000000000  0.2500000000000000
  0.5000000000000000  0.5000000000000000  0.0000000000000000
  0.6250000000000000  0.7500000000000000  0.3750000000000000
  0.8750000000000000  0.2500000000000000  0.1250000000000000
  0.7500000000000000  0.8750000000000000  0.1250000000000000
  0.1184926710220822  0.0197472695090468  0.1992268623213320
  0.6794795928122852  0.0807341912992570  0.6992268623213320
  0.1794795928122852  0.4802527304909532  0.5987454015130140
  0.3815073289779178  0.5807341912992570  0.9012545984869860
  0.0197472695090468  0.1992268623213320  0.1184926710220822
  0.4192658087007430  0.0987454015130140  0.6184926710220822
  0.5197472695090468  0.4012545984869860  0.8205204071877148
  0.0807341912992570  0.6992268623213320  0.6794795928122852
  0.3815073289779178  0.3007731376786680  0.4802527304909532
  0.6794795928122852  0.0987454015130140  0.9802527304909532
  0.1794795928122852  0.1992268623213320  0.5807341912992570
  0.1184926710220822  0.5987454015130140  0.9192658087007430
  0.1992268623213320  0.1184926710220822  0.0197472695090468
  0.5987454015130140  0.1794795928122852  0.4802527304909532
  0.0987454015130140  0.6184926710220822  0.4192658087007430
  0.3007731376786680  0.3205204071877148  0.9192658087007430
  0.8007731376786680  0.4192658087007430  0.8205204071877148
  0.3007731376786680  0.4802527304909532  0.3815073289779178
  0.4012545984869860  0.0807341912992570  0.8815073289779178
  0.0987454015130140  0.9802527304909532  0.6794795928122852
  0.9192658087007430  0.1184926710220822  0.5987454015130140
  0.5197472695090468  0.6184926710220822  0.6992268623213320
  0.4192658087007430  0.8205204071877148  0.8007731376786680
  0.4802527304909532  0.3815073289779178  0.3007731376786680
  0.5807341912992570  0.1794795928122852  0.1992268623213320
  0.0807341912992570  0.8815073289779178  0.4012545984869860
  0.0197472695090468  0.3205204071877148  0.9012545984869860
```

```
  0.6992268623213320  0.5197472695090468  0.6184926710220822
  0.1992268623213320  0.5807341912992570  0.1794795928122852
  0.9012545984869860  0.0197472695090468  0.3205204071877148
  0.9012545984869860  0.3815073289779178  0.5807341912992570
  0.4012545984869860  0.8205204071877148  0.5197472695090468
  0.8007731376786680  0.8815073289779178  0.9802527304909532
  0.6184926710220822  0.6992268623213320  0.5197472695090468
  0.4802527304909532  0.5987454015130140  0.1794795928122852
  0.9192658087007430  0.3007731376786680  0.3205204071877148
  0.9802527304909532  0.8007731376786680  0.8815073289779178
  0.6184926710220822  0.4192658087007430  0.0987454015130140
  0.8205204071877148  0.5197472695090468  0.4012545984869860
  0.3205204071877148  0.9192658087007430  0.3007731376786680
  0.8815073289779178  0.9802527304909532  0.8007731376786680
  0.5807341912992570  0.9012545984869860  0.3815073289779178
  0.8205204071877148  0.8007731376786680  0.4192658087007430
  0.8815073289779178  0.4012545984869860  0.0807341912992570
  0.3205204071877148  0.9012545984869860  0.0197472695090468
  0.6992268623213320  0.6794795928122852  0.0807341912992570
  0.5987454015130140  0.9192658087007430  0.1184926710220822
  0.9802527304909532  0.6794795928122852  0.0987454015130140
  0.1250000000000000  0.2500000000000000  0.3750000000000000
  0.3750000000000000  0.1250000000000000  0.2500000000000000
  0.1250000000000000  0.3750000000000000  0.7500000000000000
  0.6250000149000030  0.2500000149000030  0.8750000000000000
  0.2500000000000000  0.3750000000000000  0.1250000000000000
  0.7500000000000000  0.1250000000000000  0.3750000000000000
  0.7500000000000000  0.6250000000000000  0.8750000000000000
  0.2500000000000000  0.8750000000000000  0.6250000000000000
  0.6250000000000000  0.8750000000000000  0.7500000000000000
  0.3750000000000000  0.7500000000000000  0.1250000000000000
  0.8750000000000000  0.7500000000000000  0.6250000000000000
  0.8750000000000000  0.6250000149000030  0.2500000149000030
```

B.8 Nd:YAG - 1/12 Nd

```
Al5Nd(1/12)3O12Y(11/12)3
    1.000000000000000
     6.0760355910178130   -6.0708429409520700    6.0708429409520700
     6.0760355910178130    6.0708429409520700   -6.0708429409520700
    -6.0760355910178130    6.0676431900949200    6.0676431900949200
  20   1  48  11
Direct
  0.9977716032051305  0.9994210418564009  0.9990114747584258
  0.5004095670979680  0.9987601284467047  0.5009885252415742
  0.3747619323160407  0.2505390704397072  0.6258930695696634
  0.0003473404148338  0.5004128527102054  0.5001165104587457
  0.8748504748539503  0.1248504897539533  0.7500000149000030
```

0.3751495251460497	0.6251495251460497	0.7500000000000000
0.1246460157700469	0.7488688776463732	0.8741069304303366
0.7511311372536298	0.3753539991299562	0.6258930695696634
0.9997691700439120	0.9997036577485403	0.5001165104587457
0.5012398715532953	0.9995904329020320	0.9990114747584258
0.9995871472897946	0.4996526595851591	0.9998834895412543
0.5005789581435991	0.5022283967948695	0.5009885252415742
0.2501536640137374	0.6251761349444820	0.3750397955716451
0.2494609295602928	0.1252380676839593	0.8741069304303366
0.6271943360900991	0.3771943360900991	0.2500000000000000
0.1228056639099009	0.8728056639099009	0.2500000000000000
0.5002963422514597	0.5002308299560880	0.9998834895412543
0.6248861315579077	0.7498636606271631	0.3750397955716451
0.8748238650555180	0.2498463359862626	0.1249602044283549
0.7501363393728369	0.8751138684420923	0.1249602044283549
0.3750000000000000	0.1250000000000000	0.2500000000000000
0.1121441898013700	0.0159790490621603	0.1983291510020990
0.6795275308382003	0.0803499861109032	0.6995478751160249
0.1796309547601496	0.4804909759547513	0.5991029530955743
0.3813880228591842	0.5805280016645824	0.9008970469044257
0.0194649248429570	0.1989996737399053	0.1189526832206198
0.4193405850544778	0.0992197105511536	0.6183239140621595
0.5199187086912929	0.4013563279850132	0.8208766045728240
0.0804797234121963	0.6990421041184689	0.6791233954271760
0.3813893635987711	0.3042322927941825	0.4830476458338069
0.6797611525987506	0.0984568568705981	0.9793524440992485
0.1790971701733994	0.1988323039504891	0.5805752035311400
0.1182571004193420	0.5985219666422523	0.9194247964688600
0.1957677072058175	0.1186106364012289	0.0169523541661931
0.6016582822350429	0.1788153530396244	0.4830476458338069
0.0993072000888731	0.6186807750842647	0.4194371889491464
0.3011676960495109	0.3209028298266006	0.9194247964688600
0.8009578958815311	0.4195202765878037	0.8208766045728240
0.3010003262600947	0.4805350751570430	0.3810473167793802
0.4007802894488464	0.0806594149455222	0.8816760859378405
0.0986436720149868	0.9800812913087071	0.6791233954271760
0.9194719983354176	0.1186119771408158	0.5991029530955743
0.5200203442778246	0.6191978890051217	0.6995478751160249
0.4196500138890968	0.8204724691617997	0.8004521248839751
0.4840209509378397	0.3878558101986300	0.3016708489979010
0.5861849612007219	0.1823501019399174	0.1983291510020990
0.0796772176789204	0.8807092428348611	0.4015427312260584
0.0195090240452487	0.3203690452398504	0.9008970469044257
0.6989833290076888	0.5191042035110200	0.6183239140621595
0.1987041111900822	0.5800357944787606	0.1791512263987229
0.9008845680800377	0.0195528847913664	0.3208487736012771
0.9014780333577477	0.3817428995806580	0.5805752035311400
0.4015431431294019	0.8202388474012494	0.5206475559007515
0.7995912915004979	0.8808955872286575	0.9793524440992485
0.6191044127713425	0.7004087084995021	0.5206475559007515

```
  0.4804471152086336  0.5991154319199623  0.1791512263987229
  0.9199642055212394  0.3012958888099178  0.3208487736012771
  0.9808957964889800  0.8010166709923112  0.8816760859378405
  0.6192907571651389  0.4203227823210796  0.0984572687739416
  0.8218655135471451  0.5208334883911974  0.4015427312260584
  0.3176498980600826  0.9138150387992781  0.3016708489979010
  0.8808021109948783  0.9799796557221754  0.8004521248839751
  0.5800469905192713  0.9005122416223301  0.3810473167793802
  0.8201299888602804  0.8007564138648746  0.4194371889491464
  0.8813192249157353  0.4006927999111269  0.0805628110508536
  0.3211846469603756  0.8983417177649571  0.0169523541661931
  0.6992435861351254  0.6798700111397196  0.0805628110508536
  0.5994877583776699  0.9199530094807287  0.1189526832206198
  0.9791665116088026  0.6781344864528620  0.0984572687739416
  0.1245420082464079  0.2508621909183333  0.3758716698607429
  0.1250000000000000  0.3750000000000000  0.7500000000000000
  0.6251972256347642  0.2501129973684826  0.8749138307976168
  0.2491378090816667  0.3754579917535921  0.1241283301392571
  0.7513296616143350  0.1250094789423883  0.3758716698607429
  0.7497166200628627  0.6248008483291372  0.8749138307976168
  0.2498870175315204  0.8748027892652388  0.6250861692023832
  0.6250000000000000  0.8750000000000000  0.7500000000000000
  0.3749905210576117  0.7486703383856650  0.1241283301392571
  0.8751991516708628  0.7502833799371373  0.6250861692023832
  0.8750000000000000  0.6250000149000030  0.2500000149000030
```

B.9 Nd:YAG - 6/12 Nd (SQS)

```
Al5Nd(6/12)3O12Y(6/12)3
    1.000000000000000
   -12.1275820010674500   -0.0000194239128372   -0.0012257383442416
     0.0012213051468657   -0.0000707236354892   12.1284910952589900
     0.0000232603083044   12.1280729314221300   -0.0000704289617943
  40  12  96  12
Direct
  0.8749844520353136  0.7513483232068978  0.9995468589266636
  0.8750193825572765  0.2495218110688455  0.5003256347410030
  0.9994460993142553  0.9982808362925439  0.9990571920351243
  0.0005639240500415  0.5006530952769168  0.0006821862786097
  0.0005535202569007  0.8750258793678967  0.2493797959659929
  0.0006371815005721  0.3749921625215933  0.2485243245711430
  0.0007589657253888  0.9973484910394390  0.4999564805551913
  0.9996422578847515  0.5015741296920169  0.5002574305306524
  0.0005865918913130  0.1220411632190945  0.7512882891513826
  0.0004397187089324  0.6271987101436380  0.7505329094196682
  0.1229603994425403  0.2494089647751849  0.9994522818516032
  0.1232745089346778  0.7512329843746528  0.5005275596337597
  0.2504870892815916  0.5011868479982340  0.8773371135506736
```

0.2504327487611349	0.9987423297414537	0.1244300897136981
0.2496809598062271	0.2492254830682370	0.2488268292227076
0.2505705627993606	0.7518673596128238	0.2476550640018900
0.2504094636628267	0.5004559129227673	0.3728935130333610
0.2504228387243188	0.9995649201200862	0.6251851519650913
0.2502685624655783	0.2473672690163156	0.7510399656609863
0.2497802447969377	0.7513946175308135	0.7519793134279382
0.3750101685381750	0.7504830032478580	0.9994435488153641
0.3750074940759802	0.2487023190481423	0.5006175379081554
0.5002617606605284	0.9984157627264096	0.9997300713315624
0.4993485742771711	0.5027269426757144	0.0001840128010073
0.4995755595116336	0.1227662281214421	0.2496002346615995
0.4995561033681852	0.6279230333360388	0.2487216148144071
0.4996378868119606	0.9993778112017822	0.4991406682641610
0.5004615212946248	0.5016512699350884	0.5009844490089108
0.4994922016509733	0.8750197345628905	0.7511647014664362
0.4996030795254498	0.3750119051344214	0.7504388098207713
0.6267367103850319	0.2487366471740629	0.9994552690242529
0.6270376213047086	0.7504275790719674	0.5004106345619732
0.7494614254873611	0.9994920861029115	0.8771366388897448
0.7494991414177221	0.5006299817957611	0.1250133444112080
0.7500792116745103	0.2485535083213932	0.2478910738860876
0.7496575942601922	0.7524675815463269	0.2489522191325264
0.7494355857645374	0.9986574287192695	0.3726544166596284
0.7493172072189935	0.5014195997892514	0.6256534483725815
0.7495227997141001	0.2482329271211583	0.7521231778659967
0.7503133865136959	0.7508522947544876	0.7513532840459973
0.9990742101104360	0.1237536711282559	0.2488415576148171
0.0008428649291687	0.6262562473352844	0.2491032927558763
0.9989893030858283	0.3742444422738558	0.7510817325515049
0.1251230733322544	0.2487638932066645	0.4991461782623006
0.2508257171273272	0.5007655783958782	0.6259681156664385
0.3747073808633772	0.2491072348276973	0.9991740005803109
0.3752965068562162	0.7510487804596053	0.4990182460264521
0.4991229870720062	0.3757329054597989	0.2491795636520919
0.6249072931466912	0.2492508143844745	0.5008181268731633
0.7491747995302802	0.5008742543558711	0.8761766444110819
0.7508860046229273	0.5012625166666069	0.3749471760726664
0.7510414345326311	0.9989427380078979	0.6254453118989858
0.0290449850284489	0.8506779943589180	0.5516014357143604
0.0285813661499930	0.3510662567125280	0.9522438719054662
0.0294016724262605	0.1473888430446380	0.0470399429320807
0.0293403565396702	0.6498574905534724	0.4515935208805999
0.0522994591465604	0.9656237878284273	0.3522965080282532
0.0502862306787151	0.0279835759992864	0.8515578843724469
0.0526764429306752	0.4671956634911680	0.1472726814638605
0.0492254788965738	0.5342053265901257	0.6481632301808133
0.8523174049593791	0.5527532094839955	0.5347033915433528
0.8530195231192934	0.4503447965245186	0.0346745594947322
0.8506325456073398	0.0493189969527279	0.9705239565723645

```
0.8523791952832411  0.9477811449428586  0.4644824752333605
0.8974536413899870  0.7846362654210353  0.3004119519401129
0.8978152036258464  0.2835924573947679  0.1972505162763909
0.8974703360426091  0.2133480549748583  0.8022516319919717
0.8989304687314217  0.7205769090628706  0.7013707399835738
0.9485113974113872  0.9648985553688902  0.1463262871088489
0.9511081549302958  0.4666599074751119  0.3518770979196617
0.9531527565308338  0.0283707349123787  0.6490773313610845
0.9514747099354679  0.5347627381378359  0.8531331642205231
0.9700119483689775  0.8507070058206239  0.9487758970296554
0.9655754934841312  0.1451733219850979  0.4523356492844286
0.9697174653262053  0.6500044432597178  0.0478515925472891
0.9662307125967047  0.3534506414979788  0.5484054348010190
0.1024430817419670  0.2824949567148778  0.2988014617943051
0.1033805014394318  0.7849432154797213  0.1966248959411132
0.1026423586622940  0.2146317211595203  0.7011442758993311
0.1017136432665851  0.7202571710181900  0.8016040633702843
0.1497191795179873  0.0463799810502792  0.5293612207338541
0.1485925161434523  0.9500236456715925  0.0306699403294672
0.1474925554933577  0.4530116095725134  0.4657176250760742
0.1486468568985444  0.5505679243320003  0.9701655719012123
0.1998872072976070  0.8991597212208546  0.7196471732305909
0.2035484596300492  0.6028682417054156  0.2793327681075368
0.2018954989766968  0.1002127128368642  0.2187945046617443
0.2023450035318248  0.3965491839015129  0.7861982220248436
0.2157207820884253  0.7026910611883821  0.6034735025089120
0.2150997195665099  0.3000356816630827  0.1016453288852617
0.2146184988973516  0.8007490671530419  0.3966003514434320
0.2148067322954930  0.1967686937659039  0.8976892146792679
0.2846068369560868  0.1986454779101479  0.3966384610925076
0.2799359829180261  0.7004175027465607  0.0994211689151001
0.2833396846182907  0.2978263604391955  0.6036173201741875
0.2803193421316124  0.8024005814138206  0.8997206291578692
0.3012822306869793  0.8992438578336674  0.2190834158379360
0.3009012965571216  0.0994841498390926  0.7204412169491334
0.2972440672442147  0.3986115924189022  0.2785042603162893
0.3008138458293601  0.6038173655079646  0.7856516750540266
0.3509974943027174  0.9511522924907894  0.5297179827537590
0.3513342423058603  0.0464623178181682  0.0294728463234932
0.3530763815440352  0.5496082497997676  0.4654283127565151
0.3514128981318478  0.4529158131441875  0.9715245498795824
0.3987872756272708  0.2794955372332737  0.7983566893027998
0.3984595345477260  0.7803782573021465  0.7032116203321621
0.3972052116569245  0.2152764603337474  0.1998919781898607
0.3987608697678837  0.7224223416779196  0.2967274852664730
0.4524469066166361  0.4710199971197113  0.6497923374154695
0.4500021549066489  0.9691855133005447  0.8517097335570014
0.4494790475603381  0.0290734488176696  0.3507066706604789
0.4478221138899059  0.5357596802445812  0.1471489957299212
0.4663288098451304  0.1462414178805389  0.5512842112842335
```

```
0.4657364228699592  0.3532005791225643  0.4521019382480773
0.4694728322787967  0.8505243066257151  0.0506482714155681
0.4702708039696901  0.6508049997238032  0.9485955072991672
0.5354217011816829  0.8525699935456359  0.4488165160378088
0.5351414670457117  0.3531486276826712  0.0472984822175775
0.5346641708783650  0.6486581523452131  0.5520826376429326
0.5345478850800092  0.1462901045963179  0.9492482275651994
0.5469456578585863  0.9687015863562749  0.6486870257865007
0.5467239167891407  0.4702705448213536  0.8516253732811165
0.5489004498387828  0.5362018349172786  0.3523586670280636
0.5497545793692993  0.0300145453516336  0.1479416771699462
0.6014948679659682  0.7818382828668575  0.8001540279179764
0.6021553366326913  0.2156747940723776  0.2976203939050990
0.6006273033041509  0.2792371428763474  0.7041534736877111
0.6012473145225670  0.7212194262524037  0.1996135906206362
0.6475694344199709  0.0486048759684934  0.4656281391575874
0.6463202011505729  0.5528277196528535  0.0349553300828021
0.6473285879064719  0.4510062358260782  0.5334437032927823
0.6485057017739990  0.9479385971413095  0.9701890854468758
0.6973433020094362  0.1010364277751989  0.7847538880097957
0.6987262371517104  0.6036636713143011  0.7174391241540974
0.7010319815589483  0.3969145491034212  0.2162286245276093
0.6984529718197692  0.8993607880884369  0.2781191263455085
0.7208277383585937  0.7985706231618082  0.6021919533557138
0.7200900258151748  0.1981939469147562  0.1003648091390019
0.7215736143840488  0.2981945142150124  0.8995290123453898
0.7211814784829969  0.7038560243922589  0.3985163479446285
0.7840092496951883  0.2967321190841616  0.3961146502988129
0.7842825037281145  0.2006556041714163  0.6043605028532752
0.7807354845088739  0.8013729626603734  0.1004042813616337
0.7794879279462492  0.7023092822421404  0.8996882508552986
0.7975391559029177  0.3970977613844227  0.7167710807672023
0.7982800683906746  0.6045383414840302  0.2155928329312857
0.7981375445349030  0.0999139721936757  0.2784136938954376
0.8017557889999907  0.8977637912188428  0.7854660559547568
0.8748204445759384  0.2482902888556566  0.0007824685115807
0.8751909912612490  0.7508380766950538  0.5010183889634732
0.0008379523918762  0.8743340326813680  0.7510515365467327
0.1250744431504103  0.7511079273771699  0.9991001556981800
0.2489976697833782  0.9986493447881344  0.8752024805399401
0.2492857552377714  0.5016682385807059  0.1245293245428059
0.2509952520671774  0.9990974966366295  0.3740315926441582
0.5008992609398177  0.8756249816929866  0.2485170553811855
0.4990660354840983  0.1237077142291909  0.7508125485794110
0.5008224584987033  0.6263099481138994  0.7514778213890665
0.6249143229763234  0.7513661937059481  0.0010536829367638
0.7491299520124031  0.9989661901161142  0.1241272210563338
```

B.10 Nd:YAG - 11/12 Nd

```
Al5Nd(11/12)3O12Y(1/12)3
    1.000000000000000
     6.1631640089571610   -6.1690675799167930    6.1690675799167930
     6.1631640089571610    6.1690675799167930   -6.1690675799167930
    -6.1631640089571610    6.1723887388119830    6.1723887388119830
  20  11  48   1
Direct
  0.0021341910765855  0.0006543356710580  0.0008092148142680
  0.4998451208568113  0.0013249762623175  0.4991907851857320
  0.3751519652561370  0.2494216273973819  0.6241873359726711
  0.9996469903919944  0.4996035018323823  0.4999297472440531
  0.8752099111412051  0.1252099260412081  0.7500000149000030
  0.3747900888587949  0.6247900888587949  0.7500000000000000
  0.1252343063247139  0.7509646441834690  0.8758126640273289
  0.7490353707165340  0.3747657085752891  0.6241873359726711
  0.0002827568520729  0.0003262454116779  0.4999297472440531
  0.4986750237376825  0.0001548791431887  0.0008092148142680
  0.0003964981676106  0.5003530096080056  0.0000702527559469
  0.4993456643289420  0.4978658089234145  0.4991907851857320
  0.2498423776099159  0.6248710093541590  0.3749091141767380
  0.2505783726026181  0.1248480347438630  0.8758126640273289
  0.6228748999426870  0.3728748999426870  0.2500000000000000
  0.1271251000573130  0.8771251000573130  0.2500000000000000
  0.4996737545883221  0.4997172431479271  0.0000702527559469
  0.6250667365668292  0.7500381048225861  0.3749091141767380
  0.8751289906458410  0.2501576223900841  0.1250908858232620
  0.7499618951774139  0.8749332634331708  0.1250908858232620
  0.1255159619264390  0.2495954225847825  0.3744892641270141
  0.1250000000000000  0.3750000000000000  0.7500000000000000
  0.6249088205015596  0.2499925050973530  0.8750765775965519
  0.2504045774152175  0.3744840380735610  0.1255107358729859
  0.7489733022005822  0.1248938415422245  0.3744892641270141
  0.7501677719950095  0.6250840873991947  0.8750765775965519
  0.2500075098026500  0.8750911943984363  0.6249234224034481
  0.6250000000000000  0.8750000000000000  0.7500000000000000
  0.3751061584577755  0.7510266977994178  0.1255107358729859
  0.8749159126008053  0.7498322280049905  0.6249234224034481
  0.8750000000000000  0.6250000149000030  0.2500000149000030
  0.1214389300824692  0.0183229349090368  0.1959638252532017
  0.6806042252633375  0.0804016132812109  0.6946090910180942
  0.1804600168105353  0.4854202138837636  0.6001758880910586
  0.3852443257927121  0.5802841287194838  0.8998241119089414
  0.0145196094531741  0.1950937704637852  0.1145405481877759
  0.4199744644740235  0.1000666140183668  0.6149097396018703
  0.5141445029318561  0.3992933402841814  0.8190077233451660
  0.0802856169390225  0.6951367795866830  0.6809922766548340
  0.3851113250075144  0.3019843736874961  0.4831815250092291
  0.6802069845442489  0.1009237989195384  0.9867138442910743
```

```
 0.1808854239840656  0.1952395861989942  0.5801964303464189
 0.1150431558525753  0.6006889936376538  0.9198035696535811
 0.1980156263125039  0.1148886749924856  0.0168184749907780
 0.5980702000017146  0.1811971513217330  0.4831815250092291
 0.1000309273591284  0.6146631371189386  0.4198246042772240
 0.3047604138010058  0.3191145760159344  0.9198035696535811
 0.8048632204133170  0.4197143830609775  0.8190077233451660
 0.3049062295362148  0.4854803905468259  0.3854594518122241
 0.3999333859816332  0.0800255355259765  0.8850902603981297
 0.1007066597158186  0.9858554970681439  0.6809922766548340
 0.9197158712805162  0.1147556742072879  0.6001758880910586
 0.5140048657547354  0.6142074777368833  0.6946090910180942
 0.4195983867187891  0.8193957747366625  0.8053909089819058
 0.4816770650909632  0.3785610699175308  0.3040361747467983
 0.5745248951707183  0.1776408903441578  0.1959638252532017
 0.0811846482047471  0.8859593823545424  0.3991377154038602
 0.0145797861162365  0.3195399831894647  0.8998241119089414
 0.6949352751278539  0.5148431255835177  0.6149097396018703
 0.1953810912219112  0.5807888138727506  0.1808816019279433
 0.8999072119448073  0.0144994892939749  0.3191183980720567
 0.8993110063623462  0.3849568441474247  0.5801964303464189
 0.3990762010804616  0.8197930154557511  0.5132861557089257
 0.8065068597468255  0.8857900453715430  0.9867138442910743
 0.6142099546284570  0.6934931402531745  0.5132861557089257
 0.4855005107060251  0.6000927880551927  0.1808816019279433
 0.9192111861272494  0.3046189087780888  0.3191183980720567
 0.9851568744164823  0.8050647248721461  0.8850902603981297
 0.6140406176454576  0.4188153517952529  0.1008622845961398
 0.8179530671991131  0.5131783330493178  0.3991377154038602
 0.3223591096558422  0.9254751048292817  0.3040361747467983
 0.8857925222631167  0.9859951342452646  0.8053909089819058
 0.5805532222760164  0.8999790612653911  0.3854594518122241
 0.8197936769181169  0.8051614671582854  0.4198246042772240
 0.8853368628810614  0.3999690726408716  0.0801753957227760
 0.3188028486782670  0.9019297999982854  0.0168184749907780
 0.6948385328417146  0.6802063230818831  0.0801753957227760
 0.6000209387346089  0.9194467777239836  0.1145405481877759
 0.9868216669506822  0.6820469328008869  0.1008622845961398
 0.3750000000000000  0.1250000000000000  0.2500000000000000
```

B.11 Nd:YAG - 12/12 Nd (NAG)

```
Al5Nd3O12
    1.000000000000000
     6.1772917517440770   -6.1772917517440770    6.1772917517440770
     6.1772917517440770    6.1772917517440770   -6.1772917517440770
    -6.1772917517440770    6.1772917517440770    6.1772917517440770
  20  12  48
```

```
Direct
  0.0000000000000000  0.0000000000000000  0.0000000000000000
  0.5000000000000000  0.0000000000000000  0.5000000000000000
  0.3750000000000000  0.2500000000000000  0.6250000000000000
  0.0000000000000000  0.5000000000000000  0.5000000000000000
  0.8750000000000000  0.1250000149000030  0.7500000149000030
  0.3750000000000000  0.6250000000000000  0.7500000000000000
  0.1250000149000030  0.7500000149000030  0.8750000000000000
  0.7500000000000000  0.3750000000000000  0.6250000000000000
  0.0000000000000000  0.0000000000000000  0.5000000000000000
  0.5000000000000000  0.0000000000000000  0.0000000000000000
  0.0000000000000000  0.5000000000000000  0.0000000000000000
  0.5000000000000000  0.5000000000000000  0.5000000000000000
  0.2500000000000000  0.6250000000000000  0.3750000000000000
  0.2500000000000000  0.1250000000000000  0.8750000000000000
  0.6250000000000000  0.3750000000000000  0.2500000000000000
  0.1250000000000000  0.8750000000000000  0.2500000000000000
  0.5000000000000000  0.5000000000000000  0.0000000000000000
  0.6250000000000000  0.7500000000000000  0.3750000000000000
  0.8750000000000000  0.2500000000000000  0.1250000000000000
  0.7500000000000000  0.8750000000000000  0.1250000000000000
  0.1250000000000000  0.2500000000000000  0.3750000000000000
  0.3750000000000000  0.1250000000000000  0.2500000000000000
  0.1250000000000000  0.3750000000000000  0.7500000000000000
  0.6250000149000030  0.2500000149000030  0.8750000000000000
  0.2500000000000000  0.3750000000000000  0.1250000000000000
  0.7500000000000000  0.1250000000000000  0.3750000000000000
  0.7500000000000000  0.6250000000000000  0.8750000000000000
  0.2500000000000000  0.8750000000000000  0.6250000000000000
  0.6250000000000000  0.8750000000000000  0.7500000000000000
  0.3750000000000000  0.7500000000000000  0.1250000000000000
  0.8750000000000000  0.7500000000000000  0.6250000000000000
  0.8750000000000000  0.6250000149000030  0.2500000149000030
  0.1148597954842145  0.0143174634707677  0.1948958992026917
  0.6805784357319169  0.0800361037184842  0.6948958992026917
  0.1805784357319240  0.4856825365292323  0.6005423320134824
  0.3851402045157926  0.5800361037184913  0.8994576679865176
  0.0143174634707677  0.1948958992026917  0.1148597954842145
  0.4199638962815158  0.1005423320134753  0.6148597954842145
  0.5143174634707677  0.3994576679865247  0.8194215642680831
  0.0800361037184842  0.6948958992026917  0.6805784357319169
  0.3851402045157926  0.3051041007973083  0.4856825365292323
  0.6805784357319169  0.1005423320134753  0.9856825365292323
  0.1805784357319240  0.1948958992026917  0.5800361037184913
  0.1148597954842145  0.6005423320134824  0.9199638962815087
  0.1948958992026917  0.1148597954842145  0.0143174634707677
  0.6005423320134824  0.1805784357319240  0.4856825365292323
  0.1005423320134753  0.6148597954842145  0.4199638962815158
  0.3051041007973083  0.3194215642680760  0.9199638962815087
  0.8051041007973083  0.4199638962815158  0.8194215642680831
```

0.3051041007973083	0.4856825365292323	0.3851402045157926
0.3994576679865247	0.0800361037184842	0.8851402045157855
0.1005423320134753	0.9856825365292323	0.6805784357319169
0.9199638962815087	0.1148597954842145	0.6005423320134824
0.5143174634707677	0.6148597954842145	0.6948958992026917
0.4199638962815158	0.8194215642680831	0.8051041007973083
0.4856825365292323	0.3851402045157926	0.3051041007973083
0.5800361037184913	0.1805784357319240	0.1948958992026917
0.0800361037184842	0.8851402045157855	0.3994576679865247
0.0143174634707677	0.3194215642680760	0.8994576679865176
0.6948958992026917	0.5143174634707677	0.6148597954842145
0.1948958992026917	0.5800361037184913	0.1805784357319240
0.8994576679865176	0.0143174634707677	0.3194215642680760
0.8994576679865176	0.3851402045157926	0.5800361037184913
0.3994576679865247	0.8194215642680831	0.5143174634707677
0.8051041007973083	0.8851402045157855	0.9856825365292323
0.6148597954842145	0.6948958992026917	0.5143174634707677
0.4856825365292323	0.6005423320134824	0.1805784357319240
0.9199638962815087	0.3051041007973083	0.3194215642680760
0.9856825365292323	0.8051041007973083	0.8851402045157855
0.6148597954842145	0.4199638962815158	0.1005423320134753
0.8194215642680831	0.5143174634707677	0.3994576679865247
0.3194215642680760	0.9199638962815087	0.3051041007973083
0.8851402045157855	0.9856825365292323	0.8051041007973083
0.5800361037184913	0.8994576679865176	0.3851402045157926
0.8194215642680831	0.8051041007973083	0.4199638962815158
0.8851402045157855	0.3994576679865247	0.0800361037184842
0.3194215642680760	0.8994576679865176	0.0143174634707677
0.6948958992026917	0.6805784357319169	0.0800361037184842
0.6005423320134824	0.9199638962815087	0.1148597954842145
0.9856825365292323	0.6805784357319169	0.1005423320134753

Appendix C

Thermo-Calc Database

```
ELEMENT /-   ELECTRON_GAS              0.0000E+00  0.0000E+00  0.0000E+00!
ELEMENT VA   VACUUM                    0.0000E+00  0.0000E+00  0.0000E+00!
ELEMENT AL   FCC_A1                    2.6982E+01  4.5773E+03  2.8321E+01!
ELEMENT ND   DOUBLE_HCP(ABAC)          1.4424E+02  0.0000E+00  1.6990E+01!
ELEMENT O    1/2_MOLE_O2(G)            1.5999E+01  4.3410E+03  1.0252E+02!
ELEMENT SI   DIAMOND_FCC_A4            2.8085E+01  3.2175E+03  1.8820E+01!
ELEMENT Y    HCP_A3                    8.8906E+01  5.9664E+03  4.4434E+01!

SPECIES AL+3                       AL1/+3!
SPECIES ALO3/2                     AL1O1.5!
SPECIES ND+3                       ND1/+3!
SPECIES O-2                        O1/-2!
SPECIES O2                         O2!
SPECIES SI+4                       SI1/+4!
SPECIES SI2O7-6                    O7SI2/-6!
SPECIES SIO2                       O2SI1!
SPECIES SIO4-4                     O4SI1/-4!
SPECIES VA-2                       VA1/-2!
SPECIES Y+3                        Y1/+3!


FUNCTION UN_ASS     2.98140E+02  0.0 ;  3.00000E+02  N !
FUNCTION GO2GAS     2.98140E+02  -6961.74451-76729.7484*T**(-1)
    -51.0057202*T-22.2710136*T*LN(T)-.0101977469*T**2+1.32369208E-06*T**3;
    1.00000E+03  Y
     -13137.5203+525809.556*T**(-1)+25.3200332*T-33.627603*T*LN(T)
    -.00119159274*T**2+1.35611111E-08*T**3;  3.30000E+03  Y
     -27973.4908+8766421.4*T**(-1)+62.5195726*T-37.9072074*T*LN(T)
    -8.50483772E-04*T**2+2.14409777E-08*T**3;  6.00000E+03  N !
FUNCTION GAL2O3_L   2.98140E+02  -1607850.8+405.559491*T-67.4804*T*LN(T)
    -.06747*T**2+1.4205433E-05*T**3+938780*T**(-1);  6.00000E+02  Y
     -1625385.57+712.394972*T-116.258*T*LN(T)-.0072257*T**2
```

```
    +2.78532E-07*T**3+2120700*T**(-1);  1.50000E+03  Y
     -1672662.69+1010.9932*T-156.058*T*LN(T)+.00709105*T**2
    -6.29402E-07*T**3+12366650*T**(-1);  1.91200E+03  Y
     +29178041.6-168360.926*T+21987.1791*T*LN(T)-6.99552951*T**2
    +4.10226192E-04*T**3-7.98843618E+09*T**(-1);  2.32700E+03  Y
     -1757702.05+1344.84833*T-192.464*T*LN(T);  4.00000E+03  N !
FUNCTION GSIO2LIQ   2.98140E+02  -923689.98+316.24766*T-52.17*T*LN(T)
    -.012002*T**2+6.78E-07*T**3+665550*T**(-1);  2.98000E+03  Y
     -957614.21+580.01419*T-87.428*T*LN(T);  4.00000E+03  N !
FUNCTION GHSERSI    2.98140E+02  -8162.609+137.227259*T-22.8317533*T*LN(T)
    -.001912904*T**2-3.552E-09*T**3+176667*T**(-1);  1.68700E+03  Y
     -9457.642+167.271767*T-27.196*T*LN(T)-4.20369E+30*T**(-9);
    6.00000E+03  N !
FUNCTION GOBCC      2.98140E+02  +.5*GO2GAS#+1000000;  3.00000E+03  N !
FUNCTION GHSERAL    2.98140E+02  -7976.15+137.071542*T-24.3671976*T*LN(T)
    -.001884662*T**2-8.77664E-07*T**3+74092*T**(-1);  7.00000E+02  Y
     -11276.24+223.02695*T-38.5844296*T*LN(T)+.018531982*T**2
    -5.764227E-06*T**3+74092*T**(-1);  9.33600E+02  Y
     -11277.683+188.661987*T-31.748192*T*LN(T)-1.234264E+28*T**(-9);
    2.90000E+03  N !
FUNCTION GALLIQ     2.98140E+02  +11005.553-11.840873*T+GHSERAL#
    +7.9401E-20*T**7;  9.33600E+02  Y
     +10481.974-11.252014*T+GHSERAL#+1.234264E+28*T**(-9);  2.90000E+03  N !
FUNCTION GSILIQ     2.98140E+02  +50696.36-30.099439*T+GHSERSI#
    +2.09307E-21*T**7;  1.68700E+03  Y
     +49828.165-29.559069*T+GHSERSI#+4.20369E+30*T**(-9);  3.60000E+03  N !
FUNCTION GCORUND    2.98140E+02  -1707351.3+448.021092*T-67.4804*T*LN(T)
    -.06747*T**2+1.4205433E-05*T**3+938780*T**(-1);  6.00000E+02  Y
     -1724886.06+754.856573*T-116.258*T*LN(T)-.0072257*T**2
    +2.78532E-07*T**3+2120700*T**(-1);  1.50000E+03  Y
     -1772163.19+1053.4548*T-156.058*T*LN(T)+.00709105*T**2
    -6.29402E-07*T**3+12366650*T**(-1);  3.00000E+03  N !
FUNCTION GCRISTOB   2.98140E+02  -601467.73-8140.2255*T+1399.8908*T*LN(T)
    -2.8579085*T**2+.0010408145*T**3-13144016*T**(-1);  3.73000E+02  Y
     -1498711.3+13075.913*T-2178.3561*T*LN(T)+3.493609*T**2
    -.0010762132*T**3+29100273*T**(-1);  4.53000E+02  Y
     -3224538.7+47854.938*T-7860.2125*T*LN(T)+11.817149*T**2
    -.0033651832*T**3+1.2750272E+08*T**(-1);  5.43000E+02  Y
     -943127.51+493.26056*T-77.5875*T*LN(T)+.003040245*T**2
    -4.63118E-07*T**3+2227125*T**(-1);  3.30000E+03  Y
     -973891.99+587.05606*T-87.373*T*LN(T);  4.00000E+03  N !
FUNCTION GAAOMULL   2.98150E+02  -2808415.35+13484407.2*T**(-1)+1600.541*T
    -246.032747*T*LN(T)+.0138772261*T**2-8.37441995E+08*T**(-2);
    6.00000E+03   N !
FUNCTION GASOMULL   2.98150E+02  -2649812+2348905.07*T**(-1)+1050.05906*T
    -165.804515*T*LN(T)-.0160571905*T**2;   6.00000E+03   N !
FUNCTION BASOMULL   2.98150E+02  6543940.51;   6.00000E+03   N !
FUNCTION GSIO2S     2.98140E+02  -900936.64-360.892175*T+61.1323*T*LN(T)
    -.189203605*T**2+4.9509742E-05*T**3-854401*T**(-1);  5.40000E+02  Y
     -1091466.54+2882.67275*T-452.1367*T*LN(T)+.428883845*T**2
```

```
    -9.0917706E-05*T**3+12476689*T**(-1);  7.70000E+02  Y
     -1563481.44+9178.58655*T-1404.5352*T*LN(T)+1.28404426*T**2
    -2.35047657E-04*T**3+56402304*T**(-1);  8.48000E+02  Y
     -928732.923+356.218325*T-58.4292*T*LN(T)-.00515995*T**2-2.47E-10*T**3
    -95113*T**(-1);  1.80000E+03  Y
     -924076.574+281.229013*T-47.451*T*LN(T)-.01200315*T**2
    +6.78127E-07*T**3+665385*T**(-1);  2.96000E+03  Y
     -957997.4+544.992084*T-82.709*T*LN(T);  4.00000E+03  N !
FUNCTION GTRIDYM    2.98140E+02  -918008.73+140.55925*T-25.1574*T*LN(T)
    -.0148714*T**2-2.2791833E-05*T**3+66331*T**(-1);  3.88000E+02  Y
     -921013.31+224.53808*T-37.8701*T*LN(T)-.02368535*T**2-1.6835E-07*T**3;
     4.33000E+02  Y
     -919633.42+210.51651*T-35.605*T*LN(T)-.03049985*T**2+4.6255E-06*T**3
    -162026*T**(-1);  9.00000E+02  Y
     -979377.7+848.3098*T-128.434*T*LN(T)+.03387055*T**2-3.786883E-06*T**3
    +7070800*T**(-1);  1.66800E+03  Y
     -943685.26+493.58035*T-77.5875*T*LN(T)+.003040245*T**2
    -4.63118E-07*T**3+2227125*T**(-1);  3.30000E+03  Y
     -974449.74+587.37585*T-87.373*T*LN(T);  4.00000E+03  N !
FUNCTION GANDAL     2.98150E+02  -2656008.38+1091.19544*T
    -171.253095*T*LN(T)-.0136670814*T**2+2523931.61*T**(-1);   6.00000E+03
     N !
FUNCTION GHSERYY    2.98140E+02  -7347.055+117.532124*T-23.8685*T*LN(T)
    -.003845475*T**2+1.1125E-08*T**3-16486*T**(-1);  1.50000E+03  Y
     -15802.62+229.831717*T-40.2851*T*LN(T)+.0068095*T**2-1.14182E-06*T**3;
     1.79900E+03  Y
     -72946.216+393.885821*T-58.2078433*T*LN(T)+.002436461*T**2
    -7.2627E-08*T**3+20866567*T**(-1);  6.00000E+03  N !
FUNCTION GBCCYY     2.98140E+02  -1861.198+97.522398*T-20.940576*T*LN(T)
    -.007995833*T**2+7.58716E-07*T**3-54349*T**(-1);  1.75200E+03  Y
     -10207.724+195.741984*T-35.0201*T*LN(T);  1.79900E+03  Y
     +104813.954-386.167564*T+39.8075986*T*LN(T)-.019918739*T**2
    +8.41308E-07*T**3-31549963*T**(-1);  6.00000E+03  N !
FUNCTION GLIQYY     2.98140E+02  +3934.121+59.921688*T-14.8146562*T*LN(T)
    -.015623487*T**2+1.442946E-06*T**3-140695*T**(-1);  1.79900E+03  Y
     -13337.609+258.004539*T-43.0952*T*LN(T);  6.00000E+03  N !
FUNCTION GY2O3R     2.98150E+02  -1981736+763.71851*T-125.692*T*LN(T)
    -.00558*T**2+2344020.5*T**(-1)-1.1730556E+08*T**(-2);   6.00000E+03   N
    !
FUNCTION GY2O3LIQ   2.98150E+02  +2*GLIQYY#+1.5*GO2GAS#-7946.7+94.32*T
    -1813375.49+149.20552*T;   6.00000E+03   N !
FUNCTION GYAG       2.98150E+02  -7363443.37+2714.0547*T-438.9177*T*LN(T)
    -.034315335*T**2+4800831.7*T**(-1);   6.00000E+03   N !
FUNCTION GYAM       2.98140E+02  -5686303.14+2239.26502*T
    -368.158373*T*LN(T)-.018363228*T**2+4310328.16*T**(-1);  3.00000E+03  N
    !
FUNCTION GYSM       2.98140E+02  +1.0666667*GYAM#+150000;  3.00000E+03  N !
FUNCTION H17        2.98150E+02  48984.7096;   6.00000E+03   N !
FUNCTION S18        2.98150E+02  -10.7175406;   6.00000E+03   N !
FUNCTION GYAP       2.98150E+02  -72500+H17#+4.2*T+S18#*T+.5*GCOROUND#
```

```
    +.5*GY2O3R#;   6.00000E+03   N !
FUNCTION GY2SIO5    2.98140E+02  -2962274+1057.09397*T-181.294814*T*LN(T)
    -.0110113475*T**2+1803500.83*T**(-1);  3.00000E+03  N !
FUNCTION GY2SI22    2.98150E+02  -3924305+1589.97798*T-264.23561*T*LN(T)
    -.0129019088*T**2+3559383.17*T**(-1);   6.00000E+03   N !
FUNCTION GY2SI21    2.98150E+02  +GY2SI22#+2038.92-1.1*T;   6.00000E+03   N
    !
FUNCTION GY2SI23    2.98150E+02  +GY2SI22#-1785.28+1.1*T;   6.00000E+03   N
    !
FUNCTION GY2SI24    2.98150E+02  +GY2SI23#-1609.3+1.1*T;   6.00000E+03   N !
FUNCTION LOYSIO20   2.98150E+02  +64275.7706-95.015847*T;   6.00000E+03   N
    !
FUNCTION LOYSIO21   2.98150E+02  -577744.591+179.543138*T;   6.00000E+03
    N !
FUNCTION LOYSIO22   298.15 0.0; 6000.00  N !
FUNCTION LOYSIO23   298.15 0.0; 6000.00  N !
FUNCTION LOYSIO40   2.98150E+02  +1018615.91-560*T;   6.00000E+03   N !
FUNCTION ALV1       2.98150E+02  -7.18757673E+04;   6.00000E+03   N !
FUNCTION ALV2       2.98150E+02  -5.88068219E+01;   6.00000E+03   N !
FUNCTION ALV3       2.98150E+02  -4.11973465E+04;   6.00000E+03   N !
FUNCTION ALV4       2.98150E+02  -4.58427858E+01;   6.00000E+03   N !
FUNCTION ALV5       2.98150E+02  -1.04334416E+05;   6.00000E+03   N !
FUNCTION ALV6       2.98150E+02  -1.00570788E+02;   6.00000E+03   N !
FUNCTION ALV10      2.98150E+02   2.91926258E+05;   6.00000E+03   N !
FUNCTION ALV11      2.98150E+02  -3.64059856E+02;   6.00000E+03   N !
FUNCTION ALV12      2.98150E+02  -1.54644731E+05;   6.00000E+03   N !
FUNCTION ALV13      298.15 0.0; 6000.00  N !
FUNCTION F12999T    2.98140E+02  -6960.6927-51.1831467*T-22.25862*T*LN(T)
    -.01023867*T**2+1.339947E-06*T**3-76749.55*T**(-1);  9.00000E+02  Y
     -13136.0174+24.7432966*T-33.55726*T*LN(T)-.0012348985*T**2
    +1.66943333E-08*T**3+539886*T**(-1);  3.70000E+03  Y
     +14154.6459-51.485458*T-24.47978*T*LN(T)-.002634759*T**2
    +6.01544333E-08*T**3-15120935*T**(-1);  9.60000E+03  Y
     -314316.629+515.068037*T-87.56143*T*LN(T)+.0025787245*T**2
    -1.878765E-08*T**3+2.9052515E+08*T**(-1);  1.85000E+04  Y
     -108797.175+288.483019*T-63.737*T*LN(T)+.0014375*T**2-9E-09*T**3
    +.25153895*T**(-1);  2.00000E+04  N !
FUNCTION F12511T    2.98140E+02  -1845971.56+594.169159*T-109.7746*T*LN(T)
    -.02111666*T**2+1.06283883E-06*T**3+465333.3*T**(-1);  2.33300E+03  Y
     -1874805.28+952.626942*T-160*T*LN(T)-5.29959E-14*T**2
    +2.76159167E-18*T**3-9.109795E-05*T**(-1);  2.59300E+03  Y
     -1978525.28+1307.04977*T-200*T*LN(T)+3.0384975E-16*T**2
    -9.41298333E-21*T**3+1.7517065E-06*T**(-1);  6.00000E+03  N !
FUNCTION F12468T    2.98140E+02  -8402.93004+111.10259*T-27.0858*T*LN(T)
    +5.56125E-04*T**2-2.6923E-06*T**3+34887.05*T**(-1);  9.00000E+02  Y
     -6984.08331+83.6628173*T-22.7536*T*LN(T)-.00420402*T**2-1.802E-06*T**3;
      1.12800E+03  Y
     -21059.4856+242.363001*T-44.5596*T*LN(T);  1.28900E+03  Y
     -26506.5418+276.852383*T-48.7854*T*LN(T);  1.80000E+03  N !
FUNCTION ND_L       2.98150E+02  +F12468T#+10171.3-8.22626782*T;
```

```
    6.00000E+03   N !
FUNCTION ND2O3_L    2.98150E+02  +F12511T#+125000-48.2067104*T;
    6.00000E+03   N !
FUNCTION GND2O3A    2.98150E+02  -1847329+637.4243*T-116.358*T*LN(T)
    -.01468*T**2+711000*T**(-1)-10000000*T**(-2);   6.00000E+03   N !
FUNCTION GND2O3H    2.98150E+02  +33189-13.986*T+GND2O3A#;   6.00000E+03
    N !
FUNCTION GND2O3X    2.98150E+02  +44489-18.555*T+GND2O3A#;   6.00000E+03
    N !
FUNCTION GND2O3B    2.98150E+02  -399+1.684*T+GND2O3A#;   6.00000E+03   N !
FUNCTION GND2O3C    2.98150E+02  -1311+6.55*T+GND2O3A#;   6.00000E+03   N !
FUNCTION GND2O3L    2.98150E+02  +143621-56.785*T+GND2O3A#;   6.00000E+03
    N !
FUNCTION SIV1       2.98150E+02  -139228.73;   6.00000E+03   N !
FUNCTION SIV2       2.98150E+02  6.8548164;   6.00000E+03   N !
FUNCTION SIV3       2.98150E+02  -1140665.5;   6.00000E+03   N !
FUNCTION SIV4       2.98150E+02  10.881921;   6.00000E+03   N !
FUNCTION SIV5       2.98150E+02  -127444.18;   6.00000E+03   N !
FUNCTION SIV6       2.98150E+02  -18.429296;   6.00000E+03   N !
FUNCTION SIV20      2.98150E+02  -356870.98;   6.00000E+03   N !
FUNCTION SIV21      2.98150E+02  52.131791;   6.00000E+03   N !
FUNCTION SIV22      2.98150E+02  -768442.71;   6.00000E+03   N !
FUNCTION SIV23      2.98150E+02  225.50894;   6.00000E+03   N !
FUNCTION SIV30      2.98150E+02  -171104.14;   6.00000E+03   N !
FUNCTION SIV31      2.98150E+02  103.63242;   6.00000E+03   N !
FUNCTION SIV40      2.98150E+02  731821.92;   6.00000E+03   N !
FUNCTION SIV41      2.98150E+02  -573.97343;   6.00000E+03   N !
FUNCTION TOTV1      2.98150E+02 -1.1638919E+05;   6.00000E+03   N !
FUNCTION TOTV2      298.15      -105.808; 6000.00  N !
FUNCTION TOTV10     2.98150E+02  5.6000000E+04;   6.00000E+03   N !
FUNCTION TOTV11     2.98150E+02  -5;   6.00000E+03   N !
FUNCTION TOTV12      298.15 0.0; 6000.00  N !
FUNCTION TOTV13      298.15 0.0; 6000.00  N !
FUNCTION TOTV14     2.98150E+02 0;   6.00000E+03   N !
FUNCTION TOTV15      298.15 0.0; 6000.00  N !
FUNCTION YV1        2.98150E+02  684953.779;   6.00000E+03   N !
FUNCTION YV2        2.98150E+02  -276.448921;   6.00000E+03   N !
FUNCTION YV3        2.98150E+02  547912.24;   6.00000E+03   N !
FUNCTION YV4        2.98150E+02  -222.01392;   6.00000E+03   N !
FUNCTION YV10       2.98150E+02  -322541.678;   6.00000E+03   N !
FUNCTION YV11       2.98150E+02  140.28721;   6.00000E+03   N !
FUNCTION YV12       2.98150E+02  28164.6977;   6.00000E+03   N !
FUNCTION YV13       298.15 0.0; 6000.00  N !
FUNCTION YV20       2.98150E+02  99651.2541;   6.00000E+03   N !
FUNCTION YV21       2.98150E+02  -45.6588127;   6.00000E+03   N !
FUNCTION YV30       2.98150E+02  -148571.233;   6.00000E+03   N !
FUNCTION YV31       2.98150E+02  14.2388274;   6.00000E+03   N !
FUNCTION YV32       2.98150E+02  64687.5564;   6.00000E+03   N !
FUNCTION YV33       298.15 0.0; 6000.00  N !
FUNCTION YV40       2.98150E+02  -488011.718;   6.00000E+03   N !
```

```
FUNCTION YV41       2.98150E+02  162.775957;   6.00000E+03   N !
FUNCTION YV42       2.98150E+02  -97791.5755;   6.00000E+03   N !
FUNCTION YV43       2.98150E+02  97.235906;   6.00000E+03   N !
FUNCTION YV90       2.98150E+02  72852.4273;   6.00000E+03   N !
FUNCTION YV91       2.98150E+02  -26.9336241;   6.00000E+03   N !
FUNCTION YV92       2.98150E+02  69774.1266;   6.00000E+03   N !
FUNCTION YV93       298.15 0.0; 6000.00  N !
FUNCTION YV94       2.98150E+02  62640.8347;   6.00000E+03   N !
FUNCTION YV95       298.15 0.0; 6000.00  N !

TYPE_DEFINITION % SEQ *!
DEFINE_SYSTEM_DEFAULT SPECIE 2 !
DEFAULT_COMMAND DEF_SYS_ELEMENT VA !


PHASE IONIC_LIQ:Y %  2 1   1 !
   CONSTITUENT IONIC_LIQ:Y :AL+3,ND+3,SI+4,Y+3 : O-2,SIO4-4,VA,ALO3/2,SIO2
   :  !

  PARAMETER G(IONIC_LIQ,AL+3:O-2;0)  2.98150E+02  +GAL2O3_L#+1000000;
 6.00000E+03   N REF:0 !
  PARAMETER G(IONIC_LIQ,ND+3:O-2;0)  2.98150E+02  +143621-56.785*T+GND2O3A#;
    6.00000E+03   N REF:0 !
  PARAMETER G(IONIC_LIQ,SI+4:O-2;0)  2.98150E+02  +2*GSIO2LIQ#+2000000;
 6.00000E+03   N REF:0 !
  PARAMETER G(IONIC_LIQ,Y+3:O-2;0)  2.98150E+02  +GY2O3LIQ#;   6.00000E+03
  N REF:0 !
      PARA G(IONIC_LIQ,AL+3:SIO4-4;0) 298.15 0; 6000 N!
  PARAMETER G(IONIC_LIQ,ND+3:SIO4-4;0)  2.98150E+02  +2*GND2O3L#
 +3*GSIO2LIQ#+SIV30#+SIV31#*T;   6.00000E+03   N REF:0 !
  PARAMETER G(IONIC_LIQ,SI+4:SIO4-4;0)  2.98150E+02  +8*GSIO2LIQ#+2000000;
  6.00000E+03   N REF:0 !
  PARAMETER G(IONIC_LIQ,Y+3:SIO4-4;0)  2.98150E+02  +2*GY2O3LIQ#
 +3*GSIO2LIQ#+54487.7131-139.680116*T;   6.00000E+03   N REF:0 !
  PARAMETER G(IONIC_LIQ,AL+3:VA;0)  2.98150E+02  +GALLIQ#;   6.00000E+03
 N REF:0 !
      PARA G(IONIC_LIQ,ND+3:VA;0) 298.15 0; 6000 N!
  PARAMETER G(IONIC_LIQ,SI+4:VA;0)  2.98150E+02  +GSILIQ#;   6.00000E+03
 N REF:0 !
  PARAMETER G(IONIC_LIQ,Y+3:VA;0)  2.98150E+02  +GLIQYY#;   6.00000E+03   N
 REF:0 !
  PARAMETER G(IONIC_LIQ,ALO3/2;0)  2.98150E+02  +.5*GAL2O3_L#;
 6.00000E+03   N REF:0 !
  PARAMETER G(IONIC_LIQ,SIO2;0)  2.98150E+02  +GSIO2LIQ#;   6.00000E+03   N
 REF:0 !
  PARAMETER G(IONIC_LIQ,AL+3:O-2,VA;0)  2.98150E+02  -829000+106*T;
 6.00000E+03   N REF:0 !
  PARAMETER G(IONIC_LIQ,ND+3,Y+3:O-2;0)  2.98150E+02  +YV1#+YV2#*T;
 6.00000E+03   N REF:0 !
  PARAMETER G(IONIC_LIQ,ND+3,Y+3:O-2;1)  2.98150E+02  +YV3#+YV4#*T;
```

```
6.00000E+03   N REF:0 !
 PARAMETER G(IONIC_LIQ,ND+3:O-2,ALO3/2;0)  2.98150E+02  +ALV10#+ALV11#*T;
 6.00000E+03   N REF:0 !
 PARAMETER G(IONIC_LIQ,ND+3:O-2,ALO3/2;1)  2.98150E+02  +ALV12#+ALV13#*T;
 6.00000E+03   N REF:0 !
 PARAMETER G(IONIC_LIQ,ND+3:O-2,SIO4-4;0)  2.98150E+02  +SIV40#+SIV41#*T;
 6.00000E+03   N REF:0 !
 PARAMETER G(IONIC_LIQ,ND+3:O-2,SIO2;0)  2.98150E+02  +SIV20#+SIV21#*T;
6.00000E+03   N REF:0 !
 PARAMETER G(IONIC_LIQ,ND+3:O-2,SIO2;1)  2.98150E+02  +SIV22#+SIV23#*T;
6.00000E+03   N REF:0 !
 PARAMETER G(IONIC_LIQ,SI+4:O-2,VA;0)  2.98150E+02  -1482600+14.4*T;
6.00000E+03   N REF:0 !
 PARAMETER G(IONIC_LIQ,Y+3:O-2,ALO3/2;0)  2.98150E+02  -139345.93
+20.1992333*T;   6.00000E+03   N REF:0 !
 PARAMETER G(IONIC_LIQ,Y+3:O-2,ALO3/2;1)  2.98150E+02  +245749.27
-141.491633*T;   6.00000E+03   N REF:0 !
 PARAMETER G(IONIC_LIQ,Y+3:O-2,VA;0)  2.98150E+02  +209819.073
-118.227607*T;   6.00000E+03   N REF:0 !
 PARAMETER G(IONIC_LIQ,Y+3:O-2,SIO4-4;0)  2.98150E+02  +LOYSIO40#;
6.00000E+03   N REF:0 !
 PARAMETER G(IONIC_LIQ,Y+3:O-2,SIO4-4,ALO3/2;0)  2.98150E+02  -1700000;
6.00000E+03   N REF:0 !
 PARAMETER G(IONIC_LIQ,Y+3:O-2,SIO2;0)  2.98150E+02  +LOYSIO20#;
6.00000E+03   N REF:0 !
 PARAMETER G(IONIC_LIQ,Y+3:O-2,SIO2;1)  2.98150E+02  +LOYSIO21#;
6.00000E+03   N REF:0 !
 PARAMETER G(IONIC_LIQ,Y+3:O-2,SIO2;2)  2.98150E+02  +LOYSIO22#;
6.00000E+03   N REF:0 !
 PARAMETER G(IONIC_LIQ,Y+3:O-2,SIO2;3)  2.98150E+02  +LOYSIO23#;
6.00000E+03   N REF:0 !
 PARAMETER G(IONIC_LIQ,ND+3:SIO4-4,SIO2;0)  2.98150E+02  +2*SIV20#
+2*SIV21#*T;   6.00000E+03   N REF:0 !
 PARAMETER G(IONIC_LIQ,ND+3:SIO4-4,SIO2;1)  2.98150E+02  +2*SIV22#
+2*SIV23#*T;   6.00000E+03   N REF:0 !
 PARAMETER G(IONIC_LIQ,SI+4:SIO4-4,VA;0)  2.98150E+02  +250*T;
6.00000E+03   N REF:0 !
 PARAMETER G(IONIC_LIQ,Y+3:SIO4-4,SIO2;0)  2.98150E+02  +2*LOYSIO20#;
6.00000E+03   N REF:0 !
 PARAMETER G(IONIC_LIQ,Y+3:SIO4-4,SIO2;1)  2.98150E+02  +2*LOYSIO21#;
6.00000E+03   N REF:0 !
 PARAMETER G(IONIC_LIQ,Y+3:SIO4-4,SIO2;2)  2.98150E+02  +2*LOYSIO22#;
6.00000E+03   N REF:0 !
 PARAMETER G(IONIC_LIQ,Y+3:SIO4-4,SIO2;3)  2.98150E+02  +2*LOYSIO23#;
6.00000E+03   N REF:0 !
 PARAMETER G(IONIC_LIQ,Y+3:SIO4-4,ALO3/2;0)  2.98150E+02  +510558.256
-8.61930838*T;   6.00000E+03   N REF:0 !
 PARAMETER G(IONIC_LIQ,Y+3:SIO4-4,ALO3/2;1)  2.98150E+02  344332.477;
6.00000E+03   N REF:0 !
 PARAMETER G(IONIC_LIQ,Y+3:SIO4-4,ALO3/2,SIO2;0)  2.98150E+02  -2000000;
```

```
 6.00000E+03   N REF:0 !
  PARAMETER G(IONIC_LIQ,AL+3,Y+3:VA;0)  2.98150E+02  -163742.69+31.95199*T;
   6.00000E+03   N REF:0 !
  PARAMETER G(IONIC_LIQ,AL+3,Y+3:VA;1)  2.98150E+02  -45859.83+9.24704*T;
 6.00000E+03   N REF:0 !
  PARAMETER G(IONIC_LIQ,AL+3,Y+3:VA;2)  2.98150E+02  +54887.91-10.97627*T;
  6.00000E+03   N REF:0 !
  PARAMETER G(IONIC_LIQ,AL+3,Y+3:VA;3)  2.98150E+02  +19590.51-3.9181*T;
 6.00000E+03   N REF:0 !
  PARAMETER G(IONIC_LIQ,AL+3,Y+3:VA;4)  2.98150E+02  -27175.02+5.43281*T;
 6.00000E+03   N REF:0 !
  PARAMETER G(IONIC_LIQ,AL+3:VA,ALO3/2;0)  2.98150E+02  +110000+46*T;
 6.00000E+03   N REF:0 !
  PARAMETER G(IONIC_LIQ,SI+4,Y+3:VA;0)  2.98150E+02  -212656.12+25.83471*T;
   6.00000E+03   N REF:0 !
  PARAMETER G(IONIC_LIQ,SI+4,Y+3:VA;1)  2.98150E+02  +13977.08-31.08941*T;
  6.00000E+03   N REF:0 !
  PARAMETER G(IONIC_LIQ,SI+4,Y+3:VA;2)  2.98150E+02  +62049.23-50.31476*T;
  6.00000E+03   N REF:0 !
  PARAMETER G(IONIC_LIQ,SI+4:VA,SIO2;0)  2.98150E+02  +250*T;   6.00000E+03
   N REF:0 !
  PARAMETER G(IONIC_LIQ,ALO3/2,SIO2;0)  2.98150E+02  +80121-30*T;
 6.00000E+03   N REF:0 !
  PARAMETER G(IONIC_LIQ,ALO3/2,SIO2;1)  2.98150E+02  -96000+44*T;
 6.00000E+03   N REF:0 !


PHASE AL2Y  %  2 2   1 !
   CONSTITUENT AL2Y  :AL : Y :  !

  PARAMETER G(AL2Y,AL:Y;0)  2.98150E+02  -151200+16.74276*T+2*GHSERAL#
 +GHSERYY#;   6.00000E+03   N REF:0 !


PHASE AL2Y3  %  2 2   3 !
   CONSTITUENT AL2Y3  :AL : Y :  !

  PARAMETER G(AL2Y3,AL:Y;0)  2.98150E+02  -200000+20.2*T+2*GHSERAL#
 +3*GHSERYY#;   6.00000E+03   N REF:0 !


PHASE AL3Y  %  2 3   1 !
   CONSTITUENT AL3Y  :AL : Y :  !

  PARAMETER G(AL3Y,AL:Y;0)  2.98150E+02  -190000+42.4514*T+3*GHSERAL#
 +GHSERYY#;   6.00000E+03   N REF:0 !


PHASE ALY  %  2 1   1 !
   CONSTITUENT ALY  :AL : Y :  !
```

```
  PARAMETER G(ALY,AL:Y;0)  2.98150E+02  -90000+8.71568*T+GHSERAL#+GHSERYY#;
   6.00000E+03   N REF:0 !


PHASE ALY2  %  2 1   2 !
   CONSTITUENT ALY2  :AL : Y :  !

  PARAMETER G(ALY2,AL:Y;0)  2.98150E+02  -105000+13.5*T+GHSERAL#+2*GHSERYY#;
    6.00000E+03   N REF:0 !


PHASE ANDALUSITE  %  4 1   1   1   5 !
   CONSTITUENT ANDALUSITE  :AL+3 : AL+3 : SI+4 : O-2 :  !

  PARAMETER G(ANDALUSITE,AL+3:AL+3:SI+4:O-2;0)  2.98150E+02  +GANDAL#;
 6.00000E+03   N REF:0 !


PHASE BCC_A2  %  2 1   3 !
   CONSTITUENT BCC_A2  :Y : O,VA :  !

  PARAMETER G(BCC_A2,Y:O;0)  2.98150E+02  +GBCCYY#+1.5*GO2GAS#-225000+137*T;
    6.00000E+03   N REF:0 !
  PARAMETER G(BCC_A2,Y:VA;0)  2.98150E+02  +GBCCYY#;   6.00000E+03   N
 REF:0 !
  PARAMETER G(BCC_A2,Y:O,VA;0)  2.98150E+02  -2283384.08+86*T;
 6.00000E+03   N REF:0 !
  PARAMETER G(BCC_A2,Y:O,VA;1)  2.98150E+02  -757192.505;   6.00000E+03   N
 REF:0 !


PHASE CORUNDUM  %  3 2   1   3 !
   CONSTITUENT CORUNDUM  :AL+3 : VA : O-2 :  !

  PARAMETER G(CORUNDUM,AL+3:VA:O-2;0)  2.98150E+02  +GCORUND#;
 6.00000E+03   N REF:0 !


PHASE CRISTOBALITE  %  1  1.0  !
   CONSTITUENT CRISTOBALITE  :SIO2 :  !

  PARAMETER G(CRISTOBALITE,SIO2;0)  2.98150E+02  +GCRISTOB#;   6.00000E+03
  N REF:0 !


PHASE DIAMOND_FCC_A4  %  1  1.0  !
   CONSTITUENT DIAMOND_FCC_A4  :O,SI :  !

  PARAMETER G(DIAMOND_FCC_A4,O;0)  2.98150E+02  +.5*GO2GAS#+1000000;
```

```
 6.00000E+03   N REF:0 !
  PARAMETER G(DIAMOND_FCC_A4,SI;0)  2.98150E+02  +GHSERSI#;   6.00000E+03
 N REF:0 !
  PARAMETER G(DIAMOND_FCC_A4,O,SI;0)  2.98150E+02  -340000+85.3*T;
 6.00000E+03   N REF:0 !


PHASE FCC_A1  %  2 1   1 !
   CONSTITUENT FCC_A1  :AL,O,SI : VA :  !

  PARAMETER G(FCC_A1,AL:VA;0)  2.98150E+02  +GHSERAL#;   6.00000E+03   N
 REF:0 !
  PARAMETER G(FCC_A1,O:VA;0)  2.98150E+02  +GOBCC#;   6.00000E+03   N REF:0 !
  PARAMETER G(FCC_A1,SI:VA;0)  2.98140E+02  +51000-21.8*T+GHSERSI#;
 3.60000E+03  N REF:0 !
  PARAMETER G(FCC_A1,AL,SI:VA;0)  2.98140E+02  -3341.59-.43295*T;
 2.00000E+03  N REF:0 !


PHASE GAS  %  1  1.0  !
   CONSTITUENT GAS  :O2 :  !

  PARAMETER G(GAS,O2;0)  2.98150E+02  +GO2GAS#+RTLNP#;   6.00000E+03   N
 REF:0 !


PHASE HCP_A3  %  2 1   1 !
   CONSTITUENT HCP_A3  :Y : O,VA :  !

  PARAMETER G(HCP_A3,Y:O;0)  2.98150E+02  +GHSERYY#+.5*GO2GAS#-589780.33
 +71.3300504*T;   6.00000E+03   N REF:0 !
  PARAMETER G(HCP_A3,Y:VA;0)  2.98150E+02  +GHSERYY#;   6.00000E+03   N
 REF:0 !


PHASE MULLITE  %  4 1   1   1   5 !
   CONSTITUENT MULLITE  :AL+3 : AL+3 : AL+3,SI+4 : O-2,VA :  !

  PARAMETER G(MULLITE,AL+3:AL+3:AL+3:O-2;0)  2.98150E+02  +GAAOMULL#;
 6.00000E+03   N REF:0 !
  PARAMETER G(MULLITE,AL+3:AL+3:SI+4:O-2;0)  2.98150E+02  +GASOMULL#;
 6.00000E+03   N REF:0 !
      PARA G(MULLITE,AL+3:AL+3:AL+3:VA;0) 298.15 0; 6000 N!
  PARAMETER G(MULLITE,AL+3:AL+3:SI+4:VA;0)  2.98150E+02  +GASOMULL#
 +BASOMULL#;   6.00000E+03   N REF:0 !
  PARAMETER G(MULLITE,AL+3:AL+3:AL+3,SI+4:O-2;0)  2.98150E+02  -498147
 +64.083*T;   6.00000E+03   N REF:0 !


PHASE ND14SI9O39  %  3 14   9   39 !
```

```
   CONSTITUENT ND14SI9O39  :ND+3 : SI+4 : O-2 :  !

  PARAMETER G(ND14SI9O39,ND+3:SI+4:O-2;0)  2.98150E+02  +7*GND2O3A#
 +9*GSIO2S#+SIV3#+SIV4#*T;   6.00000E+03   N REF:0 !


PHASE ND2O3A  %  2 2   3 !
   CONSTITUENT ND2O3A  :ND+3,Y+3 : O-2 :  !

  PARAMETER G(ND2O3A,ND+3:O-2;0)  2.98150E+02  +GND2O3A#;   6.00000E+03   N
 REF:0 !
  PARAMETER G(ND2O3A,Y+3:O-2;0)  2.98150E+02  +GY2O3R#+YV92#+YV93#*T;
 6.00000E+03   N REF:0 !
  PARAMETER G(ND2O3A,ND+3,Y+3:O-2;0)  2.98150E+02  +YV30#+YV31#*T;
 6.00000E+03   N REF:0 !
  PARAMETER G(ND2O3A,ND+3,Y+3:O-2;1)  2.98150E+02  +YV32#+YV33#*T;
 6.00000E+03   N REF:0 !


PHASE ND2O3B  %  2 2   3 !
   CONSTITUENT ND2O3B  :ND+3,Y+3 : O-2 :  !

  PARAMETER G(ND2O3B,ND+3:O-2;0)  2.98150E+02  +GND2O3B#;   6.00000E+03   N
 REF:0 !
  PARAMETER G(ND2O3B,Y+3:O-2;0)  2.98150E+02  +GY2O3R#+YV94#+YV95#*T;
 6.00000E+03   N REF:0 !
  PARAMETER G(ND2O3B,ND+3,Y+3:O-2;0)  2.98150E+02  +YV40#+YV41#*T;
 6.00000E+03   N REF:0 !
  PARAMETER G(ND2O3B,ND+3,Y+3:O-2;1)  2.98150E+02  +YV42#+YV43#*T;
 6.00000E+03   N REF:0 !


PHASE ND2O3X  %  2 2   3 !
   CONSTITUENT ND2O3X  :ND+3,Y+3 : O-2 :  !

  PARAMETER G(ND2O3X,ND+3:O-2;0)  2.98150E+02  +GND2O3X#;   6.00000E+03   N
 REF:0 !
  PARAMETER G(ND2O3X,Y+3:O-2;0)  2.98150E+02  +GY2O3R#+YV90#+YV91#*T;
 6.00000E+03   N REF:0 !
  PARAMETER G(ND2O3X,ND+3,Y+3:O-2;0)  2.98150E+02  +YV20#+YV21#*T;
 6.00000E+03   N REF:0 !


PHASE ND2SI2O7  %  3 2   2   7 !
   CONSTITUENT ND2SI2O7  :ND+3 : SI+4 : O-2 :  !

  PARAMETER G(ND2SI2O7,ND+3:SI+4:O-2;0)  2.98150E+02  +GND2O3A#+2*GSIO2S#
 +SIV5#+SIV6#*T;   6.00000E+03   N REF:0 !
```

```
PHASE ND2SIO5  %  3 2   1   5 !
   CONSTITUENT ND2SIO5  :ND+3 : SI+4 : O-2 :  !

  PARAMETER G(ND2SIO5,ND+3:SI+4:O-2;0)  2.98150E+02  +GND2O3A#+GSIO2S#
 +SIV1#+SIV2#*T;   6.00000E+03   N REF:0 !


PHASE ND4AL2O9  %  3 4   2   9 !
   CONSTITUENT ND4AL2O9  :ND+3 : AL+3 : O-2 :  !

  PARAMETER G(ND4AL2O9,ND+3:AL+3:O-2;0)  2.98150E+02  +2*GND2O3A#+GCORUND#
 +ALV5#+ALV6#*T;   6.00000E+03   N REF:0 !


PHASE NDAL11O18  %  3 1   11   18 !
   CONSTITUENT NDAL11O18  :ND+3 : AL+3 : O-2 :  !

  PARAMETER G(NDAL11O18,ND+3:AL+3:O-2;0)  2.98150E+02  +.5*GND2O3A#
 +5.5*GCORUND#+ALV1#+ALV2#*T;   6.00000E+03   N REF:0 !


PHASE NDALO3  %  3 1   1   3 !
   CONSTITUENT NDALO3  :ND+3 : AL+3 : O-2 :  !

  PARAMETER G(NDALO3,ND+3:AL+3:O-2;0)  2.98150E+02  +.5*GND2O3A#
 +.5*GCORUND#+ALV3#+ALV4#*T;   6.00000E+03   N REF:0 !


PHASE QUARTZ  %  1  1.0  !
   CONSTITUENT QUARTZ  :SIO2 :  !

  PARAMETER G(QUARTZ,SIO2;0)  2.98150E+02  +GSIO2S#;   6.00000E+03   N
 REF:0 !


PHASE SILLIMANITE  %  4 1   1   1   5 !
   CONSTITUENT SILLIMANITE  :AL+3 : AL+3 : SI+4 : O-2 :  !

      PARA G(SILLIMANITE,AL+3:AL+3:SI+4:O-2;0) 298.15 0; 6000 N!


PHASE TRIDYMITE  %  1  1.0  !
   CONSTITUENT TRIDYMITE  :SIO2 :  !

  PARAMETER G(TRIDYMITE,SIO2;0)  2.98150E+02  +GTRIDYM#;   6.00000E+03   N
 REF:0 !


PHASE Y2O3H  %  2 2   3 !
   CONSTITUENT Y2O3H  :ND+3,Y+3 : O-2,VA-2 :  !
```

```
 PARAMETER G(Y2O3H,ND+3:O-2;0)  2.98150E+02  +GND2O3H#;   6.00000E+03   N
REF:0 !
 PARAMETER G(Y2O3H,Y+3:O-2;0)  2.98150E+02  -1956736+754.10313*T
-125.692*T*LN(T)-.00558*T**2+2344020.5*T**(-1)-1.1730556E+08*T**(-2);
6.00000E+03   N REF:0 !
     PARA G(Y2O3H,ND+3:VA-2;0) 298.15 0; 6000 N!
 PARAMETER G(Y2O3H,Y+3:VA-2;0)  2.98150E+02  +340026.026-107.540058*T
+2*GHSERYY#;   6.00000E+03   N REF:0 !


PHASE Y2O3R  %  2 2   3 !
   CONSTITUENT Y2O3R  :ND+3,Y+3 : O-2,VA-2 :  !

 PARAMETER G(Y2O3R,ND+3:O-2;0)  2.98150E+02  +GND2O3C#;   6.00000E+03   N
REF:0 !
 PARAMETER G(Y2O3R,Y+3:O-2;0)  2.98150E+02  +GY2O3R#;   6.00000E+03   N
REF:0 !
     PARA G(Y2O3R,ND+3:VA-2;0) 298.15 0; 6000 N!
 PARAMETER G(Y2O3R,Y+3:VA-2;0)  2.98150E+02  +340026.026-107.540058*T
+2*GHSERYY#;   6.00000E+03   N REF:0 !
 PARAMETER G(Y2O3R,ND+3,Y+3:O-2;0)  2.98150E+02  +YV10#+YV11#*T;
6.00000E+03   N REF:0 !
 PARAMETER G(Y2O3R,ND+3,Y+3:O-2;1)  2.98150E+02  +YV12#+YV13#*T;
6.00000E+03   N REF:0 !


PHASE Y2SI21  %  3 1   1   1 !
   CONSTITUENT Y2SI21  :Y+3 : Y+3 : SI2O7-6 :  !

 PARAMETER G(Y2SI21,Y+3:Y+3:SI2O7-6;0)  2.98150E+02  +GY2SI21#;
6.00000E+03   N REF:0 !


PHASE Y2SI22  %  3 1   1   1 !
   CONSTITUENT Y2SI22  :Y+3 : Y+3 : SI2O7-6 :  !

 PARAMETER G(Y2SI22,Y+3:Y+3:SI2O7-6;0)  2.98150E+02  +GY2SI22#;
6.00000E+03   N REF:0 !


PHASE Y2SI23  %  3 1   1   1 !
   CONSTITUENT Y2SI23  :Y+3 : Y+3 : SI2O7-6 :  !

 PARAMETER G(Y2SI23,Y+3:Y+3:SI2O7-6;0)  2.98150E+02  +GY2SI23#;
6.00000E+03   N REF:0 !


PHASE Y2SI24  %  3 1   1   1 !
   CONSTITUENT Y2SI24  :Y+3 : Y+3 : SI2O7-6 :  !
```

```
  PARAMETER G(Y2SI24,Y+3:Y+3:SI2O7-6;0)  2.98150E+02  +GY2SI24#;
 6.00000E+03   N REF:0 !


PHASE Y2SIO5  %  4 1   1   1   1 !
   CONSTITUENT Y2SIO5  :Y+3 : Y+3 : SIO4-4 : O-2 :  !

  PARAMETER G(Y2SIO5,Y+3:Y+3:SIO4-4:O-2;0)  2.98150E+02  +GY2SIO5#;
 6.00000E+03   N REF:0 !


PHASE YAG_AL5O12Y3  %  3 5   3   12 !
   CONSTITUENT YAG_AL5O12Y3  :AL+3 : ND+3,Y+3 : O-2 :  !

  PARAMETER G(YAG_AL5O12Y3,AL+3:ND+3:O-2;0)  2.98150E+02  +1.5*GND2O3A#
 +2.5*GCORUND#+TOTV1#+TOTV2#*T;   6.00000E+03   N REF:0 !
  PARAMETER G(YAG_AL5O12Y3,AL+3:Y+3:O-2;0)  2.98150E+02  +GYAG#;
 6.00000E+03   N REF:0 !
  PARAMETER G(YAG_AL5O12Y3,AL+3:ND+3,Y+3:O-2;0)  2.98150E+02  +TOTV10#
  +TOTV11#*T;     6.00000E+03   N REF:0 !
  PARAMETER G(YAG_AL5O12Y3,AL+3:ND+3,Y+3:O-2;1)  2.98150E+02  +TOTV12#
  +TOTV13#*T;     6.00000E+03   N REF:0 !
  PARAMETER G(YAG_AL5O12Y3,AL+3:ND+3,Y+3:O-2;2)  2.98150E+02  +TOTV14#
  +TOTV15#*T;     6.00000E+03   N REF:0 !


PHASE YAM_AL2O9Y4  %  4 2   4   1   9 !
   CONSTITUENT YAM_AL2O9Y4  :AL+3,SI+4 : Y+3 : O-2,VA : O-2 :  !

  PARAMETER G(YAM_AL2O9Y4,AL+3:Y+3:O-2:O-2;0)  2.98150E+02  +GYAM#;
 6.00000E+03   N REF:0 !
  PARAMETER G(YAM_AL2O9Y4,SI+4:Y+3:O-2:O-2;0)  2.98150E+02  +GYSM#;
 6.00000E+03   N REF:0 !
  PARAMETER G(YAM_AL2O9Y4,AL+3:Y+3:VA:O-2;0)  2.98150E+02  +GYAM#;
 6.00000E+03   N REF:0 !
  PARAMETER G(YAM_AL2O9Y4,SI+4:Y+3:VA:O-2;0)  2.98150E+02  +GYSM#;
 6.00000E+03   N REF:0 !
  PARAMETER G(YAM_AL2O9Y4,AL+3,SI+4:Y+3:O-2:O-2;0)  2.98150E+02
 +706342.874+10.1111582*T;   6.00000E+03   N REF:0 !
  PARAMETER G(YAM_AL2O9Y4,AL+3:Y+3:O-2,VA:O-2;0)  2.98150E+02  -265100
 +110.449011*T;   6.00000E+03   N REF:0 !
  PARAMETER G(YAM_AL2O9Y4,SI+4:Y+3:O-2,VA:O-2;0)  2.98150E+02  -453406.101
 -220.2521*T;   6.00000E+03   N REF:0 !
  PARAMETER G(YAM_AL2O9Y4,AL+3,SI+4:Y+3:VA:O-2;0)  2.98150E+02  -202926.265
 +103.756041*T;   6.00000E+03   N REF:0 !


PHASE YAP_ALO3Y  %  3 1   1   3 !
   CONSTITUENT YAP_ALO3Y  :AL+3 : Y+3 : O-2 :  !
```

```
  PARAMETER G(YAP_ALO3Y,AL+3:Y+3:O-2;0)  2.98150E+02  +GYAP#;   6.00000E+03
   N REF:0 !

LIST_OF_REFERENCES
NUMBER  SOURCE
 !
```

Bibliography

[1] T. H. Maiman. Stimulated optical radiation in ruby. *Nature*, 187(4736):493–494, 1960.

[2] J. E. Geusic, H. M. Marcos, and L. G. Vanuitert. Laser oscillations in Nd-doped yttrium aluminum yttrium gallium + gadolinium garnets. *Appl. Phys. Lett.*, 4(10):182–184, 1964.

[3] V. Lupei, A. Lupei, and A. Ikesue. Single crystal and transparent ceramic Nd-doped oxide laser materials: a comparative spectroscopic investigation. *J. Alloy. Compd.*, 380(1-2):61–70, 2004.

[4] A. Ikesue, T. Kinoshita, K. Kamata, and K. Yoshida. Fabrication and optical-properties of high-performance polycrystalline Nd-YAG ceramics for solid-state lasers. *J. Am. Ceram. Soc.*, 78(4):1033–1040, 1995.

[5] S. H. Lee, S. Kochawattana, G. L. Messing, J. Q. Dumm, G. Quarles, and V. Castillo. Solid-state reactive sintering of transparent polycrystalline Nd:YAG ceramics. *J. Am. Ceram. Soc.*, 89(6):1945–1950, 2006.

[6] S. H. Hong and D. Y. Kim. Effect of liquid content on the abnormal grain growth of alumina. *J. Am. Ceram. Soc.*, 84(7):1597–1600, 2001.

[7] O. Fabrichnaya, H. J. Seifert, R. Weiland, T. Ludwig, F. Aldinger, and A. Navrotsky. Phase equilibria and thermodynamics in the Y_2O_3-Al_2O_3-SiO_2-system. *Z. Metallk.*, 92(9):1083–1097, 2001.

[8] M. Hillert. On theory of normal and abnormal grain growth. *Acta Metallurgica*, 13(3):227–238, 1965.

[9] A. T. Dinsdale. SGTE data for pure elements. *Calphad-Comput. Coupling Ph. Diagrams Thermochem.*, 15(4):317–425, 1991.

[10] B. Sundman and J. Agren. A regular solution model for phases with several components and sub-lattices, suitable for computer-applications. *J. Phys. Chem. Solids*, 42(4):297–301, 1981.

[11] O. Redlich and A. T. Kister. Algebraic representation of thermodynamic properties and the classification of solutions. *Industrial and Engineering Chemistry*, 40(2):345–348, 1948.

[12] M. Hillert, B. Jansson, B. Sundman, and J. Agren. A 2-sublattice model for molten solutions with different tendency for ionization. *Metallurgical Transactions a-Physical Metallurgy and Materials Science*, 16(2):261–266, 1985.

[13] P. Hohenberg and W. Kohn. Inhomogeneous electron gas. *Phys. Rev. B*, 136 (3B):864–871, 1964.

[14] W. Kohn and L. J. Sham. Self-consistent equations including exchange and correlation effects. *Physical Review*, 140(4A):1133–1138, 1965.

[15] G. Kresse and J. Furthmuller. Efficiency of ab-initio total energy calculations for metals and semiconductors using a plane-wave basis set. *Comput. Mater. Sci.*, 6(1):15–50, 1996.

[16] J. P. Coutures. The Al_2O_3-Nd_2O_3 phase-diagram. *J. Am. Ceram. Soc.*, 68 (3):105–107, 1985.

[17] N. A. Toropov and T. P. Kiseleva. The binary system neodymium oxide-aluminum oxide and some data on the ternary system Nd_2O_3-Al_2O_3-SiO_2. *Russ. J. Inorg. Chem.*, 6:1193–1196, 1961.

[18] M. Mizuno, T. Yamada, S. Kitade, K. Sakamoto, and T. Noguchi. Phase diagram of the system Al_2O_3-Nd_2O_3 at high temperature. *Rep. Gov. Ind. Res. Inst., Nagoya*, 27(4):131–137, 1978.

[19] Y. Kanke and A. Navrotsky. A calorimetric study of the lanthanide aluminum oxides and the lanthanide gallium oxides: Stability of the perovskites and the garnets. *J. Solid State Chem.*, 141(2):424–436, 1998.

[20] Y. H. Zhang and A. Navrotsky. Thermochemistry of rare-earth aluminate and aluminosilicate glasses. *J. Non-Cryst. Solids*, 341(1-3):141–151, 2004.

[21] P. Wu and A. D. Pelton. Coupled thermodynamic phase-diagram assessment of the rare-earth-oxide aluminum-oxide binary-systems. *J. Alloy. Compd.*, 179:259–287, 1992.

[22] L. Li, Z. Tang, W. Sun, and P. Wang. Calculation of phase diagrams of Al_2O_3-SiO_2-R_2O_3 systems. *Phys. Chem. Glasses*, 38(6):323–326, 1997.

[23] O. Fabrichnaya and H. J. Seifert. Assessment of thermodynamic functions in the ZrO_2-Nd_2O_3-Al_2O_3 system. *Calphad*, In Press, Corrected Proof, 2007.

[24] N. Iyi, Z. Inoue, and S. Kimura. The crystal-structure of neodymium hexaaluminate. *J. Solid State Chem.*, 54(1):123–125, 1984.

[25] R. W. G. Wyckoff. *Crystal Structures*. Interscience Publishers, New York, 2nd edition, 1963.

[26] M. Marezio, P. D. Dernier, and J. P. Remeika. Crystal-structures of orthorhombic $SmAlO_3$ and of trigonal $NdAlO_3$. *J. Solid State Chem.*, 4(1): 11–19, 1972.

[27] M. C. Martin-Sedeno, D. Marrero-Lopez, E. R. Losilla, S. Bruque, P. Nunez, and M. A. G. Aranda. Stability and oxide ion conductivity in rare-earth aluminium cuspidines. *J. Solid State Chem.*, 179(11):3445–3455, 2006.

[28] J. Dohrup, A. Hoyvald, G. Mogensen, C. J. H. Jacobsen, and J. Villadsen. Formation of new compounds $Ln_4Al_2O_9$ in the Ln_2O-Al_2O_3 system (Ln=La, Pr, Tb). *J. Am. Ceram. Soc.*, 79(11):2959–2960, 1996.

[29] S. Huang, O. Van der Biest, J. Vleugels, and L. Li. Experimental investigation and thermodynamic assessment of the Nd_2O_3-Y_2O_3 system. *J. Am. Ceram. Soc.*, 89(8):2596–2601, 2006.

[30] W. D. Zhuang, J. K. Liang, Z. Y. Qiao, J. Y. Shen, Y. Shi, and G. H. Rao. Estimation of the standard enthalpy of formation of double oxide. *J. Alloy. Compd.*, 267(1-2):6–10, 1998.

[31] N. A. Toropov. Some rare earth silicates. *Trans. Intern. Cerara. Congr. 7th, London, Engl.*, 1960:435–42, 1961.

[32] R. O. Miller and D. E. Rase. Phase equilibrium in the system Nd_2O_3-SiO_2. *J. Am. Ceram. Soc.*, 47(12):653–654, 1964.

[33] Y. Masubuchi, M. Higuchi, and K. Kodaira. Reinvestigation of phase relations around the oxyapatite phase in the Nd_2O_3-SiO_2 system. *J. Cryst. Growth*, 247 (1-2):207–212, 2003.

[34] H. Okudera, A. Yoshiasa, Y. Masubuchi, M. Higuchi, and S. Kikkawa. Temperature dependence of structural parameters in oxide-ion-conducting $Nd_{9.33}(SiO_4)_6O_2$: single crystal X-ray studies from 295 to 900 K. *J. Solid State Chem.*, 177(12):4451–4458, 2004.

[35] A. C. Tas and M. Akinc. Crystal-structures of the high-temperature forms of $Ln_2Si_2O_7$ (Ln=La, Ce, Pr, Nd, Sm) revisited. *J. Am. Ceram. Soc.*, 77(11): 2968–2970, 1994.

[36] J. Felsche. The crystal chemistry of rare-earth silicates. In J.D. Dunitz, editor, *Structure and Bonding*, volume 13, pages 99–197. Springer-Verlag, New York, 1973.

[37] K. Gschneidner Jr. The Nd-Y(Neodymium-Yttrium) system. *Bull. Alloy Phase Diagrams*, 3(2):202–205, 1982.

[38] J. Coutures, R. Verges, and M. Foex. High temperature studies of systems formed by neodymium sesquioxide with yttrium sesquioxide and ytterbium sesquioxide. *Mater. Res. Bull.*, 9(12):1603–1612, 1974.

[39] P. A. Tikhonov, A. K. Kuznetsov, E. F. Zhikhareva, K. Y. Merezhinskii, and V. N. Yuneev. Structural diagram of Y_2O_3-Nd_2O_3 system and physicochemical properties of solid-solutions. *Zhurnal Neorg. Khimii*, 22(4):1057–1061, 1977.

[40] G. T. Adylov, V. G. Voronov, and L. M. Sigalov. The system Nd_2O_3-Y_2O_3. *Inorg. Mater.*, 23(11):1644–1646, 1987.

[41] M. Zinkevich. Thermodynamics of rare earth sesquioxides. *Prog. Mater. Sci.*, 52(4):597–647, 2007.

[42] A. Kaiser, R. Telle, M. Herrmann, H. R. Richter, and W. Hermel. Subsolidus phase relationships of the beta-sialon solid solution in the oxygen-rich part of the Nd-Si-Al-O-N system. *Z. Metallk.*, 92(10):1163–1169, 2001.

[43] R. V. Bakradze, L. M. Kovba, Kuznetso.Gp, and V. K. Trunov. Phase equilibria in Y_2O_3-Al_2O_3-Nd_2O_3 system. *Doklady Akademii Nauk Sssr*, 179(4): 849–851, 1968.

[44] L. V. Soboleva and A. P. Chirkin. Y_2O_3-Al_2O_3-Nd_2O_3 phase diagram and the growth of $(Y,Nd)_3Al_5O_{12}$ single crystals. *Crystallogr. Rep.*, 48(5):883–887, 2003.

[45] D. Klimm, S. Ganschow, A. Pajaczkowska, and L. Lipinska. On the solubility of Nd^{3+} in $Y_3Al_5O_{12}$. *J. Alloy. Compd.*, 436(1-2):204–208, 2007.

[46] D. E. Eakins, M. Held, M. G. Norton, and D. F. Bahr. A study of fracture and defects in single crystal YAG. *J. Cryst. Growth*, 267(3-4):502–509, 2004.

[47] L. Lipinska, L. Lojko, A. Klos, S. Ganschow, R. Diduszko, W. Ryba-Romanowski, and A. Pajaczkowska. Nanopowders and crystals in $(Y_{1-x}Nd_x)_3Al_5O_{12}$ system: Preparation and properties. *J. Alloy. Compd.*, 432(1-2):177–182, 2007.

[48] A. Zunger, S. H. Wei, L. G. Ferreira, and J. E. Bernard. Special quasirandom structures. *Phys. Rev. Lett.*, 65(3):353–356, 1990.

[49] I. MacLaren, R. M. Cannon, M. A. Gulgun, R. Voytovych, N. Popescu-Pogrion, C. Scheu, U. Taffner, and M. Ruhle. Abnormal grain growth in alumina: Synergistic effects of yttria and silica. *J. Am. Ceram. Soc.*, 86(4): 650–659, 2003.

[50] R. B. Rogenski, K. H. Sandhage, A. L. Vasiliev, and E. P. Kvam. The effect of excess neodymia on the grain growth of $Nd_{1+x}Ba_{2-x}Cu_3O_y$ solid solutions. *Journal of Materials Research*, 13(10):2819–2832, 1998.

[51] D. A. Porter and K. E. Easterling. *Phase Transformations in Metals and Alloys*. CRC Press, Boca Raton, 1992.